Master Thesis

Msc offshore & dredging engineering

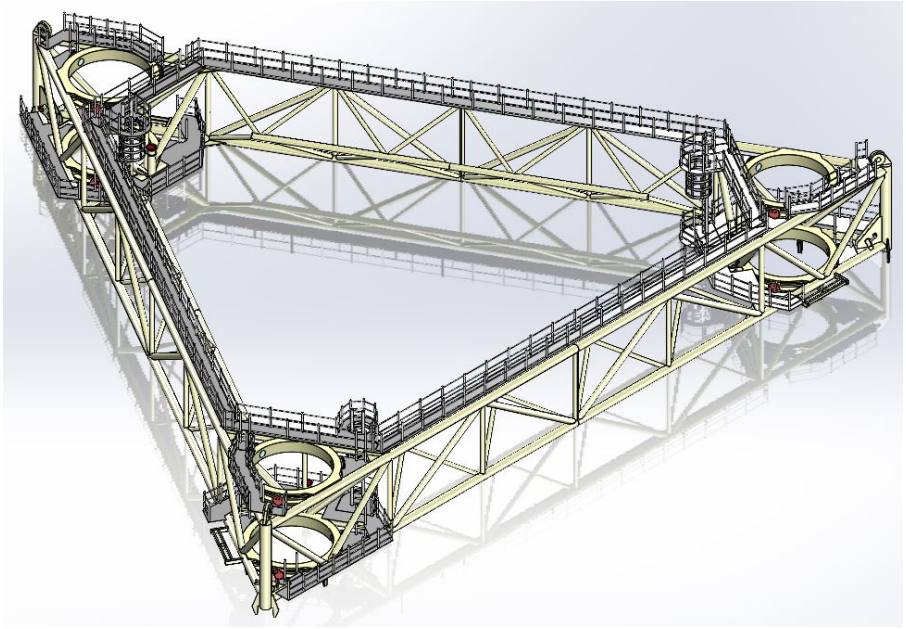

Design of a suction pile installation template

A case study on the implementation and design of a suction pile installation template as an installation aid for suction pile foundation installations

Author:

Laurens Berkouwer (4700228) |

Under TUDelft supervision of:
Oriol Colomés Gené & André van der Stap

Under SPT-offshore supervision of:
Peter Kromwijk & Erik ter Horst

August 12, 2023

Preface

This master thesis is submitted as part of the requirements for the Master of Science degree in Offshore and Dredging Engineering at TUDelft. Building upon my Bachelor's degree in Mechanical Engineering, the two-year master program provided me with a comprehensive understanding of various aspects of offshore engineering, which prepared me well for conducting research on the design of a suction pile installation template. This thesis was carried out in collaboration with SPT Offshore.

My passion for designing large structures led me to contact Erik ter Horst at SPT Offshore, and when I first learned about this graduation topic, I knew it was a perfect fit for me. Recognizing the potential in the topic, I hoped to play a key role in pioneering a new installation method for suction pile jacket foundations. From the start of this thesis, my goal was to address all aspects of the suction pile installation template design. However, it became clear that my proposed scope of work was too ambitious. Narrowing down the scope and make the work feasible within the nine-month time-frame allotted for this thesis was a challenge. Additionally, expressing my research thoughts and creating a cohesive narrative proved to be more challenging than I initially anticipated.

My thesis follows a typical design report format, emphasizing the presentation of results and a summary of the data collection process to maintain conciseness and prevent readers from becoming overwhelmed by intricate details of the suction pile installation template design. Those interested can find more comprehensive analyses in the Appendix.

Overall, I am satisfied with the work I have produced and the lessons I have learned. However, I am aware that there is still much more work to be done in this field, and it is difficult to conclude my research solely on the design of the suction pile installation template. I wish future researchers the best of luck and hope that my work can provide valuable insights.

I would like to express my gratitude to my two TUDelft committee members: Oriol Colomes Gene (supervisor), who consistently made time for me despite supervising many other theses, and Andre van der Stap (chairman), whose invaluable guidance and feedback helped me focus on the key aspects of my research. Additionally, I am grateful to my SPT Offshore committee members: Peter Kromwijk (supervisor), who provided constant support and was available for progress discussions throughout the week, and Erik ter Horst (supervisor), who entrusted me with this assignment, introduced me to relevant contacts, and meticulously reviewed and provided feedback on my draft reports. I would also like to acknowledge my SPT Offshore & DEME colleagues who warmly welcomed me into their team, shared their knowledge, and provided insights into work experiences. To all of you, I sincerely appreciate your time and expertise.

Lastly, I would like to express my heartfelt appreciation to my family and friends for their interest in my thesis development and for their support in helping me find balance between my work and social life. In particular, I want to thank my parents for equipping me with the tools, responsibility, and confidence to achieve my goals.

Abstract

For the installation of suction pile jackets, a new installation method initiated by SPT Offshore could extend the allowable size for suction pile jackets used as foundations for offshore wind turbines. This method involves installing the suction piles separately from the jacket frame. First, the suction piles are installed on the seabed. Then, the jacket frame is placed on top of the suction piles, and the piles and the frame are connected. The installation of the suction piles in the seabed requires a certain level of precision to ensure a proper connection with the jacket frame. This can be achieved by introducing an installation tool called the suction pile installation template (SPIT). The goal of this thesis is to take the first steps towards realizing the SPIT installation method by designing the suction pile installation template and identifying key design challenges for the SPIT.

To bound the scope of the research, assumptions are made regarding the installation vessel, foundation dimensions, jacket-pile connection, and site specifications based on a case study and the resources of DEME. To design the SPIT, the use of the SPIT is analysed, considering a wide range of design options. The most significant inputs to the analysis are the limitations of the installation vessel and operational efficiency. Next, the changes to the suction pile and jacket frame are examined. The selected grout connection between the suction pile and the jacket frame creates a jacket frame similar to a standard pin pile jacket. The suction pile requires a stub on top of the top-plate. An optimization study is conducted to determine the size of the stub. These two analyses provide the general design requirements for the SPIT, which is then checked for structural strength, installation tolerance of the suction piles and lift capacity. The checks are based on industry standard codes.

Analysis shows that the hydrodynamic loading on the suction piles induces the largest loads on the SPIT. However, if the suction piles are incorrectly placed in the seabed, the interaction between the soil and the suction piles could result in even larger loads on the SPIT. The models used in this thesis should provide conservative estimates. In future research, the analysis of hydrodynamic loading, geotechnical analysis, and dynamic response of the SPIT should be verified and justified using more sophisticated models and/or simulation software.

The results from this thesis indicate that the proposed design of the SPIT provides a solution to extent the installation of SPJ for OWT. The research identifies four key design challenges. Each challenge indicates solvable obstacles to the design of the SPIT. Based on the results, the estimated total weight of the SPIT is $240mt$. DEME's installation vessel, the Orion, has sufficient lift capacity to perform the installation and deck-space to perform up to 13 installation in one trip.

Keywords: Suction pile installation, Installation template, Suction pile jacket, Heavy lift operation, Concept design, Offshore wind farm foundation, Offshore installation method.

Nomenclature

Abbreviation	Description
CTC	Center to center
DAF	Dynamic amplification factor
DNV	Det norske veritas
DOF	Degrees of freedom
FBD	Free body diagram
GW	Gigawatt
HLV	Heavy lift vessel
KC	Keulegan-Carpenter
MDS	Mass damping spring
MSL	Mean sea level
NC	Non consolidated
OWF	Offshore wind farm
OWT	Offshore wind turbine
PPJ	Pin pile jacket
PTG	Penetration target
ROV	Remotely operated vehicle
RAO	Response amplitude operator
SHL	Static hook load
SPJ	Suction pile jacket
SPIT	Suction pile installation template
SP	Suction pile
T&I	Transport and installation
UC	Utilization coefficient
WSD	Working stress design

Contents

Preface **I**

Abstract **II**

Nomenclature **III**

1 Introduction **1**

2 Background **2**
2.1 Suction pile jacket . . . 2
2.1.1 Working principle . . . 2
2.1.2 Installation method . . . 4
2.1.3 Advantages & disadvantages . . . 5
2.2 Potential for pre-installation with template . . . 6
2.2.1 Offshore wind farm trends . . . 6
2.2.2 Vessel capacity of DEME . . . 6
2.2.3 Financial gains . . . 8
2.3 Research gap . . . 9
2.3.1 Literature related to the SPIT installation method . . . 9

3 Scope of research **11**
3.1 Research goal . . . 11
3.1.1 Research questions . . . 11
3.2 Research setup . . . 11
3.3 Case study . . . 12
3.4 Assumptions . . . 12

4 Transport & installation strategy **15**
4.1 On-site . . . 15
4.1.1 Installation options . . . 15
4.1.2 Concept strategy . . . 18
4.2 Offshore transport . . . 20
4.2.1 Offshore transport options . . . 20
4.2.2 Concept strategy . . . 21
4.3 Answer to sub-research question 1 . . . 22

5 Suction pile - jacket connection **23**
5.1 Connection configuration . . . 23
5.2 Design requirements . . . 23
5.3 Grout connection dimensions . . . 24
5.4 Tolerance margin for the grouted connection . . . 25
5.5 Concept design . . . 26
5.6 Answer to sub-research question 2 . . . 28

6 Design of the SPIT **29**
6.1 SPIT design requirements . . . 29
6.2 Design choices . . . 30
6.2.1 SPIT . . . 30
6.2.2 SPIT-SP engagement . . . 31
6.2.3 SPIT-Orion connection . . . 33
6.2.4 Safety . . . 34
6.3 Concept design . . . 34
6.4 Requirements check for SPIT . . . 37
6.4.1 Strength of the SPIT frame during operation . . . 38
6.4.2 Padeye strength . . . 46
6.4.3 Capacity of hydraulic cylinders . . . 47
6.4.4 Installation tolerance of the SPs with the SPIT . . . 48

6.4.5 Weight of the SPIT . . . 50
6.4.6 Crane curve Orion . . . 51
6.5 Answer to the research questions . . . 53
6.5.1 Sub-research question 3 . . . 53
6.5.2 Main research question . . . 53

7 Discussion **55**
7.1 Hydrodynamic loads on SP . . . 55
7.2 Geotechnical analysis . . . 55
7.3 Weight and structural strength of the SPIT . . . 56
7.4 Jamming forces on the SPIT-SP connection . . . 56
7.5 Top-plate grouting . . . 56
7.6 Orion as installation vessel . . . 56

8 Conclusion **58**

9 Recommendations **59**
9.1 SPIT functions . . . 59
9.2 Detailed load analyses . . . 59
9.3 Commercial feasibility . . . 59

References **60**

A Suction pile stub analysis **62**
A.1 Design maximum loads . . . 62
A.2 Design capacity . . . 62
A.3 Grout thickness relation . . . 63
A.4 Results . . . 63
A.5 Total stub length . . . 65

B Horizontal hydrodynamic load analysis on the SP **66**
B.1 Morison coefficients . . . 66
B.2 Water particle motions . . . 67
B.3 Load case . . . 68
B.4 Results . . . 69
B.5 Stub loads . . . 70

C Horizontal hydrodynamic load analysis on the SPIT frame **73**

D Soil pile interaction **76**
D.1 Clay . . . 77
D.1.1 Uniform clay . . . 77
D.1.2 Normally consolidated clay . . . 79
D.2 Sand . . . 80

E Venting of a SP **83**
E.1 Buoyancy development over time . . . 84
E.2 Minimum perforation . . . 85

F Truss frame analysis **86**
F.1 Load distribution from gripper ring to the frame . . . 87
F.2 Loads on the main members of the SPIT . . . 88
F.3 Shear in frame due to bending moments . . . 91
F.4 Shear in pocket frame . . . 93
F.5 Member sizing . . . 94

G Padeye analysis **96**
G.1 SPIT-sling padeye . . . 97
G.2 SPIT-SP padeye . . . 98

H Tolerance analysis for the SP-jacket connection **100**
H.1 Fabrication tolerances . . . 101
H.1.1 Jacket pin . . . 101
H.1.2 SP stub . . . 101
H.1.3 Total fabrication tolerances . . . 102
H.2 installation tolerances . . . 102
H.2.1 Height of the SP (Heave): . . . 102
H.2.2 Horizontal misalignment of the SP (Surge and sway) . . . 102
H.2.3 Rotational misalignment of the SP (Pitch and roll): . . . 103
H.2.4 Total installation tolerances . . . 103
H.3 Total tolerances . . . 104

I Metocean data **105**

J Frame numbering **106**

1 Introduction

In 2021, the United Nations Energy Compact was signed by the Global Wind Energy Council (GWEC) and the International Renewable Energy Agency (IRENA), pledging to work together to install 2000 GigaWatts (GW) of offshore wind generated power globally by 2050 [20]. Both GWEC and IRENA are international organizations that represent over 1500 companies, organisations and institutions [18] and 167 countries & the EU [23]. These organizations should make sure that on average, 35 GW of offshore wind generated power is added to local grids per year to reach this goal. Due to the necessary growth of offshore wind generated power and limited suitable offshore sites near the coast, offshore wind farms are built further away from shore and into deeper waters [30]. In order to safely commission the wind turbines, the offshore sites require larger foundation structures. Installation limitations for installation vessels create additional challenges for the installation of these foundation structures.

One foundation type used for offshore wind turbines is the suction pile jacket (SPJ) [24]. This foundation type has a reduced environmental impact and installation time over the standard pin pile jacket (PPJ) [45]. However, one disadvantage is the increased size and weight of the SPJ due to the attached suction piles (SPs) to the jacket frame.

Separating the installation of the SPs from the jacket frame, can allow installation vessels to extend installations for larger SPJ. An installation tool is required in order to install the SPs separate from the jacket and have the SPs placed with the correct orientation on the seabed. A frame template can provide the necessary functions of the tool. Figure 2 illustrates a schematic representation of the proposed pre-installation process of the suction piles with a template frame and the installation of the jacket frame. First, the installation of the SPs are performed with the help of the installation tool. Then, the tool is removed and can be reused for the next offshore foundation. The last step is to connect the jacket frame to the SPs.

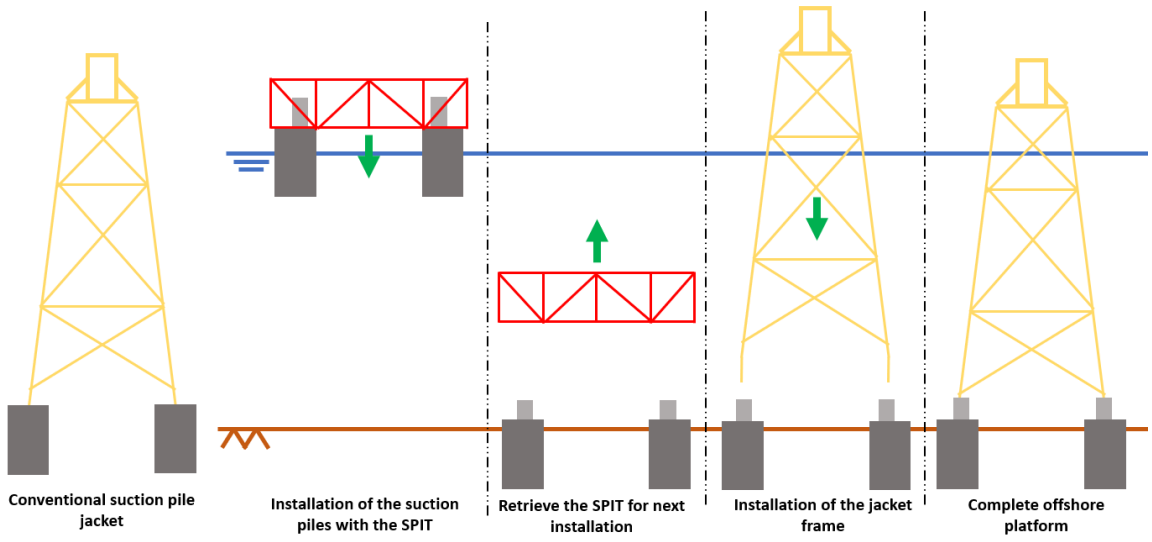

Figure 2: Schematic sketch for the pre-installation of the suction piles for suction pile jackets

Pre-installation with a suction pile installation template (SPIT) for SPJs is an installation method considered by SPT-offshore (DEME). The master thesis will conceptualise and justify the design of the SPIT for this installation method, based on the resources of DEME.

This thesis is structured as follows. Chapter 2 provides background information on why pre-installation of SPs is considered. This Chapter also identifies the research gap for the installation method. Chapter 3 defines the research scope. Here, the goal of this thesis is stated and a case study is introduced. In Chapter 4, the transport and installation (T&I) of the SPIT strategy is visualised. The considered strategy is worked out from port to on-site operations. Chapter 5 explains the changes for the SP - jacket connection necessary for pre-installation of SPs. Lastly, the conceptual design of the template is worked out in Chapter 6. In this Chapter, analyses are performed to justify that the SPIT design satisfies the design requirements.

2 Background

In this Chapter, the working principle and installation strategy of a SPJ is explained. Then, the potential of the SPIT method is explained. The third section identifies the research gap for the proposed installation method.

2.1 Suction pile jacket

This section provides information on the working principle of the suction pile foundation and the conventional installation method of the SPJ. The advantages and disadvantages are explained in section 2.1.3 to give a clear overview of when SPJs are preferred over PPJs. The section concludes by relating this information to the SPIT installation method.

2.1.1 Working principle

The described working principle for the SPs and the installation of the SPJ is based on the common practice at SPT-offshore [39]. A SPJ is a steel frame structure with 3 or 4 legs and attached to each leg is a SP [24]. SPs represent the piled foundation in the seabed of the SPJ. A SP is a large round steel tubular where the top of the tubular is closed by a top-plate. The SP steel tubular is called the SP shell. A schematic side-view of a suction pile is shown in Figure 3a. When the SP is placed on the seabed, the soil creates a seal around the shell enclosing the inside volume of the SP. A pump connected to a valve located on the top-plate, can displace water from the inside to the outside of the pile and in turn lowers the SP into the seabed. More detail about the suction process is explained in section 2.1.1.2. The process can also be reversed if the SP should be removed from the seabed.

2.1.1.1 Bearing capacity The bearing capacity of the SP should satisfy the loads occurring during the SPJ lifetime. Combined loading cases consisting of later loads, overturning moments and vertical loads are a critical topic for the design of the SPs [43] [45]. The bearing capacity of the SP is created by two bearing types on the SP:

- **Shear bearing:** The shear bearing is the friction between the soil and the steel caused by the pressure of the soil against the shell of the SP. The shear bearing depends on the soil type and dimension of the SP [43] [44].
- **Compression bearing:** The compression bearing is caused by the vertical and lateral compressive strength of the soil and is dependent on the contact area of the SP with the soil, soil type and submerged height of the SP in the soil [43] [44].

In Figure 3b, the shear (blue) and compression (red) bearing on a SP is depicted.

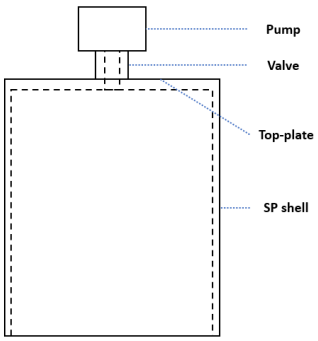

(a) Schematic side-view of the SP with pump

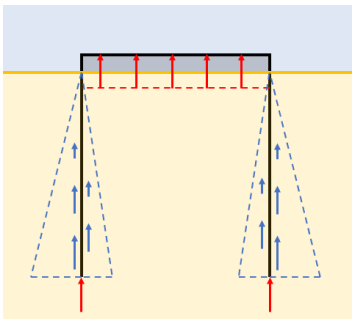

(b) Vertical forces on the suction pile due to soil interaction

Figure 3

2.1.1.2 Pump The pump is attached to the top of the suction pile before the SP is lifted to the seabed. The pump is powered and controlled by a pump control container on board of the installation vessel. The pump is attached to the control container via an umbilical cord. The designed bearing capacity of the SP is calculated for a specific embedded length called penetration target (PTG). The capacity of the pump is selected to allow for the SP to reach this PTG. The pump systems provided by SPT-offshore [39] for the SP installation have two functions:

- **Suction pile lowering:** The pump discharges water from inside the pile to the outside creating an under-pressure inside the pile with respect to the outside pressure. Due to the under-pressure the pile is slowly forced into the soil. When the vertical bearing capacity of the soil on the SP equals the suction force created by the pump, the suction process is stopped. If the SP needs to be removed, this suction process can be reversed.

  During the suction process, the soil on the inside of the pile can expand or the top soil layer can separate from the soil layer below, resulting in plug heave [42]. What the actual plug heave will be during installation is hard to predict and measure. When the soil on the inside of the SP reached the top-plate, the pump is unable to create an under-pressure in the pile and the suction process is stopped. An extra offset from the PTG can be considered for potential plug heave. Figure 4 gives an overview of the sensors and the parameters used during installation of a suction pile.

- **Sensor tool:** Different sensors are attached to the pump to monitor the installation of the SP. A sensor for the verticality of the pile gives feedback to the control system whether verticality adjustments need to be made. For a single SP used as an anchor, the lift line is adjusted accordingly to correct the verticality. For multi chambered suction piles or multiple single chamber suction pile installations, changing the under-pressure for different chambers will adjust the verticality [45]. The easy regulation of the pump discharge rate results in high installation precision [39]. An echo sensor is installed on the bottom of the pump to measure height of the soil inside the pile. The sensor is used to measure the plug heave. A height sensor in combination with a reference sensor are used to measure the penetration depth. The reference sensor is attached to an external umbilical and placed on the seabed to reference the measured data on the SP to a fixed point.

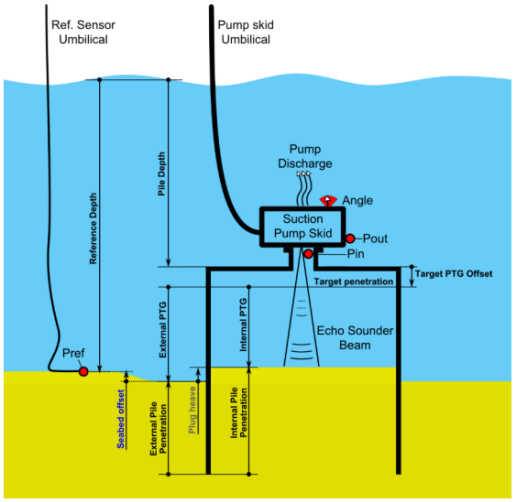

Figure 4: Overview of suction pile and sensor measurements. Picture taken from the Database of SPT-offshore [39]

2.1.1.3 Top-plate grouting When the pile is at its PTG, the pump is stopped and removed. Because of the PTG offset, there is a small volume left between the soil and the top-plate. Depending on the permeability of the soil, water can flow through the soil when the pile is loaded, making the foundation unstable. It is therefore necessary that the leftover volume, now occupied by water, is filled with a medium unable to move through the soil. Heavy grit grout is used to fill up the volume. When the grout is fluid it distributes itself in the pile. After the grout has dried, the contact between the grout and the top-plate add bearing capacity to the SP. Top-plate grouting is a labour-intensive process and is preferably avoided. Alternatives to grouting have been suggested internally at SPT-offshore [39], but no competitive large-scale proof of concepts exist.

2.1.1.4 Scour protection Scour is the excessive sediment erosion around an offshore structure [42] [43]. The erosion occurs due to the motion of the water near the seabed, which is caused by the current on the seabed. The structure disturbs the flow of the water resulting in accelerated flows and/or turbulent phenomena such as vortexes. The disturbance can cause excessive sediment erosion around the structure. Thus, scour puts the stability of the foundation at risk. Since SP lengths are significantly less than driven piles, a $1m$ scour has

a greater impact on suction piles. Scour protection systems, such as subsea rock installation [21], are required to minimise the erosion [42]. However, the jacket structure limits the accessibility to perform subsea rock installation on the inside of the jacket legs [42]. Scour treatment takes up a significant part of the installation budget [8] and alternative low-cost scour treatments are being researched [1].

2.1.1.5 Suction pile - structure connection The SP-jacket connection is always on the top-plate of the SP. The top-plate is more suitable for distributing the loads over the SP, as the thin shell of the SP allows for poor local lateral strength. The top-plate of the SP can be easily increased in stiffness and strength with beams and panels to satisfy for the required loads. To ensure that the loads from the jacket is transferred directly to the centre of forces of the suction pile, the SP-jacket connection is generally located with an offset from the middle axis of the SP shell. This is to avoid additional bending moments in the jacket leg and SP.

2.1.2 Installation method

After the fabrication of the SPJ at the fabrication yard, the platform is transported to site. Due to the large footprint of the SPJ, crane vessels are limited in the number of SPJs they can transport on deck. Barges or transport ships can be used as an additional transportation method, as multiple SPJs can usually be fitted on these decks. When the installation vessel is in position, the barge will approach the site and the jacket can be prepared for installation. The pumps are placed on the SP and operated via the control containers stationed on the installation vessel. The umbilical cord from the control containers are carefully guided to the pumps to avoid entanglement of the cords during the installation of the SPJ.

The SPJ is now lowered to the seabed. Figure 5 depicts the installation sequence at the seabed of the SPJ.

a. Due to the self-weight of the jacket, the piles are forced into the soil. When the resistance of the soil is equal to the self-weight of the structure, the self-weight penetration in the seabed is reached and the structure is stationary. After the self-weight penetration, the pumps are activated and the SPs are lowered to the required height. In paragraph 2.1.1.2 the pump operation is explained in more detail.

b. The pumps are removed from the SPs. Remotely operated vehicle (ROV) support is used to detach the pumps.

c. Top-plate grouting is performed. This is the process where the remaining water volume in the suction piles is replaced with grout. Paragraph 2.1.1.1 & 2.1.1.3 explain top-plate grouting in more detail. The grout is guided to the SPs through grout lines via the jacket structure or an ROV.

d. Scour protection is added to the base of the jacket. Rock dumping techniques are mainly used for the application of the scour protection layer. Paragraph 2.1.1.4 explains scour protection in more detail.

The SPJ is now ready for the installation of the topside structure.

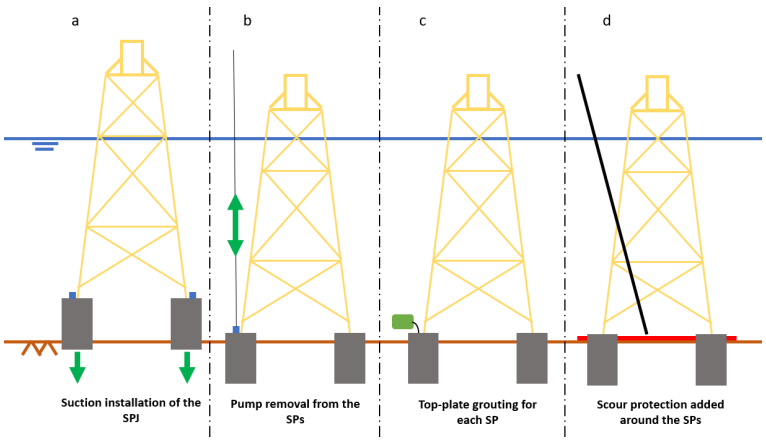

Figure 5: Installation sequence of a SPJ at the seabed

2.1.3 Advantages & disadvantages

Jacket structures are considered for water depth ranges of $30 - 80m$ [10] [45]. The two main foundation types for jackets are a PPJ or a SPJ [24]. The advantages and disadvantages listed below for SPJs are made in comparison with PPJs only. There are four main advantages of SPJs:

- **Installation speed:** The installation operation of a SPJ is faster. PPJ installation operations on average take up to three to four days per platform [28]. A SPJ operation takes less than 12 hours per platform on average [39].
- **Installation precision:** The verticality precision of SPJ installation is better. The precision of suction piles are of order of magnitude $10mm$ [46] whereas pile driven piles are of order of magnitude $100mm$ [9]. The installation precision of SPJs is due to the controllability of the pumps that suck the foundation into the seabed.
- **Environmental impact:** SPJs have a reduced environmental strain. Driving piles into the seabed creates disrupting noises for marine life around the site. The installation process of SPJs however, does not create harmful noises to the environment [45]. Additionally, the SP installation is reversible, making it possible to decommission the complete structure without leaving piles in the soil, thus allowing for complete seabed restoration.
- **Soft soils:** For soft soil top layers, driven piles have poor stability performance. These piles are elongated to improve the stability in deeper layers. However, SPs can be sized to have sufficient stability in soft top layers, significantly reducing the amount of steel necessary for the foundation [39].

Four main disadvantages of the SPJs are:

- **Shell structure of SP:** SPJs are more vulnerable to accidental loads due to the thin shell structure of the SPs. The SP has low later strength before installation. An accidental lateral load can dent the shell, increasing local buckling failures, resulting in unusable SPs for installation [39].
- **Jacket size:** The total jacket size for SPJs is larger. The integrated SPs to the jacket increase the weight, height and footprint of the jacket frame compared to a PPJ at the offshore location [10].
- **Infrastructure:** The infrastructure for jacket platforms is much more advanced for PPJs. Manufacturers and offshore companies have more experience with PPJs and have fabrication lines & equipment adjusted for these platform types. This can scare off potential customers for SPJs [39] [45].
- **Hard soils:** SPs do not have the capacity to penetrate hard soil types or debris such as boulders in the soil [39] [45]. Driven piles can be driven through these layers or holes can be drilled for the piles to be installed later [43].

Whether SPJs are preferred over PPJs depends on the location and demand of the customer. SPT-offshore states that generally SPJs are the cheaper alternative. With growing environmental demands by local governments, PPJ are required to use advanced noise mitigation systems. The noise mitigation systems add additional costs to the installation operation and might not satisfy the environmental requirements in practise. The rise of environmental awareness in offshore projects increases the demand for SPJs.

The installation method of pre-installation of the SPs for SPJs has significant impact on multiple parts of the installation procedure:

- Pre-installation of the SPs will reduce the necessary lift capacity since the SPs will be installed separately from the jacket frame. However:
  - More lift operation actions will be introduced offshore.
  - An installation template is required for accurate SP placement.

  Both bullets result in additional costs for the installation operation for SPJs.
- The SPIT installation method reduces the footprint of the SPJ during transportation. The deck-space required for the jacket frames of SPJs and PPJs will be equal.
- The SPIT can be designed to individually lower the SPs. The top-plate can be levelled with the inside of the soil, reducing top-plate grouting or even making the grout obsolete.

- The scour treatment can be done before the jacket frame is installed. The pre-installation of the suction pile foundation enables easier access for scour treatment methods.
- The lift operations for the pump systems can be reduced by integrating these systems into the SPIT. Individual attachment and removal of the pumps on the SP by the crane is not required anymore.

The mentioned bullets impact the required resources and time necessary for the SPIT installation method. This translates to commercial benefits and drawbacks of the installation methods.

2.2 Potential for pre-installation with template

In this section, the challenges and costs of SPJ installations are explained. The section concludes on why the novel installation method is worth considering for future SPJ installations.

2.2.1 Offshore wind farm trends

The offshore environment significantly increases installation and foundation costs for offshore wind farms (OWFs) compared to onshore wind farms. However, due to the limited space available in high populated coastal areas and favourable wind conditions offshore, OWF are constructed to supply green energy to the grid. To reduce foundation and installation costs, OWF are built in shallow waters and close to the shore. As the current development progresses, OWF sites are increasingly expanding in both depth and distance from shore. Figure 6, taken from the offshore wind market report 2021 [30], illustrates the global trend for water depth of OWF installations.

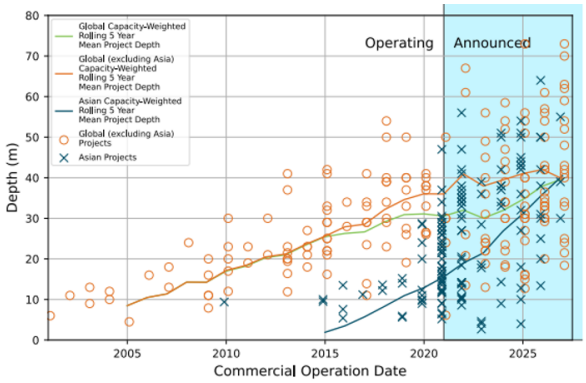

Figure 6: Offshore wind farm commercial operation date plotted against the average water depth

As water depth increases, the foundation structure also increases in weight and size. Not only are OWFs moving to greater water depths, but the wind turbines are also increasing in size [20]. The foundation structure should therefore also increase in strength resulting in even larger and heavier structures.

For water depths up to $30m$, monopile foundations are generally used for OWF [30]. In deeper water, structures with more complex geometries that reduce hydrodynamic loads are preferred over monopiles. Jacket structures are most commonly used for these water depths. Floating foundations for OWF are considered for even larger water depths. However, when floating foundations are considered over jacket foundations is arbitrary. DEME foresees demand for jacket installation for water depths up to at least $80m$.

2.2.2 Vessel capacity of DEME

For the installation of jacket foundations at water depths of $80m$, the crane of the installation vessel should satisfy the requirements. The limiting factors for installation vessels are:

- Crane capacity
- Lift height
- Weather conditions

When the environmental conditions are known, a crane curve can be constructed that relates the crane capacity, lift height and lifting radius. For offshore installations, DEME wants to maximise the use of their own fleet. The largest installation vessel in their fleet is the Orion. In good weather conditions, when dynamic factors are considered below 1.1 in all capacity curves, the Orion has a maximum lift capacity of $5000mt$ and a maximum lift height of $120m$. SPJ weight estimations for a $120m$ tall jacket is $3200mt$ [10]. Therefore, in the case of the Orion, the limiting factor for SPJ in good weather conditions is the lift height.

In Figure 7a, the jacket foundation height is split into four parts:

- **Transition piece (TP):** Top part of the jacket that connects the wind turbine shaft to the foundation.
- **Air-gap:** Necessary gap to avoid wave slamming to the deck of the jacket [43].
- **Water depth:** The mean water depth at the site.
- **Suction pile (SP):** Pile that transfers the loads from the jacket to the soil.

Each part has a height design envelope depending on the OWT type & location and are indicated in Figure 7a. Height limitations for the Orion can occur for water depths when the maximum range of the TP, airgap and SP are considered. The pink area in Figure 7b indicates potential height limitations for SPJ. If even deeper water depths are considered, the jacket without the SPs will also exceed the lift height capacity of the Orion. Pre-installation of the suction pile will not be enough to reduce the height of the SPJ. The corresponding design envelope is indicated in red in Figure 7b. This problem would occur for both SPJs and PPJs. Splitting the jacket frame (SPLIT) can be considered to install these large jacket structures. To clearly indicate the regions where the SPIT or SPLIT method can be considered for jacket foundations, the plots in Figure 18a and 8b are constructed.

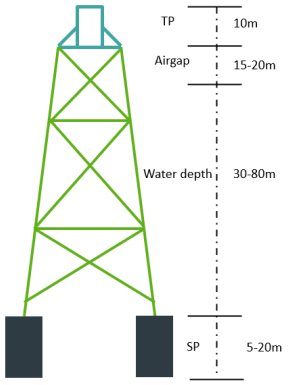

(a) Jacket height split in four parts. The height ranges are estimations from previous and future projects.

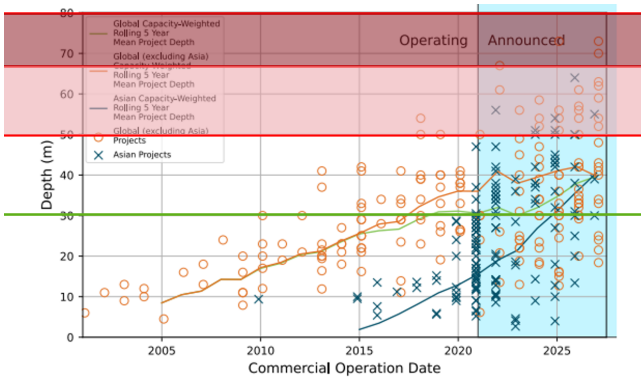

(b) Offshore wind farm commercial operation date plotted against water depth. The pink area indicates potential limitation problems for SPJ. The red area indicates potential limitation problems for the SPJ without the SPs.

Figure 7: Height limitations for jacket foundation for DEME

The plot in Figure 18a is based on the height limitations of the Orion. The area below the purple line indicates the range for conventional SPJ installations. The orange area indicates the range where the SPLIT and the SPIT method can both be considered. If the jacket exceeds the height limit, only the SPLIT method can be considered. The design envelope for SPJs is indicated by the area encircled by the red line and located in the top left corner of the plot. The jacket/suction pile height ratio is larger than 1. The plot for the combined suction pile weight and jacket weight is similar (Figure 8b). The main difference is the location change of the design envelope. The jacket/SP weight ratio is around 1.

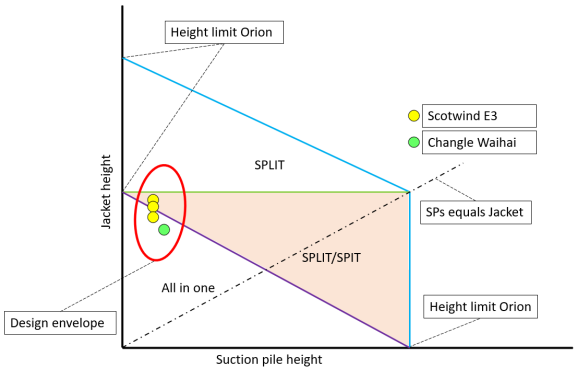

(a) Suction pile height plotted against jacket height. Different areas exist corresponding to the suitable installation methods. The encircled red area indicates the design envelope for SPJ.

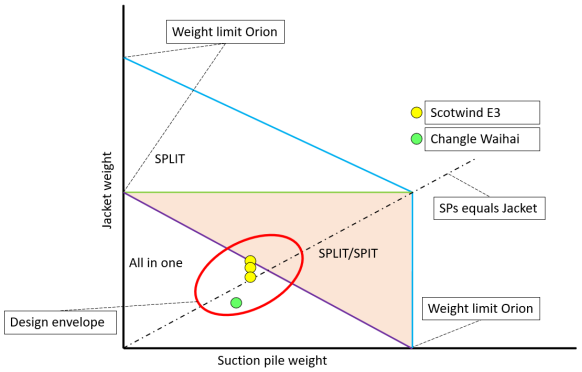

(b) Suction pile weight plotted against jacket weight. Different areas exist corresponding to the suitable installation methods. The encircled red area indicates the design envelope for SPJ.

Figure 8

The data point of ScotWind E3 SPJ indicates that the height limit of the Orion is exceeded. The SPIT or SPLIT method can both be considered in this case. Due to the large crane capacity of the Orion, SPJ installations in general will be limited by the lift height. However, for different installation vessels such as the Green Jade, weight limitations for SPJs are more likely to occur. If a different installation vessel is selected the axis of the plots should be properly scaled.

2.2.3 Financial gains

The installation of the foundation is only one part of the development needed for OWFs. Whether pre-installation of the SPs is commercially feasible depends on the cost gains or losses introduced with this novel installation method.

In Figure 9a, the cost percentages for development of a representative offshore wind farm up to commissioning are shown. The data is taken from the Beatrice wind farm guide [8]. Roughly 27% of development costs is spent on installation and commissioning. From this 27%, only 15% is spent on the T & I of the foundation for the wind turbine. 4% of the complete development of the windfarm is spent on the T & I of the foundation. For a typical $1GW$ OWF this 4% would translate to €100 million.

These Figures are based on a guide released in 2019. The COVID-19 pandemic and the extremely volatile oil and gas prices had a negative impact on the T & I cost [20]. Moreover, this guide was based on OWF for water depths of $30-40m$. For this thesis, relevant water depths of $70m$ should be considered. For larger water depths, the jacket foundation size will also increase, which requires bigger and more expensive installation vessels. These factors most likely increase the absolute and relative costs of T & I for OWF.

Yet, the estimated 4% translates to a significant amount of the OWF budget. Companies which are specialised in offshore T & I projects such as DEME can benefit from installation methods that drive down the project costs.

However, what should be noted is that at specific offshore locations, DEME can only perform the jacket installations if a SPIT or SPLIT installation method is used. In this specific case, the financial differences with other methods will not play a role and only the SPIT or SPLIT method should be compared to each other. The SPIT method has significant transport logistical advantages over the SPLIT method. However, the SPIT method requires the fabrication of the SPIT. From this can be reasoned that if few jacket installations are necessary, the SPLIT method is preferred. When the SPIT can be reused, the SPIT method is estimated to be more cost efficient after a certain amount of installations. However, the research that should be performed to justify this claim is outside of the scope of this thesis.

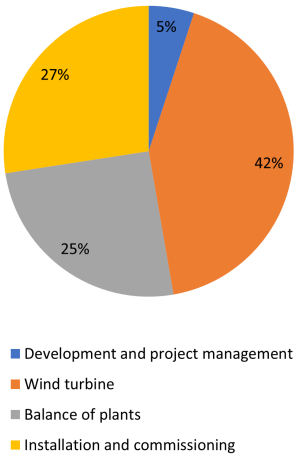

(a) Cost percentages for development of an offshore wind farm up to commissioning

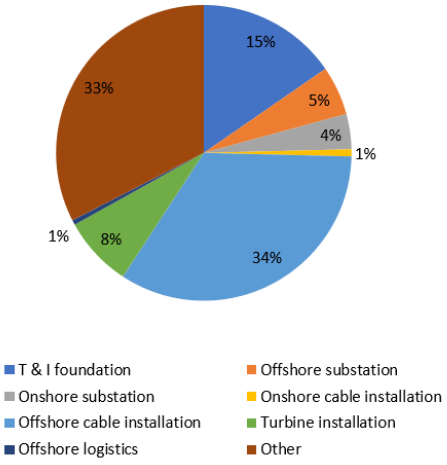

(b) Installation & commissioning cost percentages for offshore windfarm development

Figure 9: Pie charts containing the cost percentage of the development for an offshore wind farm.

2.3 Research gap

To identify in which area additional research is required for the SPIT installation method, public literature is reviewed. The complete scope of research for the SPIT installation method is divided into four parts. Figure 10 illustrates the four parts with a schematic sketch. This is done to order the wide scope of the SPIT installation method and to indicate what the scope of research for this thesis will be. Chapter 3 will explain which parts will be in the scope of research.

1. **Installation sequence:** This part covers what actions are required to perform the SPIT installation method.
2. **Suction pile jacket changes:** This part covers how the jacket frame will be connected to the SPs and what changes are required to the conventional SPJ in order for this installation method to work.
3. **Suction pile placement:** This part covers how the SPs are placed in the seabed with the help of the SPIT.
4. **Commercial feasibility:** This part covers how the SPIT installation method compares financially to other methods.

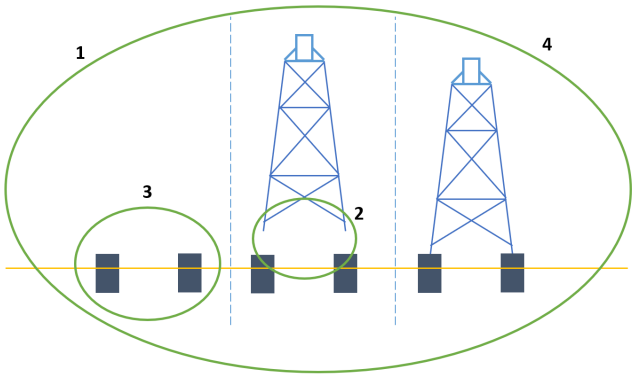

Figure 10: Total overview of the four parts of the SPIT installation method

2.3.1 Literature related to the SPIT installation method

Only patents have been found directly related to the SPIT installation methods. N Prior Energy GmbH and Boskalis B.V. have both submitted a patent that is directly related to the proposed SPIT method. The patent

of N Prior Energy GmbH [22] indicates multiple installation methods for a suction pile tripod. Two methods in the patent describe the installation of the SPs in the seabed. The two methods described are:

- Three SPs are lifted to the seabed with a lifting tool. After the installation is done the tool is removed and the tripod frame is placed on top of the SPs.
- SPs are individually placed in the seabed without the help of an installation tool. After the SPs are in the seabed, the tripod frame is placed on top of the SPs.

The patent of Boskalis B.V. [41] indicates three types of installation methods for a four legged suction pile jacket. The three methods are:

- Four SPs are lifted to the seabed with a lifting tool. After the installation is done the tool is removed and the jacket frame is placed on top of the SPs. This method is similar to the first method described by N Prior Energy GmbH.
- A template frame is placed on the seabed with four large holes. Then, in each hole a SP is placed such that the SPs are correctly placed on the seabed. After the SPs are in the seabed, the template frame is removed and the jacket frame is placed on top of the SPs. This installation method is similar to the pre-piling method for pin pile jackets.
- SPs are lifted to the seabed connected to a frame. This frame represents a part of the jacket frame. After the SPs are in the seabed, the remaining jacket frame is placed on top of the frame. This installation method describes a split jacket method installation.

Also included in the patent is the connection method described of the jacket frame to the SPs. This description is similar to the grout connection used for conventional pin pile jackets used for OWF. Multiple claims in the patent of Boskalis B.V. have been rejected, stating that these claims are too vague or not novel. A similar connection method and split jacket method have also been claimed by the patent of Charles W. Nelson [31].

These patents indicate that the installation of the SPs first for a SP foundation platform is known and at least two companies are developing a version of this installation method. The mentioned patents lack description of how their claims are technically feasible. Thus, these patents only indicate the idea of a SPIT installation method but not how the idea will be executed and satisfy design requirements. The patents form a basis of research for parts 1, 2 and 3 mentioned in section 2.3.

The background information presented in this Chapter highlights the potential for pre-installation of SPs using a SPIT. Since the SPIT installation method has only been proposed in patents, the installation method lacks research regarding details in all four parts. Therefore, any research regarding the SPIT installation method can be used to help fill the research gap.

3 Scope of research

The complete scope of research for the SPIT installation method introduced in section 2.3 requires too much research for a nine months master thesis. With the help of a case study and assumptions, the scope of research in parts 1, 2 and 3 are narrowed down such that the master thesis main focus is on the design of the SPIT. Part 4, the commercial feasibility, has been left outside the scope of this thesis.

The research goal is stated in section 3.1 and will be achieved by answering the research questions. Section 3.2 gives an overview of how the master thesis research is set up and explains the order of answering the research questions. In sections 3.3 and 3.4, the case study is explained and assumptions are made for parts of the design choices.

3.1 Research goal

The goal of the research is to visualise & justify a design of the SPIT through a technical review of the SPIT to identify key design challenges. In doing so, further understanding and important details are created for the SPIT installation method that can be used for future research.

3.1.1 Research questions

The main research question that results from the research goal is:

> **What are key design challenges of a suction pile installation template that is used as an installation tool for suction pile jackets for a representative OWF?**

To oversee the scope of the main research question, three sub-research questions are proposed and provide a benchmark to help answer the main research question. The sub research questions are based on the research gaps discovered in section 2.3, with the main focus on discovering key factors in the design of the SPIT. The three sub research questions are the following:

> **1: What will the installation strategy of suction pile jackets look like by implementing an installation template for pre-installation of the suction pile foundation for a representative OWF?**
>
> **2: How will the suction piles and jacket frame change with respect to conventional suction pile jackets by using an installation template for pre-installation of the suction pile foundation for a representative OWF?**
>
> **3: How will the design of an installation template for pre-installation of the suction pile foundation for jackets satisfy the design requirements to perform safe offshore operations at a representative OWF?**

3.2 Research setup

The three sub research questions proposed in section 3.1 provide the answer for the main research question. The research is split into three sections corresponding with the following three Chapters. Each Chapter answers one sub research question. Chapter 6 also answers the main research question

Chapter 4: In this Chapter the use of the SPIT is analysed by researching the transport and installation strategy for the SPIT method. Chapter 4 concludes on question 1 of the sub research questions. The conclusion of this Chapter provides the basis for the following sections. However, design choices have been made from feedback in Chapters 2 & 3 regarding practical matters.

Chapter 5: In this Chapter the suction pile-jacket connection is analysed and what changes need to be made with respect to a conventional SPJ. The design changes are based on the findings of Chapter 4. Chapter 5 concludes on question 2 of the sub research questions.

Chapter 6: In this Chapter the design of the SPIT is visualised and justified on the design requirements resulting from the previous two Chapters. A technical review is performed to check the leading load cases for the design and if the design requirements are satisfied. The Chapter provides the answer to question 3 of the sub research questions and the main research question.

3.3 Case study

The Crown Estate Scotland seabed leasing, or in short ScotWind, has auctioned OWF sites in 2021. DEME Concessions participated in the auctioning and have identified multiple fields for study purposes. An internal report has been written stating the general data of the OWF sites and the estimated dimensions of the OWT foundations [10]. The auctioned offshore sites are located in average water depths of $> 50m$. The E3 site showed great potential for suction pile jackets due to the soil type. The soil data predicts an 82% probability of bedrock at a seabed depth of $30 - 50m$. This is highly disadvantageous for driven pile foundations as expensive drilling equipment is necessary for the penetration of the piles through the bedrock. Suction piles would be able to provide sufficient strength at the top layer of the seabed where there is only a 2% probability of bedrock. The water depth range at the E3 site is divided into three ranges:

- Shallow: 55m
- Intermediate: 63m (SPJ exceeds lift height limit)
- Deep: 70m (SPJ exceeds lift height limit)

With preliminary calculations done by DEME in their internal report [10], the last two ranges indicate capacity problems for DEMEs largest crane vessel; the Orion [17]. Specifically, the height of the suction pile jacket is the limiting factor. DEME has started research on a split jacket concept for these ranges. The SPIT method also provides a solution for the installation of the SPJ at the last two ranges. Future research can analyse how both the SPIT and SPLIT method compare in this situation. In Table 1 & 2, the data gathered from ScotWind E3 [10] is shown.

Site designation	E3	-
Area	187	km^2
Turbine capacity	18	MW
Average water depth	63,1	m
Min water depth	53,3	m
Max water depth	91	m
Number of jacket legs	3	-
Bucket jacket footprint	50x50	m
Bucket diameter	12	m
Bucket height	15	m

Table 1: General data ScotWind

	Water depth (m)	Total weight (mt)	Total height (m)
Shallow-SBJ	53,3	2898	95,4
Intermediate SBJ	63,1	3133	105,4
Deep-SBJ	70	3313	112,1

Table 2: Preliminary dimensions estimated from the DEME database for the 3 water depth ranges at ScotWind E3

The SPIT method is applicable at the E3 site and the preliminary dimensions of the jacket structures are known. Previous internal reviews on the split jacket concepts provided by DEME can be used by DEME as comparison with the SPIT method. Also, metocean data from the NE2 neighbouring windfarm is available for offshore weather condition estimations. Many of the assumptions made in the next subsection are based on this case study. The data used in this case study is estimated from general OWF data gathered by DEME and is therefore selected as a representative OWF for this master thesis.

3.4 Assumptions

For the research to perform as a good benchmark for other projects where the SPIT method can be considered and narrow the scope of this thesis, assumptions are made that need to represent general conditions. Design assumptions have been made in four parts of the design process: Vessel type, SPJ dimensions, jacket-pile

connection type and site specifications. Below, the assumptions made in all four parts are explained and an overview of the assumptions are displayed in Table 3.

T & I vessel	Orion	-
Number of legs	3	-
Bucket diameter	12	m
Bucket height	15	m
Bucket weight	300	t
SBJ footprint	50x50	m
Jacket footprint	36	m
Jacket clusters	1	-
Jacket weight	2400	mt
Jacket height	97	m
Jacket-pile connection	Grout	-
Site location	East Scotland	-
Water depth	70	m
Number of installations	50	-
Travel distance	80	nmi

Table 3: Assumptions made for research

Vessel type: The vessel that is made available for the pre-installation of the SPs with the SPIT influences the use of the SPIT and the T & I strategy of the SPJ. The installation options are discussed in detail in Chapter 4. Since DEME is looking for installation opportunities for their own fleet, the vessel used for the SPIT method is required to be in DEMEs fleet. The height and weight capacity for the crane vessel to install the jacket part of the platform can only be done by two vessels in the fleet: The Green Jade [16] and the Orion [17]. Both vessels are monohulls and are equipped with dynamic positioning and water ballasting systems. The Green Jade is stationed in Taiwan for Asian related projects. The Orion, stationed in Belgium, is primarily available for European and American projects. ScotWind E3 is used as case study, the pre-installation of the suction piles will be assumed to be done by the Orion since the Orion is stationed close by and will also be required for the jacket installations. The Orion will be used as the main T & I vessel. Vessels necessary for smaller installation procedures will be mentioned otherwise.

SPJ dimensions: The preliminary calculations done by DEME for the ScotWind E3 windfarm provides a set of dimensions for the SPJ [10]. The preliminary calculations are based on extrapolated input taken from the internal database of DEME from previous projects. Since the dimensions follow the average trend of the DEME database, the SPJ dimensions can be assumed to represent a relevant OWF. The shallow SPJ range at E3 would not require pre-installation of the suction piles. The intermediate and deep SPJ range at the E3 site are clustered [42] that can structurally satisfy for one footprint. Therefore, only one jacket type and footprint for the pre-installation of suction piles is assumed for this thesis research. The dimensions for the SPJ are displayed in Table 3.

Jacket-pile connection type: As the piles are installed separate from the jacket, the jacket needs to be connected to the suction piles near the seabed. The jacket-pile connection needs to consider 2 main aspects:

- **Strength of connection:** Due to the size of the OWT and jacket platform, the environmental loads cause heavy fatiguing at the jacket-pile connection. Connection methods such as pins or hooks have very localised stress contact area [5] [26]. The heavy fatiguing for these connection methods is disadvantageous.
- **Tolerance margins of the jacket pile and suction pile stub:** The pre-installation of the suction piles with an external frame creates necessary tolerance margins of order of magnitude $100mm$ [9] [34]. Bolted connections [33], welding [43], swaging [40] [43] and slipjoints [7] do not allow tolerances of that magnitude.

Grout connections perform well on fatigue strength and tolerance margins [33] [38]. However, the installation process for grout connections is labour intensive and requires sufficient space for the grout lengths that negatively impacts the structural strength of the jacket frame [24] [33]. Chapter 5 explains this in more detail. DEME has used grout connections for monopile & pin pile jacket installations. The cost and resources necessary for this connection type are known within the organization and therefore, it is most probable that grouted connections would be used for the SPIT method in future projects. Since no alternative connection method exist that satisfies

the criteria of strength and tolerances next to grout, and the experience DEME has with grout connections, this type of connection method for the jacket-pile connection is assumed for the master thesis.

Site specifications: The case study provides a site location where metocean data, available ports and OWF size are known. The location specifications are relevant for multiple OWFs found in the North Sea and therefore serves as a solid benchmark. In Appendix I, the metocean data is provided and the overview of the travel distance from available ports to the E3 site. The assumed data for the site specifications are displayed in Table 3.

4 Transport & installation strategy

This Chapter identifies and visualises the T & I strategy of the SPs and the SPIT. The installation of jacket platforms with grouted connections have already been extensively researched and put into practice by DEME. Therefore this part of the installation requires no further research at this stage. In this Chapter the T & I is assessed in two parts:

- On-site installation strategy, explained in section 4.1.
- Offshore transport from port to site, explained in section 4.2.

The first sub-research question is answered in section 4.3. The general use of the SPIT results from the findings of this Chapter and is translated to design requirements for the SPIT stated in section 6.1.

4.1 On-site

This section focuses on the installation strategy of the suction piles and when the 3 sub-actions: pump removal, top-plate grouting and scour protection, explained in section 2.1.2, will take place. Many design options are considered to install the SPs in the seabed with the SPIT. There are three main factors that the design options are rated on:

- Required crane capacity for the lift operations
- Required deck-space of the heavy lift vessel (HLV)
- Installation speed of the SPs

In section 3.4 the assumption is made that the Orion will be used as the installation vessel. Compared to other installation vessels in the DEME fleet, the crane capacity and available deck-space is largest for the Orion. If the required crane capacity and deck-space is sufficient for the Orion, the design choices are optimised for the installation speed of the SPs.

4.1.1 Installation options

Design options are considered for the following functions of the SPIT during the installation of the SPs:

- General SPIT use
- SPIT-crane connection strategy
- SPIT-SP connection strategy
- Individual pile lowering at the seabed
- Pump installation
- Top-plate grouting

All design options for the functions are explained in the following paragraphs. In section 4.1.2, the most suited design option for this case study is explained and the installation sequence of the SPs with the SPIT is visualised.

4.1.1.1 General SPIT use This paragraph describes design options on how the SPs are lowered and placed on the seabed with the help of the SPIT. Figure 11 shows a schematic depiction of the design options.

- **Option 1:** The SPIT and SPs are connected to each other on deck and are lifted as one object to the seabed. The SPIT is first used as a lifting tool and after the SPs are lifted to the seabed, it functions as a tool to correctly place and adjust the SPs on the seabed. The installation vessel only requires one lift to lower the three SPs to the seabed and therefore reduces installation time. However, the required lift capacity for the SPIT and the SPs should not exceed the lift capacity of the installation vessel. Also, the deck-space required for the SPIT is equal to the footprint of the SPJ and should not exceed the available deck-space of the installation vessel.

- **Option 2:** The SPIT and the SPs are each individually lowered to the seabed. The SPIT is first lowered and functions as a guide frame for the SPs. The SPs are lowered one-by-one through the SPIT frame to the seabed. This option requires a low lifting capacity of the installation vessel since the SPIT and SPs are lifted separate. However, the installation vessel does require multiple lifts, therefore increasing the installation time. Because the SPs are lifted through the SPIT, the footprint of the SPIT is larger than the footprint of the SPJ and this should not exceed the available deck-space of the installation vessel.
- **Option 3:** The SPIT and the SPs are each individually lowered to the seabed. The SPIT is first lowered and functions as a guide frame for the SPs. However, different from option 2, the frame can rotate to a specific location where it can guide a SP into the seabed. When one SP is successfully installed in the seabed, the frame rotates to the next location for the second SPs. This process is repeated for the last SP. By rotating the SPIT on the seabed, the required footprint of the SPIT is reduced by one-third of the footprint of option 2. The required lift capacity for the installation vessel is low since the SPIT and SPs are lifted separate. The SPIT does require a complex frame to be able to rotate on the seabed

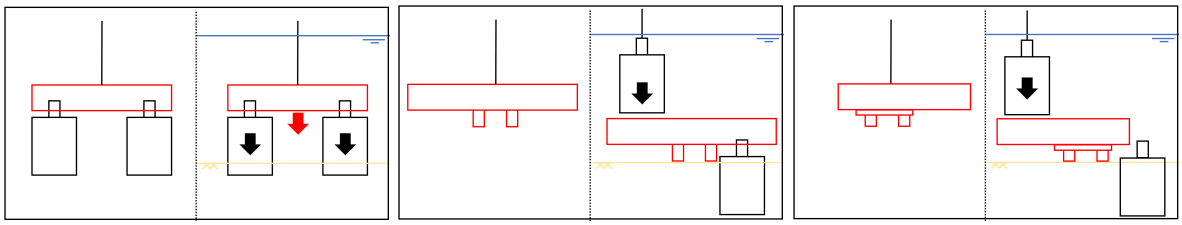

(a) Option 1 **(b)** Option 2 **(c)** Option 3

Figure 11: General use of the SPIT visualised for the 3 options. In each Figure depicted on the left Figure is the template on deck and on the right depicted the template at the seabed. The SPIT is depicted in red and the SPs are depicted in black

4.1.1.2 SPIT-crane connection strategy This paragraph describes design options on when and how the crane will be connected and disconnected from the SPIT. Figure 12 shows a schematic depiction of the design options.

- **Option 1:** The SPIT is connected to the crane from a single point on the SPIT. The rigging of the crane to the SPIT is equipped with a tool that can be disconnected and reconnected with the SPIT at the seabed when the SPIT needs to be retrieved. Reconnecting the SPIT to the crane requires ROV support [26]. On the other hand, lifting the SPIT from a single point can cause large bending moments in the SPIT during lift.
- **Option 2:** The SPIT is connected to the crane with slings at the corners of the SPIT. When the SPIT is at the seabed, the slings reach above the waterline. This allows for the SPIT to be disconnected from the crane above the water and the slings are temporarily connected to the hull of the vessel. The slings are in slack when connected to the hull to avoid loads on the SPIT by the movement of the vessel. Reconnecting the crane to the slings can be done on deck. This option only works in finite water depths depending on the crane height. The effect of the slings attached to the vessel requires analysis of the stability of the vessel.
- **Option 3:** The SPIT is connected to the crane with slings at the corners of the SPIT. The SPIT is not disconnected from the crane underwater. Additional crane operations that are required for the installation strategy of the SPs need to be performed after the SPIT is retrieved to the deck of the vessel.
- **Option 4:** The SPIT is connected to the crane with slings at the corners of the SPIT. The SPIT is disconnected from the crane at the bridle that connects the slings and is placed on the seabed floor. With ROV support the crane can be reconnected to the bridle on the seabed when the SPIT needs to be retrieved.

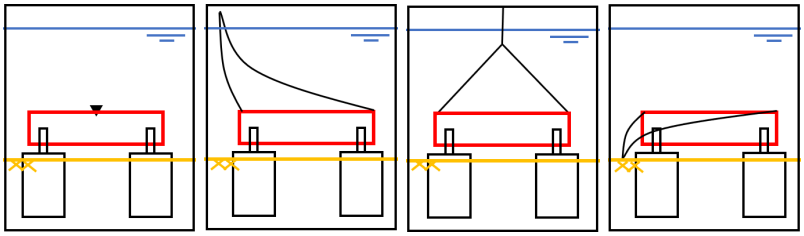

(a) Option 1 **(b)** Option 2 **(c)** Option 3 **(d)** Option 4

Figure 12: SPIT-crane connection strategy options

4.1.1.3 SPIT-pile connection strategy This paragraph describes design options on how the SPs are connected to the SPIT on deck, if the SPs and the SPIT are lowered to the seabed together. Figure 13 shows a schematic depiction of the design options.

- **Option 1:** The SPIT is placed on top of three SPs on deck. In order for the SPIT to connect to the SPs, the SPs must be carefully positioned at the deck of the vessel before the SPIT is placed on top of the SPs. The positioning of the SPs is performed at a designated preparation area at the deck of the vessel. After each installation three new SPs should be prepared for the next installation.
- **Option 2:** The SPIT is placed on deck of the vessel and the SPs are individually inserted into the SPIT. The SPIT is placed on a preparation frame that elevates the SPIT from the deck in order for the SPs to be leveled at height where the SPIT will connect to the SPs.

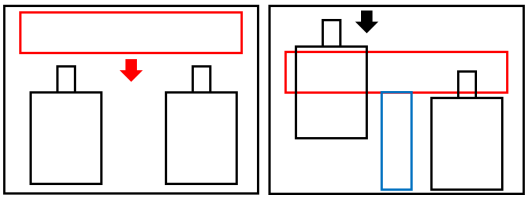

(a) Option 1 **(b)** Option 2

Figure 13: SPIT-pile connection methods on deck

4.1.1.4 Individual pile lowering at seabed As mentioned in section 2.1, top-plate grouting can be made obsolete by individually lowering the SPs. Removing top-plate grouting from the installation strategy removes the cost of top-plate grouting, but increases the complexity of the SPIT to allow for individual lowering of the SPs.

4.1.1.5 Pump installation

- **Option 1:** The conventional pump attachment and removal method is applied as explained in section 2.1.1.2. This requires individual lift operations to attach and remove the pumps from the SPs.
- **Option 2:** The pumps for the SPs are integrated into the SPIT, reducing the lift operations necessary for pump attachment and removal with respect to option 1. Integrating the pumps into the SPIT will increase the complexity of the SPIT.
- **Option 3:** The pumps are individually attached to the SPs on deck. However, the pumps are removed by a secondary vessel. This option optimises on the main installation vessels time. The main installation vessel can remove the template when the SPs are sufficiently lowered and move to the next location. Time is saved because the main installation vessel does not have to remove the SPs. The pumps are removed and transported back to the main installation vessel by the secondary vessel. As a benefit, the pumps can be reused for a next installation sequence.

4.1.1.6 Top-plate grouting

- **Option 1:** The conventional top-plate grouting method is applied as explained in section 2.1.1.3
- **Option 2:** The top-plate grouting systems are integrated into the SPIT. The integrated systems will increase the speed of the top-plate grouting procedure. As a disadvantage the SPIT is increased in complexity.

4.1.2 Concept strategy

Out of the design options, the best option is selected for this case study. In this section the final design choices are explained and the installation sequence is visualised.

4.1.2.1 Design choices

- **General SPIT use:** The estimated weight of the SPIT is 300mt and the estimated weight of a SP is 300mt. The required static hook load (SHL) of the SPIT with the SPs attached is $300 \cdot 4 = 1200mt$. The dynamic response of the SPIT during lift will amplify the SHL but is estimated not to exceed the lift capacity of the Orion. Also, the available deck-space of the Orion is sufficient for the footprint of the SPJ (see section 4.2). Therefore, using the SPIT as a lifting frame to lift the three SPs to the seabed in one lift (option 1) results in the fastest installation of the SPs with respect to the other options. Option 1 is selected for the general SPIT use.
- **SPIT-crane connection strategy:** The suction process of the SPs requires on average three to four hours [39], during this time the crane can be used for other operations if the crane can be disconnected from the SPIT. When dangerous weather conditions appear, the SPIT should be able to be disconnected from the crane and temporarily abandoned. When calmer weather conditions return, the SPIT should be able to be reconnected to the crane. Therefore, option 3 is not an option for the SPIT-crane connection.

  Option 1 has become an unattractive solution due to the added weight of the SPs to the SPIT. Large bending moments are created by the SPs in the frame of the SPIT due to the single lift point. These bending moments are reduced when the SPIT is lifted at the corners of the SPIT. Option 2 suggests a quick solution of disconnecting and reconnecting the SPIT to the crane but is not seen in practice. Further research for this option could prove that this is a viable solution but until proof of concept exists the option is not selected. Option 4 remains and is selected for the SPIT-crane connection strategy.
- **SPIT-SP connection strategy:**For this design choice, the available deck-space is an important factor. Option 1 requires a preparation area in order to prepare the SPs before the SPIT is placed on top of the SPs. The SPIT needs to be stored somewhere during the preparation of the SPs. If the SPIT is stored on deck, few deck area is left to transport additional SPs for next installation sequences. Option 2 however combines the SPIT storage and the SP preparation area. With the selected SPIT-crane connection strategy, the crane can be used to prepare the SPs for the next site while the SPs and the SPIT are at the seabed. When the SPIT is retrieved to deck, the SPIT can be placed directly on top of the SPs and the new installation sequence can begin. If option 2 is considered, crane operations during the suction process are not necessary but the SPs can only be prepared after the SPIT is retrieved to deck. Therefore option 1 offers a faster installation sequence than option 2. Option 1 is selected for the SPIT-SP connection strategy.
- **Individual pile lowering at seabed:** The option to individually lower the SPs at the seabed is selected since the added complexity of the SPIT is estimated to reduce the total installation cost by removing the top-plate grout procedure.
- **Pump system:** With the previous selected design choices, the pumps can be integrated into the frame of the SPIT and easily connect and disconnect from the SPs simultaneously when the SPIT is connected and disconnected from the SPs. Option 1 is selected for the pump installation.
- **Top-plate grouting:** Top-plate grouting has become obsolete since the piles can be individually lowered. No option is selected for top-plate grouting.

4.1.2.2 Installation sequence With the selected design choices, the installation sequence of the SPs with the SPIT is formulated and visualised. Figure 14 shows the schematic depiction of the installation sequence.

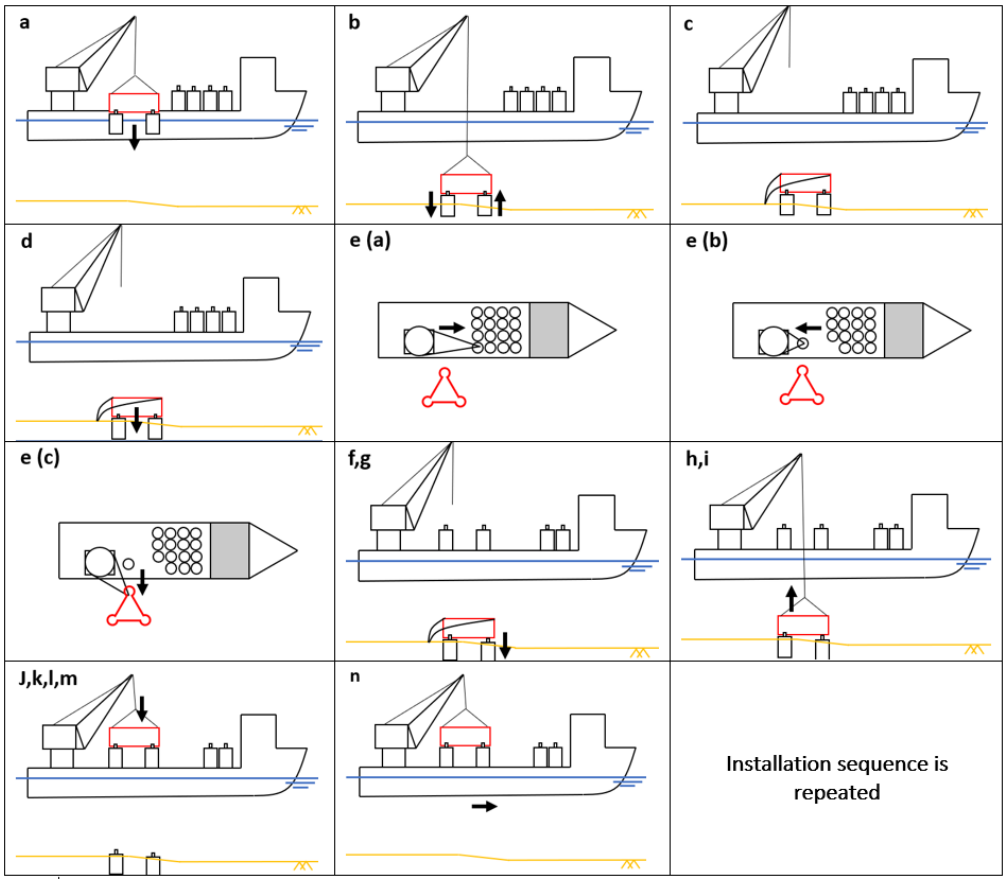

Figure 14: Schematic overview of the installation sequence on-site

a. Lift SPIT and SPs from deck to seabed.

b. Start the suction process, adjust verticality by regulating the under-pressure for each SP.

c. Detach the crane cable from the SPIT.

d. Lower the SPs into the seabed.

e. While the SPs are lowered into the seabed, the crane can start to prepare the SPs on deck for the next location. The next sequence is repeated 3 times:

   (a) Attach crane cable to SP

   (b) Position SP on deck for next location

   (c) Detach crane cable from SP

f. Detach the SPs from the SPIT.

g. Individually lower SPs if PTG is not yet reached.

h. Detach the pump from the SPs.

i. Reattach the crane cable to the SPIT.

j. Retrieve the SPIT to deck.

k. Lower the SPIT over the SPs prepared on deck.

l. Attach the SPs to the SPIT.

m. Attach the pumps to the SP.

n. Sail to next location.

Before the jacket frame is placed on the stubs of the SPs, subsea rock installation is performed for scour protection around the SPs on the seabed. The accessibility for subsea rock installation is improved by the absence of the jacket frame.

4.2 Offshore transport

The offshore transportation focuses on the transport between port and OWF site. In the assumptions made in 3.4, the travel distance from port to site is $80nmi$. The maximum transit speed for heavy lift installation vessels is $14kn$ [8]. The transit time for the Orion to make the trip from port to site and back takes a minimum of $80 \cdot 2/14 = 11.4$ hours. Valuable time can be saved by reducing the amount of trips necessary for the installation of the OWT foundations.

In Figure 15, the deck layout of the Orion is shown. The bridge and living quarters are located at the bow of the vessel. The Orion is equipped with one main crane located in the middle of the vessel and a secondary crane located at the stern of the vessel. A free deck area of $8000m^2$ and a maximum deck payload of $30000mt$ [17] is available.

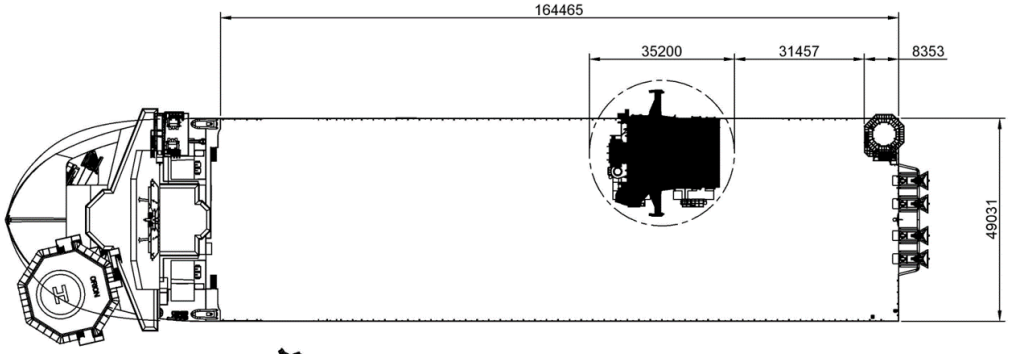

Figure 15: Deck layout of the Orion. Dimensions are given in mm.

4.2.1 Offshore transport options

The design options that are considered for the offshore transport of the SPIT and SPs are based on the efficiency of the deck-space and the stability of the vessel and the crane.

4.2.1.1 SPIT preparation location For the installation sequence explained in 4.1, part of the deck is necessary to place the SPIT and prepare the SPs for the next location. The preparation area can be located in 3 places: front, middle and aft of the deck. The sub-Figures in Figure 16 sketch the different layout options. The blue contour indicates the estimated size of the SPIT with SPs.

- **Option 1:** The preparation location for the SPIT is at the front of the vessel. Figure 16a shows the orientation of the SPIT at the location.
- **Option 2:** The preparation location for the SPIT is in the middle of the vessel. Figure 16b shows the orientation of the SPIT at the location.
- **Option 3:** The preparation location for the SPIT is in the back of the vessel. Figure 16c shows the orientation of the SPIT at the location.

4.2.1.2 SP stacking The free deck area around the SPIT is used to transport the SPs. The thin shell structure of the SPs does not have enough strength to support its own weight when the SP is placed horizontally. Therefore, the SPs are required to be transported vertically. The sketch layout for the SPs is shown in Figure 17. The 39 SPs placed on deck translate to 13 foundation installations that the Orion can perform in one trip.

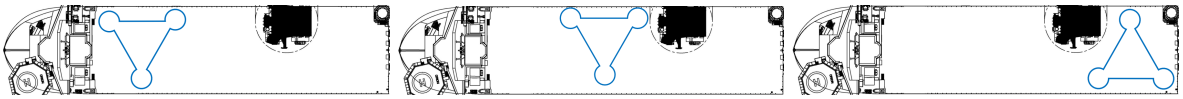

(a) Option 1: Front preparation location for the SPIT

(b) Option 2: Middle preparation location for the SPIT

(c) Option 3: Back preparation location for the SPIT

Figure 16: Different SPIT layout options. The blue contour indicates the estimated size of the SPIT with SPs.

Sufficient space for safe walkways, rigging and other equipment on deck must be taken into consideration and might reduce the total number of SPs on deck.

For the case study, 50 foundations, resulting in 150 SPs, have to be installed. With the layout proposed in Figure 17, four trips are required. The number of trips will be reduced if SPs are stacked on top of each other. The upper limit of SPs that can be transported by the Orion based on the maximum deck pay load of $30000mt$ is 100 SPs for a $300mt$ SP. Two trips are still required for the installation of all SPs. However, the practical maximum number of SPs that can be transported by the Orion is significantly lower. Other equipment and the SPIT also have to be taken into account and should be subtracted from the $30000mt$. Also, the shift in COG of the Orion due to the deck loading can create stability problems. A stability check is necessary to determine the actual maximum payload of the deck and the number of SPs that can be transported.

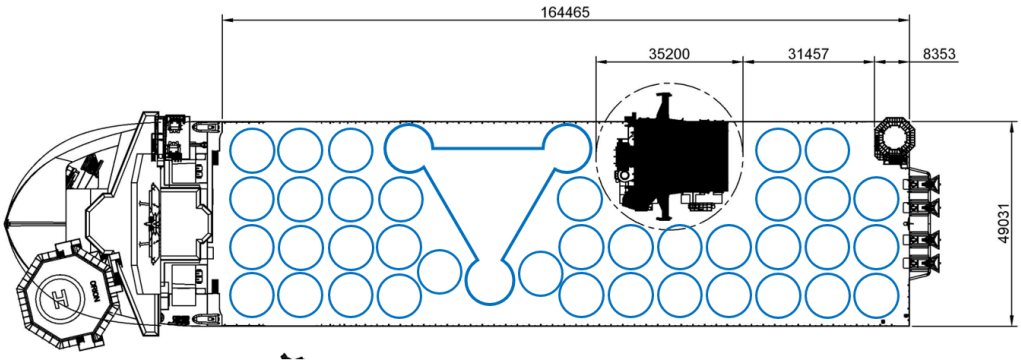

Figure 17: Deck layout with SPs vertically placed on deck. The SP diameter is $12m$. The current layout has 39 piles on deck, including the SPs already attached to the SPIT. 13 foundation installations are possible per trip.

4.2.2 Concept strategy

From the design options, the best option for this case study is selected. In this section the final design choices are explained.

- **SPIT preparation location:** The required crane capacity of the installation vessel is smallest for options 2 & 3 since the reach necessary of the crane for lifting the SPIT and SP are small compared to option 1. As the crane tip approaches the center of rotation for the vessel's roll, pitch and yaw motion, the influence of these motions on the crane tip's movement decreases. Consequently, the crane tip experiences its least motion when positioned in the middle of the vessel. This positioning yields the most favorable dynamic responses during lifting operations. Also, for option 3, the secondary crane at the aft of the vessel blocks a direct path for the SPIT to be lifted to the seabed. The SPIT should be lifted around or above the secondary vessel. Therefore option 2 is selected for the SPIT preparation location.
- **SP stacking:** Stacking the SPs does not impact the installation strategy of the SPs with the SPIT. However, it is an option to consider when the installation efficiency should be optimized. Additional research that is required for this transport method for sea-fastening of the SPs and vessel stability is outside the scope of this thesis. Without stacking, the deck-space would have sufficient space for a maximum of 39 SPs in order to perform 13 installations in one trip. This is considered as the base case for the SPIT installation strategy.

A secondary vessel can be introduced for the installation strategy to transport additional SPs to site. The main installation vessel would be required to only make one single trip to site and can be restocked by the secondary vessel. If the reduced transport cost and time for the Orion is compensated by the added cost of the secondary vessel, depends on the secondary vessel's transport capacity & cost and environmental conditions. Lifting objects from one vessel to another vessel requires calm weather conditions. The workability of the operations on-site would decrease depending also on the location and time period of the installation. This analysis is outside the scope of this thesis. Also, adding a secondary vessel requires little modification to the installation sequence of the SPs and the use of the SPIT.

4.3 Answer to sub-research question 1

From sections 4.1 and 4.2 the T & I strategy of the SPs with the SPIT is visualised. The answer to the first sub-research question results from the findings.

> **What will the installation strategy of suction pile jackets look like by implementing an installation template for pre-installation of the suction pile foundation for a representative OWF?**

Answer: The installation strategy will look like as described in section 4.1.2.2 with the corresponding deck-layout sketch in Figure 17. The design choices were made based on optimising the installation speed. The two key design choices of this strategy are:

- The general use of the SPIT: The SPIT will be used as a lifting tool to lift three SPs together to the seabed. This requires sufficient lift capacity and deck-space since an area is required to connect the SPs to the SPIT on deck.
- The SPIT-crane attachment strategy: The SPIT is connected to the crane with slings attached to each corner of the SPIT. This connection creates an effective load path when the SPIT and SPs are lifted. It is crucial to disconnect and reconnect the slings to the crane when the SPIT is submerged. This is to save on deck-space and increase the installation speed during the installation sequence.

The limitations in crane capacity and deck-space of the installation strategy should be considered if the assumptions made in Chapter 3 are not applicable for a different OWF site. Limits of the installation vessel can be exceeded when:

- The footprint of the SPJ is increased.
- The weight and diameter of the SPs are increased.
- The Orion is unavailable and a smaller installation vessel is appointed to the project.

If these limits are exceeded, the installation strategy needs to be re-evaluated and might have a drastic impact on the T & I strategy and the design of the SPIT.

5 Suction pile - jacket connection

In this Chapter the grout connection of the SP and jacket is worked out in detail. The dimensions of the grout connection translates to the required installation tolerance of the SPs on the seabed. This is an important design requirement for the SPIT. In section 5.1, the grouted connection configuration is explained. Then, the design requirements for the SP are stated in section 5.2. An analysis is performed to optimize the required installation tolerance of the SPs and to estimate the dimensions of the grouted connection in section 5.3. The tolerance margin for the grouted connection is analysed in section 5.4. The concept design of the SP with the SP stub is explained in section 5.5. The results of the chapter are concluded in section 5.6 by answering the second sub-research question.

5.1 Connection configuration

For a grouted connection, a pin is inserted into a sleeve and the gap between the pin and the sleeve is filled with grout. Two grouted connection configurations are considered. A schematic side view of the two configurations are displayed in Figure 18.

- Configuration 1 is similar to the standard practise configuration for a grouted connection of a pin pile jacket. The suction pile jacket frame is changed at the bottom end of the jacket legs. A vertical pin is now at each leg of the frame. On top of the top-plate of the SP a stub is attached. The stub provides the sleeve for the jacket pin to be inserted in.
- Configuration 2 switches the functions of the leg of the jacket and the stub of the SP. The stub on the SP is the pin and the jacket leg is the sleeve.

(a) Configuration 1 **(b)** Configuration 2

Figure 18: Grouted connection configurations. Highlighted in red is the jacket frame and in black the SP with a stub on top.

For an efficient jacket structure, the lowest bracing should be as close to the seabed as possible to reduce the bending moments at the bottom end of the jacket. For the first configuration, the lowest bracing is attached to the jacket leg above the stub of the SP. Configuration 2 provides a solution to start the lowest bracing at the tip of the jacket frame. The structural effectiveness depends on the height difference that can be achieved for the lowest bracing and is directly related to the height of the stub.

However, the grout in the connection is preferred to be loaded in shear. The second configuration applies horizontal loads directly on the connection reducing the strength and fatigue life of the grout. To quantify the effects of the bracing height of the jacket frame and the horizontal loads on the grout, requires research that is outside the scope of this thesis. Configuration 1 is selected for the design of the grouted connection. The estimated loss of structural efficiency for the jacket frame is accepted at this stage for the design of the SPIT. Also, DNVGL-ST-0126 [6] can be used to dimension the connection for configuration 1.

5.2 Design requirements

The design requirements are based on the dimensions of the SP from the design report for ScotWind [10] and the lift operations that are required for the SPs for the installation sequence stated in section 4.1.2.2.

- The outer diameter of the shell of the SP is 12m and the height is 15m.

- The top-plate of the SP is stiffened by beams to support the loads transferred from the jacket to the shell of the SP.
- A stub connected to the top-plate is used to connect the SP to the jacket pin.
- The grout connection between the SP stub and jacket pin has sufficient strength for 30 a year operation lifetime of an $18MW$ turbine at ScotWind.
- The stub has an out of center offset of 2m with respect to the suction pile skirt.
- A single padeye, located on the symmetry plane of the SP, is used to restrain the SP in heave direction.
- The stub of the SP is used to restrain the SP in surge, sway, pitch and roll direction.
- The stub and top-plate stiffener on the symmetry plane of the SP are used to restrain the SP in yaw direction.
- The SP can be lifted with a crane.
- The SP can be precisely positioned on deck at the preparation site.

5.3 Grout connection dimensions

In Figures 19a and 19b, a schematic Figure shows the jacket pin inside the pile stub for the selected grouted connection configuration. The strength of the connection is enhanced by welded shear keys on the inside of the stub and on the outside of the jacket leg. A stabbing cone on the end of the jacket pin allows for the crane operator to handle the jacket placement easier. The upper centralizer is used to create a minimum grout thickness. A lower centralizer is sometimes also used for the same purpose. The grout is pumped through a tube inside the jacket leg and exits at the stabbing cone. The pile stopper is used during the cure process of the grout in order to restrain the jacket pin from any movement. The pile stopper is removed after the grout cure process to create only steel on grout contact. This is crucial for the fatigue life of the grout connection.

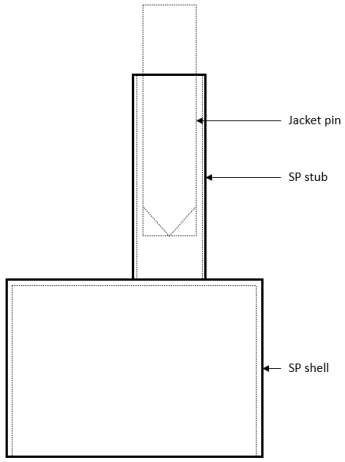

(a) Schematic side-view of the stub on the SP

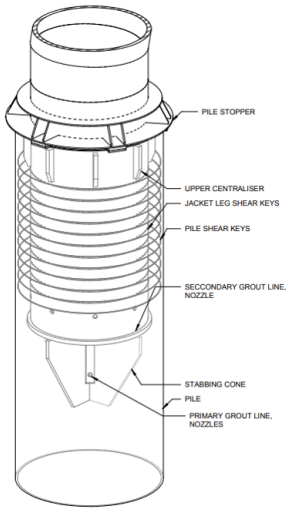

(b) Pile-jacket connection

The strength of the grout connection in this Chapter is analysed for two variables: the diameter and length of the stub. For the design of the SP for use of the SPIT installation method, two design options are considered:

- Option 1: Large stub diameter, small stub length
- Option 2: Small stub diameter, large stub length

Both options will result in the same strength of the grouted connection but differ in the following practical aspects:

- **Bracing height:** For structural efficiency of the jacket, the lowest bracing should begin as close to the seabed as possible. Option 1 is preferred in this aspect.

- **Weight:** The grouted connection for option 2 is more weight efficient. This claim results from the performed analysis in Appendix A.
- **Tolerance margins:** The grout thickness is the space between the SP stub and the jacket pin. If the grout thickness is increased, the tolerance margins of the SP installations are also increased. From the calculations performed in Appendix A can be concluded that the maximum grout thickness equals 10% of the stub diameter. A bigger stub diameter therefore, results in an increased tolerance margin.

  In addition, the induced verticality of the SP in the seabed during installation is translated to a larger deflection of the stub when the stub length is increased. This negatively impacts the required SPIT installation tolerance. Therefore, for the tolerance margins of the grouted connection, option 1 is preferred.
- **Load transfer to SPIT:** The SPIT will use the SP stub to constrain the SP during the installation sequence. The loads on the SPs are transferred through the stub to the SPIT. A larger stub length will reduce the loads transferred from the SPs to the SPIT. Option 2 is preferred for this aspect.

The expected installation tolerances of the SPs with the SPIT are still unknown. A stub size that optimizes on the tolerance margins is preferred to make the installation tolerance of the SPIT less critical. Therefore, the SP stub is modeled after option 1. The reduced bracing height of the jacket frame is an added bonus. Since the weight of the stub only contributes to a small part of the total weight of the SP, the added weight for option 1 with respect to option 2 is manageable. The analyses in section 6 will indicate what the transferred loads of the SPs to the SPIT will be. The transferred loads of the SPs to the SPIT are higher for option 1 than for option 2. However, the structural strength of the SPIT can be adjusted accordingly and from the analyses performed in section 6 is proven to be structurally feasible.

In Appendix A, the grout connection analysis is performed according to DNVGL-ST-0126 [6]. The relevant loads used in the analysis are based on previous internal project reports by DEME [9] [34]. The stub dimensions for safe operation during the entire lifetime of the foundation results from Appendix A and is displayed in Table 4.

Stub outer diameter	4100	mm
Stub thickness	30	mm
Stub minimal total length	6400	mm
Stub maximum total length	7900	mm

Table 4: Dimensions of the stub resulting from the calculations in Appendix A.

5.4 Tolerance margin for the grouted connection

During the installation of the jacket frame on the SPs and the grout cure period, the jacket pin and the SP stub should avoid clashing. The distance between the jacket pin and the SP stub result in the tolerance margins for the installation of the SPs and the jacket frame. Three clash cases are considered for the tolerance margin calculations. Figure 20 indicates the point of contact for each clash case.

- Upper centralizer clash with the tip of the SP stub
- Lower centralizer clash with the lowest shear key in the stub (1)
- Lower centralizer clash with the tip of the SP stub (2)

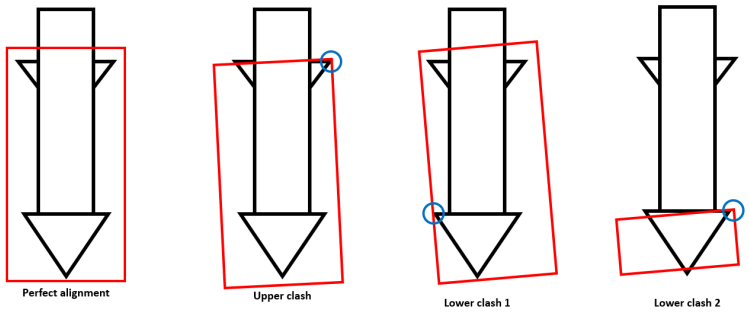

Figure 20: Potential clash cases for the grouted connection

The allowable tolerance margin is the distance the SP stub and the pin are allowed to deflect. The required tolerance margin is the distance the SP stub and the pin can be expected to deflect to. The allowable tolerance margin is the maximum distance from the centralizers to the stub. Table 5 displays the parameters used for the grout tolerance. The allowable tolerance margin is displayed in Table 6.

Stub inner diameter	4040	mm
Jacket pin outer diameter	3240	mm
Jacket stab in length	6100	mm
Grout thickness	400	mm
Width upper centralizer	150	mm
Width lower centralizer	140	mm
Shear key height	18	mm
Gap upper centralizer-stub	250	mm
Gap lower centralizer-shear key	242	mm

Table 5: Important dimensions of the grout connection

The required tolerance margin for the grouted connection results from two categories:

- Installation tolerances
  - SP height difference
  - Horizontal misalignment SP
  - Rotational misalignment SP
- Fabrication tolerances
  - Fabrication of the SP stub
  - Fabrication of the JP

In Appendix H, the fabrication tolerances of the SP stub and jacket pin have been calculated. The remaining tolerance margin indicates the maximum allowable installation tolerances. Table 6 shows the results. The installation tolerance depends on the design of the SPIT. Therefore, an important design requirement for the SPIT is to not exceed the remaining tolerances indicated in Table 6.

	Upper clash	Lower clash 1	Lower clash 2
Maximum tolerance margin	242mm	232mm	250mm
Fabrication tolerance SP and jacket pin	92mm	92mm	113mm
Remaining tolerance margin	150mm	140mm	137mm

Table 6: Results from the tolerance calculations in Appendix H.

5.5 Concept design

The concept design of the SP is displayed in Figure 21. The 3D model of the SP is created in SolidWorks. The added weight of the stub results in an estimated total weight of the SP of $340mt$. The minimum and maximum total height of the SP equals $21.4m$ and $22.9m$ respectively.

During the installation of the SPs, the SPs are constrained in motion by the SPIT to install the SPs with the required installation tolerance. The design choices on how the SP is constrained by the SPIT are explained in section 6.2. The heave motion is constrained by the main padeye on the SP. The main girder and SP stub are used to constrain the five other DOF of the SPIT.

The top-plate of the SP is stiffened to distribute the load from the stub to the shell of the SP. The three secondary padeyes on the top-plate are used to move the SP onshore and on deck.

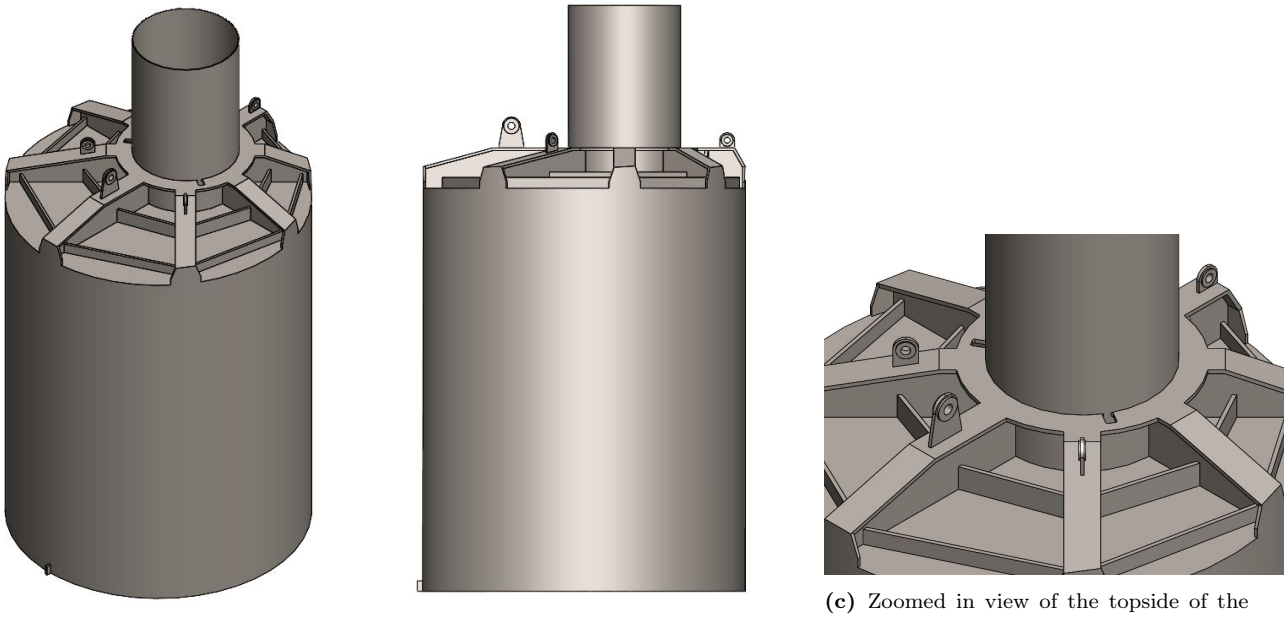

(a) Isometric view

(b) Side view

(c) Zoomed in view of the topside of the SP

Figure 21: Concept design of the SP

During the installation sequence explained in section 4.1.2.2, the SPs are positioned on deck in order for the SPIT to be placed on top of the SPs. The positioning of the SPs at the preparation site on deck is depicted in Figure 22. The CTC distance of the SP stubs should correspond with the assumed jacket footprint in section 3.4. The total footprint of the SP foundation is approximately $50m$. The orientation of the SPs should make sure that the main girder is in line with the centre of the virtual triangle. The two plates on the bottom of the SP are used to position the SP with the required spacing and rotation on deck. The preparation area on deck will require a guide frame where the two plates on the SP can slot into.

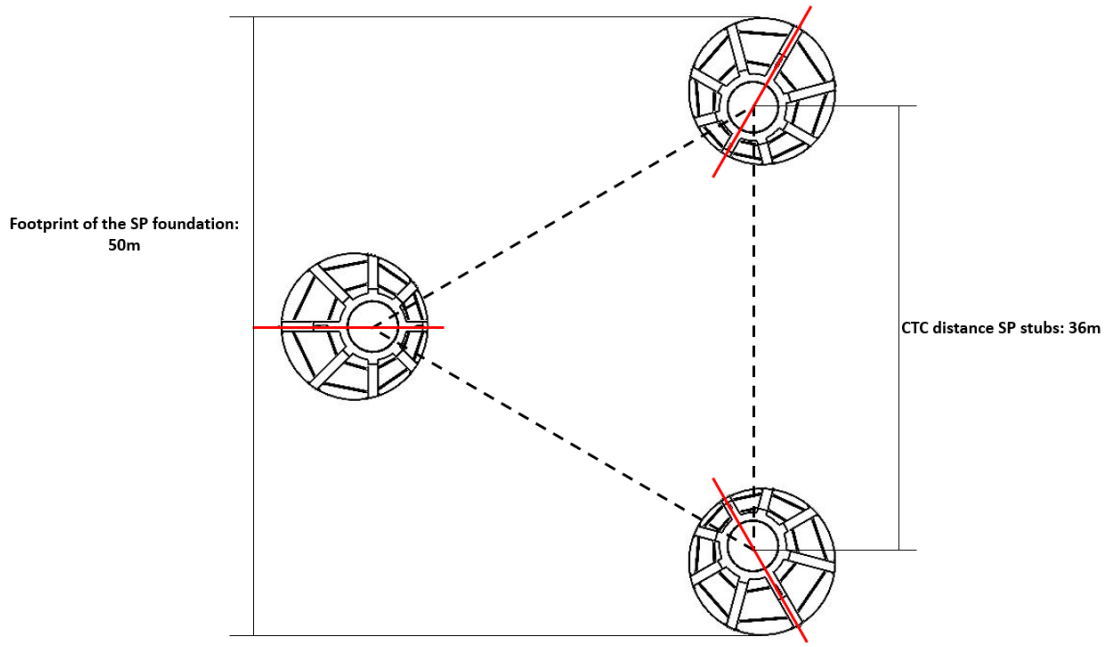

Figure 22: Top view of the spacing of the SPs on deck

5.6 Answer to sub-research question 2

In this Chapter, the dimensions of the SP-jacket connection are calculated and the design of the SP is visualised. The answer to the second sub-research question results from the findings.

> **2: How will the suction piles and jacket frame change with respect to conventional suction pile jackets by using an installation template for pre-installation of the suction pile foundation for a representative OWF?**

Answer: The conventional welded connection of the SPs and the jacket frame is changed to a grouted connection. The bottom end of the jacket frame legs are changed to vertical pins. The jacket frame is similar to a pin pile jacket. The SPs are modified by adding a vertical stub on the top-plate. The stubs act as a sleeve for the pins of the jacket legs. This connection method introduces the required installation tolerance of the SPs to avoid clashes between the SP stub and the jacket pin. For the design of the SP stub, the installation tolerance is optimised. Two important factors should be considered for the size of the stub:

- The size of the stub relative to the size of the jacket leg pin determines the maximum installation tolerance of the SPs in the seabed. This is used as an important design requirement for the SPIT.
- The stub of the SP can be used by the SPIT to constrain the SP. The size of the stub is used as an important input for the loads that are transferred to the SP and the SPIT.

If the SPIT cannot satisfy the maximum installation tolerance design requirement, the connection method should be re-evaluated. This could result in a completely different approach for the installation of the SPs with the SPIT.

6 Design of the SPIT

Chapter 4 proposes the general use and features of the SPIT required for the installation sequence. Chapter 5 provides the dimensions of the stub that should be constrained by the SPIT and the required installation tolerance of the SPs. These aspects are translated to design requirements of the SPIT and are stated in section 6.1. In section 6.2, the design choices made for the SPIT are explained in order to satisfy the design requirements. The result is visualised in a 3D model and is explained in section 6.3. In section 6.4, design requirements regarding the size of the SPIT and its features are justified based on the estimated SPIT design loads. At the end of the Chapter in section 6.5, the results are used to answer sub-research question 3 and the main research question.

6.1 SPIT design requirements

- The SPIT places three SPs spaced with a CTC distance of the SP stubs of $36m$. This design requirement is based on the assumptions made in section 3.4, taken from the preliminary design report of the foundations at the ScotWind E3 site [10].
- The SPIT is attached to the SPs on deck and in a single lift, the SPIT and SPs are lifted to the seabed. This design requirement results from the proposed installation sequence in section 4.1.2.2.
- Installation tolerance of the SPs with the SPIT does not exceed the allowable tolerance margins stated in Table 6.
- The installation height of the SPs can be individually lowered with a maximum height difference between top-plates of $1.5m$. The design requirement is based on the maximum seabed slope considered at the OWF location [10].
- The yaw movement of the SP is constrained by the SPIT during installation and has an installation tolerance of 1%. This design requirement is based on the stability margin taken for the design of a SPJ [39].
- The SPIT can operate in a water depth of $70m$, representing the maximum installation depth at the ScotWind E3 site.
- The maximum design wave height during operations is 3m and is based on the offshore workability of pre-piling templates [8].
- The structural strength of the SPIT is designed to withstand all the loads during the installation sequence of the SPIT mentioned in section 4.1.2.2.
- During operation of the SPIT, the safety of the crew and other assets should be considered.
- The SPIT is able to be retrieved/abandoned from seabed at all times to protect the assets of DEME when offshore conditions change unexpectedly.
- The SPs can always be released from the SPIT during installation, without jamming or critically damaging the SPIT to make sure that the SPIT can always be safely retrieved from the seabed.
- The lifts performed during operation of the SPIT are below the maximum lift capacity of the Orion, based on the crane curves provided by DEME [10].
- The deck-space required for the SPIT, SPs and other equipment necessary for the installation sequence fits on the available deck-space of the Orion.
- Critical parts of the SPIT are easily accessible for the crew of the vessel to perform maintenance work or inspections.
- The SPIT has integrated pump systems to assist the suction process of the SP. The pumps can be remotely attached and detached from the SPs.
- The impact damage on the stub of the SPs due to potential re-contact with the SPIT during retrieval of the SPIT from the seabed is minimized.

6.2 Design choices

The design choices for the concept design of the SPIT can be split into 3 parts.

- **SPIT:** Design choices regarding the function of the frame.
- **SPIT-SP engagement:** Design choices regarding the interaction between the SPIT and the SPs.
- **SPIT-Orion connection:** Design choices regarding the connection between the SPIT and the Orion.

Each part is explained in more detail in the following subsections. A 3D model of the SPIT is displayed in section 6.3 and will be referred to, to clarify specific design choices. At the end of the section, safety considerations for the design of the SPIT are mentioned.

6.2.1 SPIT

From the proposed installation sequence, the SPIT can be summarised as a lifting tool with integrated features. The SPIT is required to safely lift and install the SPs to the designated location on the seabed with the required installation tolerances. This section explains the general lay-out of the frame and its functions.

6.2.1.1 Frame design The primary function of the frame is to lift three SPs to the seabed where the SPs stubs are spaced 36m from each other. The frame can be separated in sections with two distinct uses:

- **Pocket frame:** The part of the frame where the SPIT is connected to the crane and the SP
- **Connecting frame:** The part of the frame spacing the pocket frames

The three SPs should be spaced equally in which the SPs are placed at the corners of a virtual equilateral triangle. The frame of the shape is therefore chosen to be an equilateral triangle with on each corner a pocket frame. The pocket frames are connected by a connecting frame to create the triangular frame. A top-view sketch of the triangular frame consisting of the different frame types is illustrated in Figure 23a.

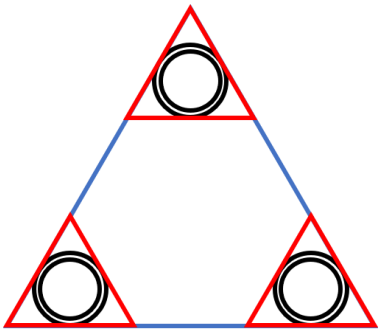

(a) Top-view sketch of the frame. In red: the pocket frames. In blue: the connecting frames. The SP stub and the hydraulic mechanism fit in the pocket frames.

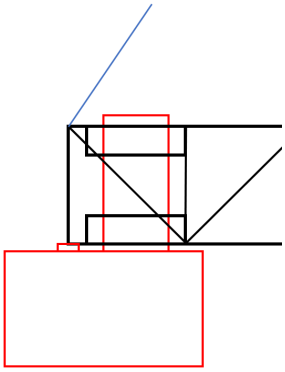

(b) Side-view sketch of the pocket frame. In red: the suction pile with the stub inserted into the pocket frame. In blue: the sling connecting the crane and the SPIT. The connections with the SP and crane are located on the same vertical line.

Figure 23

On each corner of the frame, the SP is connected to the frame with a padeye. The stub of the SP is restrained by a hydraulic mechanism that is fitted on the inside of the pocket frame. See paragraph 6.2.2.2 for more detail of the hydraulic mechanism. Figure 23b presents a side-view sketch of the frame. When the frame or SP stubs are subjected to bending loads, the area moment of inertia of the SPIT should be maximised to reduce the axial loads in the frame members. Therefore, the frame consists of two levels of members: upper and lower level. The distance between the upper and lower level should be small enough for the stub to fit through the frame. By placing the sling connection point above the connection of the SPIT and the stub, an efficient load-path through the members of the frame is created and the sling, connecting the SPIT to the crane, is not hindered by the stub.

The upper and lower levels are connected by vertical and diagonal braces. The braces also make the frame less sensitive to buckling failures and increases the shear strength of the frame. The design of the configuration of the diagonal braces is created to limit the number of braces. In practice, the angle of the diagonal brace is between 30-60° with the horizontal members [43]. Figure 33b presents the configuration of braces in the SPIT. An additional member connected with braces is added to the connecting frame. This is done to increase the strength of the frame against environmental loads in the horizontal plane to the SPIT. Figure 33a in section 6.3 depicts how the added member is connected to the connecting frame. The frame is correctly sized for its strength to satisfy the design requirements. This claim will be analysed and justified in section 6.4.

6.2.1.2 Pump docking station The pump docking station is placed on the outside of the pocket frame. This makes the pump easily accessible for the crew of the vessel and the crane hook. When the SPs are individually lowered, the SPs move with respect to the SPIT. Additional research is required to detail the variable length between the pump and the SPs when the SPs are individually lowered.

6.2.1.3 Accessibility of crew The frame has integrated walkways, stairs and ladders to get the crew to the critical parts of the SPIT for inspection or maintenance. Additional space is considered for work areas where maintenance such as replacement of hydraulic cylinders or pumps will be performed. Figure 31 presents a zoomed in view of the pocket frame where the walkways and work areas are displayed.

6.2.2 SPIT-SP engagement

The connection between the SPIT and the SP has four factors to consider that makes the design of the SPIT complex. The connection constrains the motion of the SP. In Figure 24, the six DOF of the SP are labeled.

- **Asymmetry of the stub on the SP:** The asymmetry of the stub makes it hard to place a single connection point directly above the COG of the SP. Multiple connection points should be considered or an additional bending moment is created during the lift of the SP.
- **Large hydrodynamic loads on the SP:** The hydrodynamic loads on the SP induce significant loads on the SP. These loads are transferred to the SPIT through the SP stub.
- **Small installation tolerances:** The mechanism in the SPIT that constrains the SP in all DOF during operation should allow enough space to place the SPIT over the SP, while still satisfying the required tolerance margin during installation. After a certain period during the suction process, in order for the SP to be individually lowered into the seabed, the heave DOF should be released by the mechanism of the SPIT.
- **Potential for high jamming forces in the connection mechanism:** Installation & fabrication tolerances or seabed irregularities might tilt the SP during the suction process in the seabed. The SP stub or padeye can clash with the SPIT. This creates friction between the SPIT and SP, resulting in jamming forces. High jamming forces can damage the SPIT and SPs or obstruct the retrieval of the SPIT.

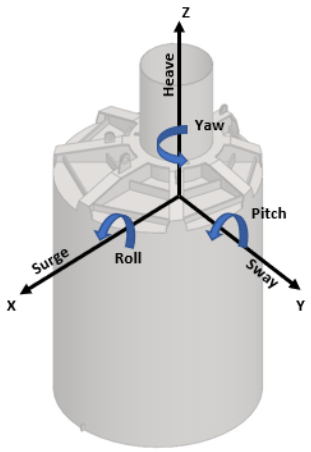

Figure 24: All degrees of freedom for a SP

A mechanism has been devised where the vertical force from the SP is separated from all other loads on the SP. In this way, the constrained heave DOF can be raised without other DOF. The mechanism can be split into four areas of contact between the SPIT and the SPs:

- **Padeye lock mechanism:** Constrains the heave motion of the SP.
- **Upper hydraulic gripper:** Constrains the surge and sway motion at the upper part of the SP stub. In combination with the lower hydraulic gripper constraints the roll and pitch motion.
- **Lower hydraulic gripper:** Constrains the surge and sway motion at the lower part of the SP stub. In combination with the upper hydraulic gripper constraints the roll and pitch motion. In combination with the girder guide restraints the yaw motion.
- **Girder guide:** Constrains the sway motion at the main girder. In combination with the lower hydraulic gripper restraints the yaw motion.

All four parts of the mechanism will be explained next.

6.2.2.1 Padeye lock mechanism The padeye lock mechanism is a remotely operated pin connection. The main padeye located on the SP top-plate is used to constrain the heave DOF of the SP to the SPIT. Figure 21c shows the location of the padeye. The pin connection is a safe design choice that during lift operations ensures that the SPs are locked to the SPIT. If the hydraulics systems unexpectedly fail a release of the SPs out of the SPIT is avoided. A robust locking mechanism with a large hydraulic cylinder should always be able to retrieve the pin while containing the damage done to the padeye and the locking mechanism. Figure 25 shows a schematic side view of the mechanism in locked and unlocked position. The lock mechanism is located on the inside of the outer corners of the triangular frame. Figure 31 shows the exact location on the SPIT. Attention should be given to the size of the SP padeye. The padeye requires sufficient space to fit inside the SPIT frame.

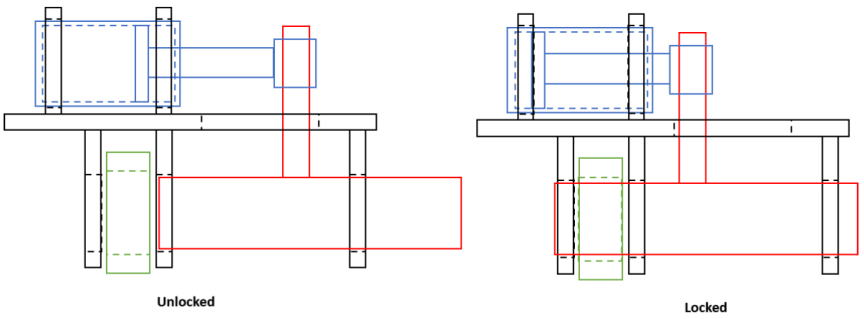

Figure 25: Schematic pictures of the lock mechanism. In green: the SP padeye. In red: the pin. In blue: the hydraulic cylinder

6.2.2.2 Hydraulic gripper A hydraulic gripper is an offshore tool used to lift or restrain cylindrical objects. The hydraulic gripper is a steel ring with integrated hydraulic cylinders to clamp to the cylindrical object. Figure 26a depicts a top-view sketch of a hydraulic gripper. This mechanism can be used to constrain the stub of the SP in the SPIT from all directions in the horizontal plane. By combining two hydraulic grippers, where one is located on the upper level of the frame and one on the lower level of the frame, the roll and pitch motion can be constrained. Because of the controllability of the hydraulic cylinders, the mechanism can adjust the tilt of the SP. In this way, the SP can be perfectly aligned before the suction process starts, reducing the potential of large tilt misalignment in the seabed. Figure 26b shows a schematic depiction of the hydraulic mechanism. The stroke of the hydraulic cylinders is designed to be large enough to release its constraints on the stub when the SPIT is retrieved from the seabed.

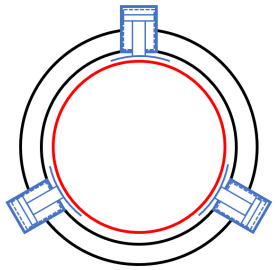

(a) Schematic top-view of the hydraulic gripper. In blue: the hydraulic cylinders attached to the steel ring. In red: the SP stub.

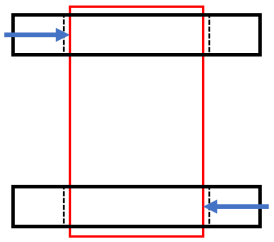

(b) Schematic side-view of the upper and lower hydraulic gripper. In black: the hydraulic grippers. In red: the SP stub. The grippers can push the stub, adjusting the stub and SP if necessary.

Figure 26

6.2.2.3 Girder guide The girder guide is a steel funnel that is inserted over the main girder of the SP when the SPIT is placed on the SP. Figure 31 shows how the funnel is positioned over the main girder of the SP. A small gap between the funnel and the girder is taken into consideration for small misalignment of the SPs on the preparation area. However, the gap is small enough that the maximum yaw misalignment does not exceed the design requirement. When the girder guide and the main girder are in contact, further yaw movement is constrained. The girder guide is also a guide for the SP padeye to make the alignment with the pin.

6.2.2.4 Individual SP lowering A hydraulic mechanism is integrated into the pocket frame on the inside of the SPIT. Figure 32a shows the location of the mechanism. The mechanism consists of a vertical hydraulic cylinder that is used to jack-up the SPIT, while the SP underneath the SPIT is lowered. In this way, the SP can be individually lowered into the seabed while the SPIT remains horizontally leveled.

6.2.2.5 Stub guide funnels At the bottom of the SPIT, steel funnels are attached to the lower hydraulic gripper. Figure 32b shows the location and configuration of the steel funnels. These funnels help to guide the SPIT over the stub when the SPIT is lifted over the SPs. They are also used as a bumper to mitigate the potential impact forces of the SPIT against the stub. Potential high impact forces between the SPs and SPIT can occur due to the dynamic response of the SPIT excited by environmental loads and the motions of the vessel. High impact loads occur when the SPIT is lifted over the SPs or during recontact of the SP stubs when retrieving the SPIT from the seabed. After a high impact load on the funnels the function of the funnels should be re-evaluated and might require repairing or replacement.

6.2.3 SPIT-Orion connection

The SPIT is connected by multiple points to the Orion. The connections should all be detachable if the situation demands it. Details on how this can be achieved requires additional research to justify the claims.

6.2.3.1 SPIT to sling The SPIT is connected to the crane hook by slings. The slings are attached to the SPIT with a padeye shackle connection. The padeyes on the SPIT are showed in Figure 30. The loads that result from the slings to the SPIT can be minimised by increasing the angle of the sling with the horizontal plane. For a conservative estimate, a sling angle of 60° [26] is selected. With the connection method proposed in section 4.1.1, the slings are attached to the SPIT during the installation of all the SP foundations of the OWF. Remotely attaching and detaching of the sling is therefore not necessary. The crane hook can be detached from the sling during the installation sequence or, if the SPIT on the seabed should be temporarily abandoned due to weather conditions. A short description of how this can be achieved is proposed in section 4.1.1.

6.2.3.2 Tuggerlines The tuggerlines are used to dampen the horizontal movement of the SPIT during the overboarding operation of the SPIT and the SP and to correctly adjust the orientation of the SPIT before the SPs land on the seabed. The tuggerlines are attached to the SPIT by slings looped around at the top corners of the SPIT below the padeye to the crane. Figure 30 shows the location of the tuggerline-SPIT connection. The slings leading to the tuggerlines can be detached from the SPIT if the SPIT on the seabed should be temporarily abandoned due to weather conditions.

6.2.3.3 Umbilical The umbilical leading to the SPIT is used to feed the SPIT with electricity. The main features to power are the hydraulic and pump systems and controls. By having a central umbilical, the lines going to the SPIT are easy to manage. The umbilical can be detached from the SPIT if the SPIT on the seabed should be temporarily abandoned due to weather conditions.

6.2.4 Safety

The safety design requirement is satisfied if the following is considered during the design and use of the SPIT:

- Correctly sizing the dimensions of the SPIT will avoid dangerous mechanical or structural failures.
- The mentioned walkways, ladders and work-areas on the SPIT are designed with safety rails for safe working conditions on the SPIT.
- The weather windows should be carefully analysed before the installation sequence is initiated to avoid environmental loads that can exceed the SPIT design loads.
- Sufficient space between the crew and other assets is considered to avoid collisions during lift operations of the SPIT.

The estimated requirements to satisfy these claims are considered in this thesis. However, more detailed safety and risk analysis should be performed in future research of the SPIT.

6.3 Concept design

From the design choices explained in the section above, a 3D concept design is modeled in Solidworks. The renders in the Figures below show how the design choices have been incorporated in the concept design.

In Figures 27, 28 and 29, the 3D renders are shown of the SPIT structure. Each corner of the triangular frame encloses the hydraulic grippers and at the tip, padeyes are welded to the SPIT to connect the slings of the cranes to the SPIT. Walkways and work areas create the necessary access to all critical parts of the SPIT. Ladders, positioned at the inside of each corner of the SPIT, are designed with backscratchers to allow for safe access to the lower and upper part of the frame. The connecting frame is strengthened by a back brace connected to the frame with smaller braces.

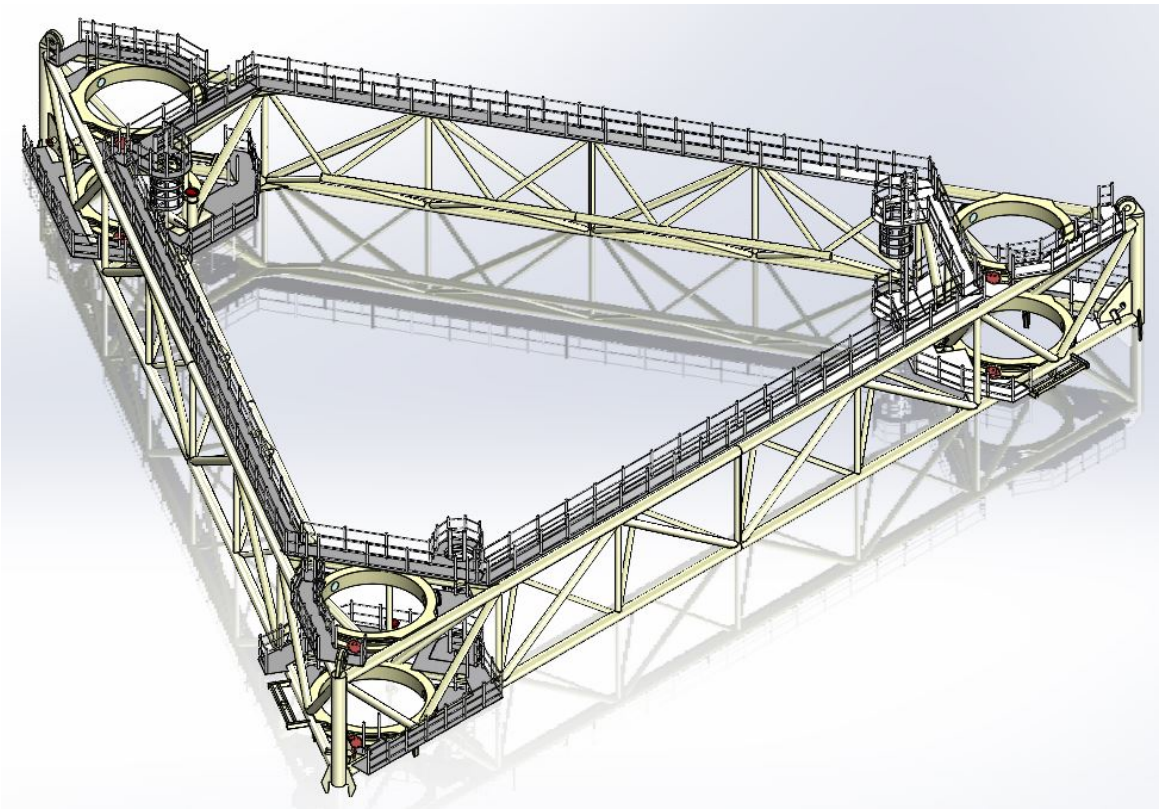

Figure 27: Concept design of the SPIT

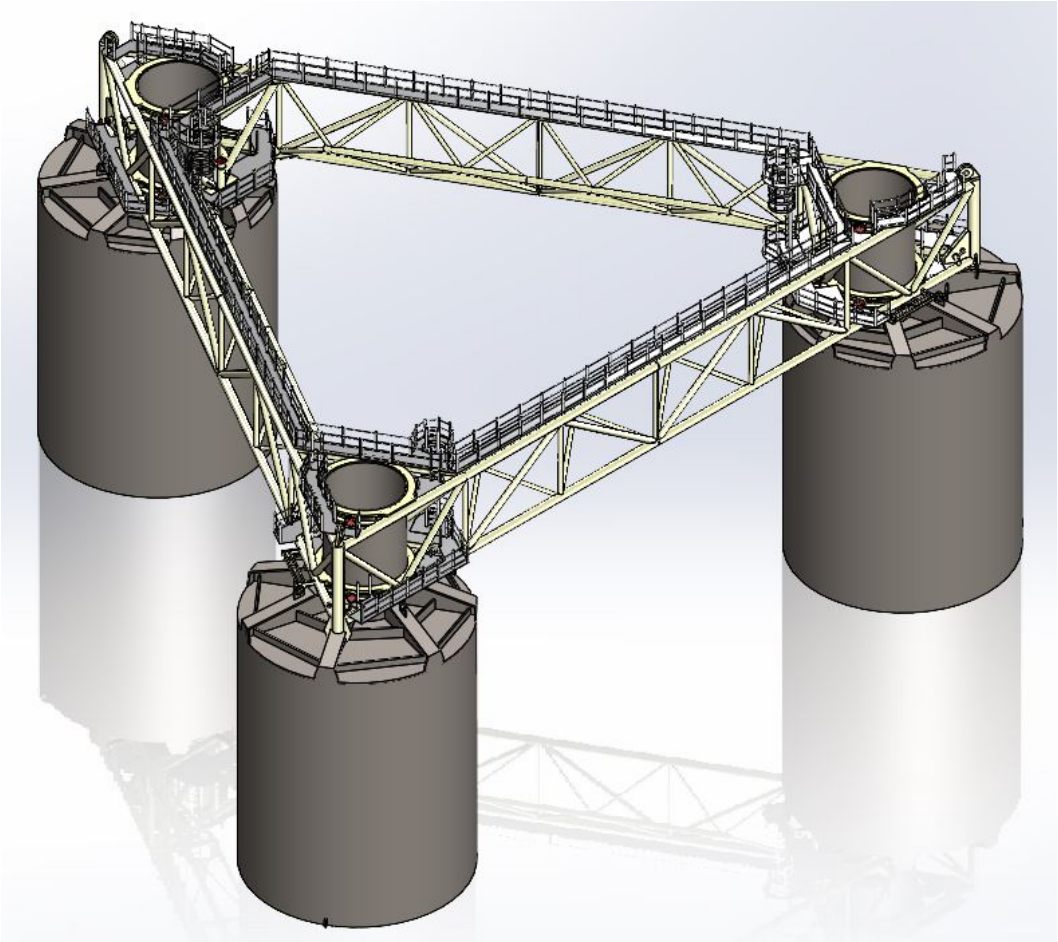

Figure 28: Concept design of the SPIT with SPs

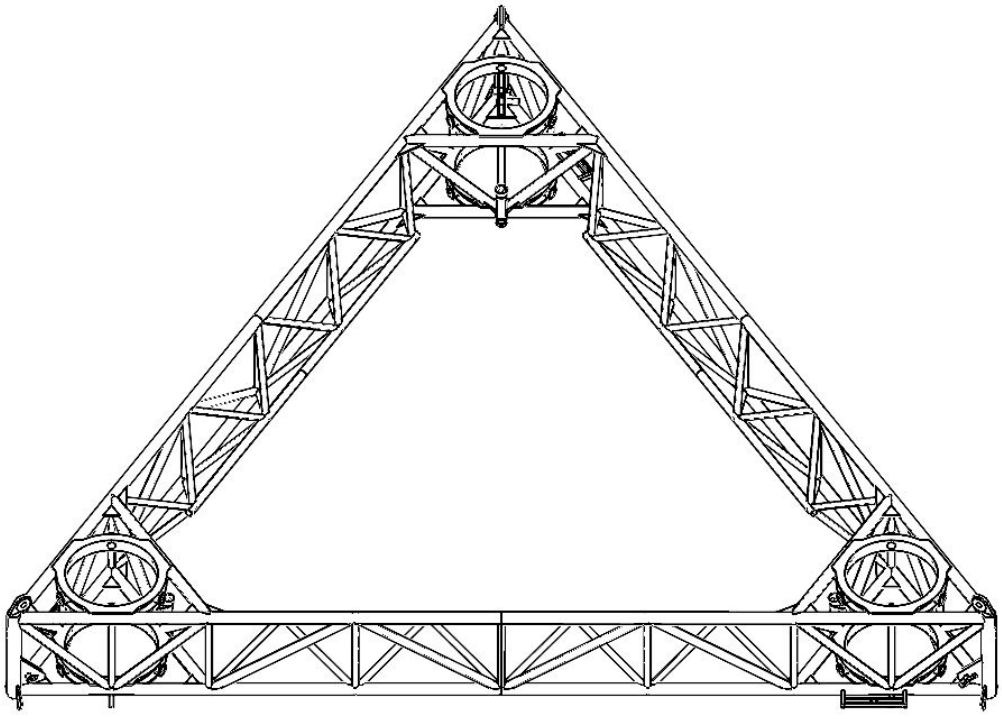

Figure 29: Black and white render of the SPIT without walkways

Figure 30 shows a close-up of the SP stub inside the frame of the SPIT. The hydraulic grippers enclose the stub of the SP in order to constrain the necessary DOF. All hydraulic cylinders are inserted into tubes to hold the cylinders in place. The back of the cylinders are highlighted in red. The cylinders are bolted to the tubes with flanges and the hydraulic connections are easily accessible. All hydraulic cylinders have enough space to be removed and replaced if necessary. The connection point of the sling to the SPIT is highlighted in red below the top corner of the frame.

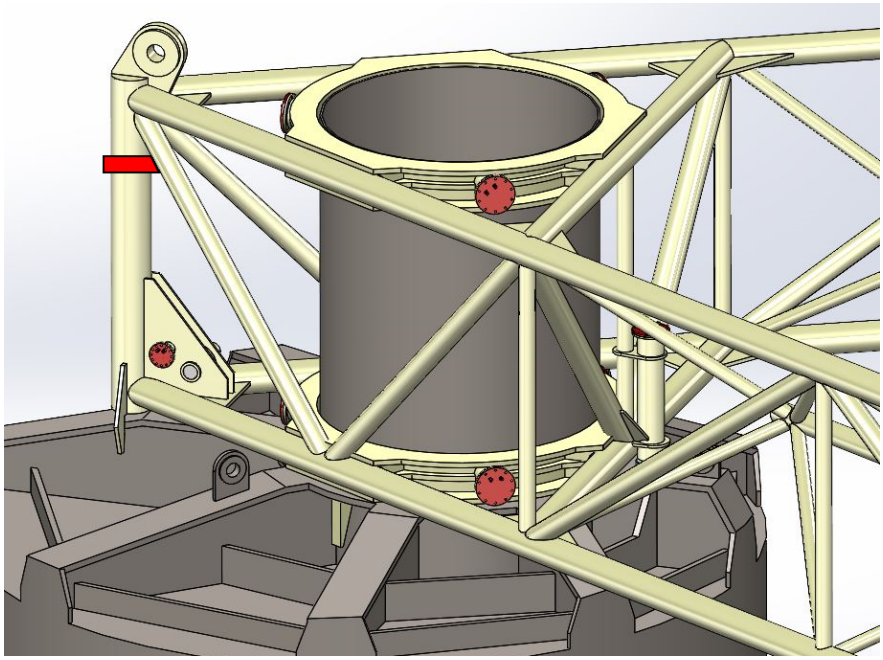

Figure 30: Close-up of the SP stub in the pocket of the SPIT without walkways.

Figure 31 shows a close-up of the SPIT frame with the pump docking station attached to the lower level of the frame. At the edge of the lower triangle, the Figure shows how the girder guide falls over the main girder of the SP. The locking mechanism to connect the SP to the SPIT is located next to the girder guide at the left.

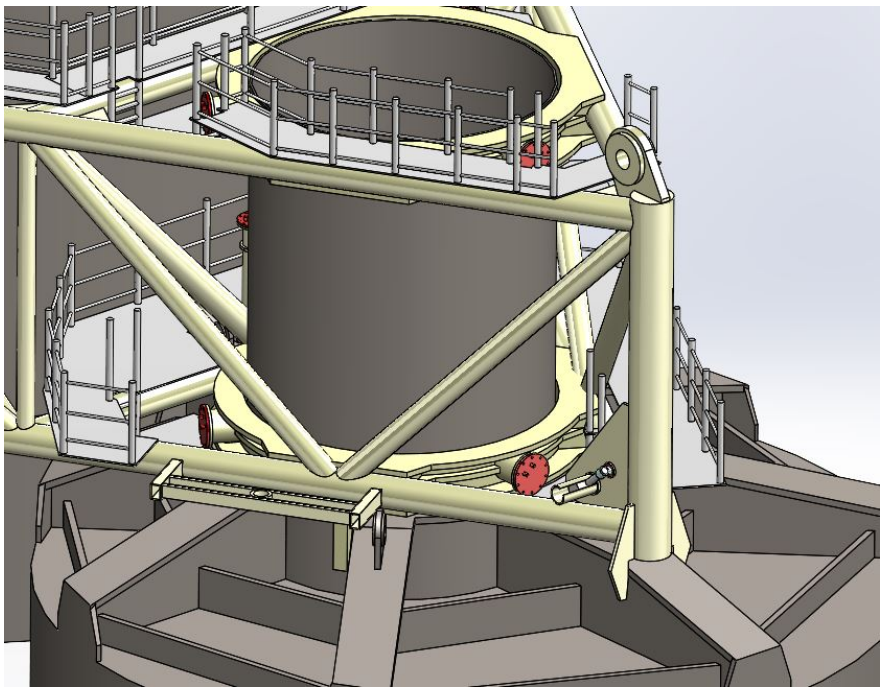

Figure 31: Close-up of the SPIT frame with the pump docking station

Figure 32a shows how the hydraulic mechanism is attached to the SPIT. The head of the hydraulic cylinder presses down on the back girder of the SP to adjust the height of the SPIT accordingly. Figure 32b shows how the stub guides are attached to the SPIT. Figures 33a and 33b show the top and side-view of the SPIT with the SPs.

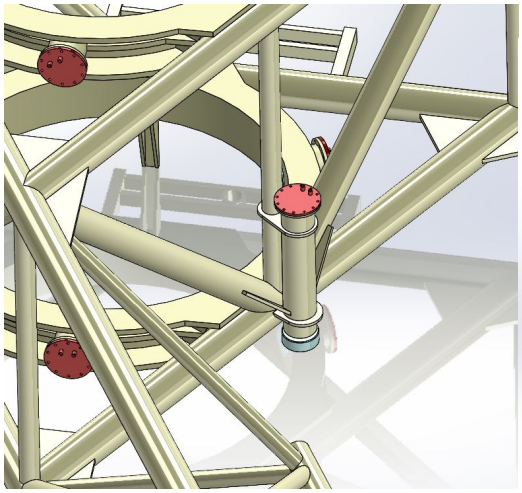

(a) Close-up of the hydraulic mechanism to adjust for the height difference of the SPs

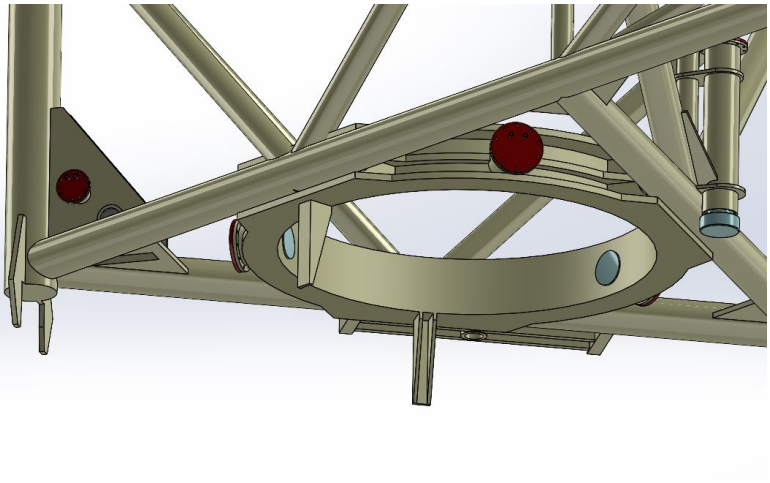

(b) View of the underside of the SPIT

Figure 32

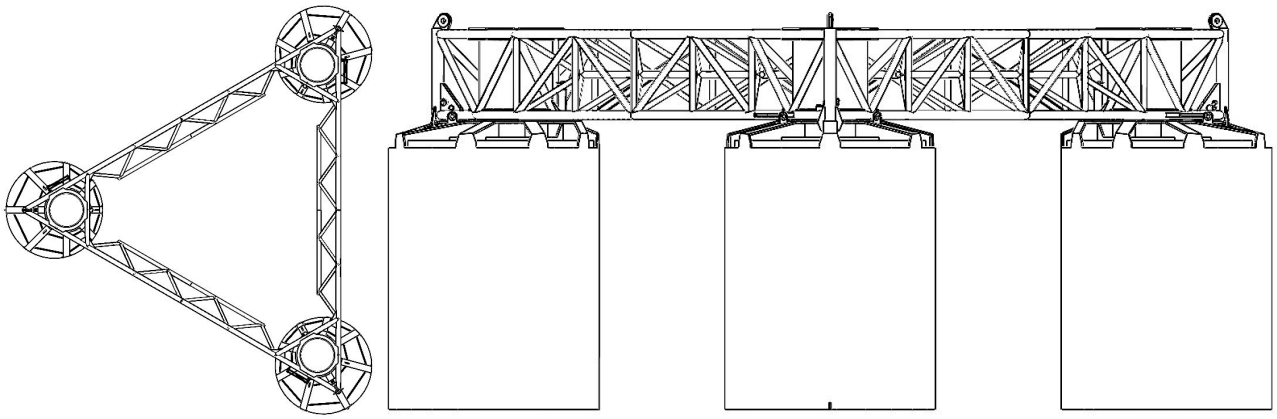

(a) Top-view of the SPIT with SPs

(b) Side-view of the SPIT with SPs

Figure 33

6.4 Requirements check for SPIT

The design presented in section 6.3 covers all design requirements stated in section 6.1. In this section, the claims that state that the design requirements are satisfied regarding three topics are justified. The three topics are:

- Strength of the frame and important features of the SPIT
- Installation precision of the SPs with the SPIT
- Required crane capacity for the installation sequence

These topics are analysed further to describe and understand critical aspects of the SPIT design. All checks regarding the three topics are done based on high level load estimations. Conservative estimates should result from the analyses.

6.4.1 Strength of the SPIT frame during operation

The SPIT is loaded during the installation sequence by various loads and directions. The strength of the frame is dependent on the highest load cases during this installation sequence. In this section, the highest expected loads on the SPIT are quantified. Three horizontal load cases are considered:

- Horizontal hydrodynamic loads on the SPs
- Horizontal hydrodynamic loads on the SPIT frame
- Horizontal loads on the SP in the seabed

The maximum dynamic response of the SPIT during lift is also analysed. The horizontal load cases and the dynamic response of the SPIT are used to determine the axial loads on the members of the SPIT frame. The size of the members results from the stress and buckling check for each member. The weight of the SPIT is further analysed in section 6.4.5 and is used to check the required crane capacity.

6.4.1.1 Horizontal hydrodynamic loads on the SPs The SPs first make contact with the water during the lift operation of the SPIT and SPs. The cylinder shells of the SPs create forces and bending moments in the stub where the SPs is connected to the SPIT. Figure 34 depicts the load case of the horizontal loading of the SP by a wave.

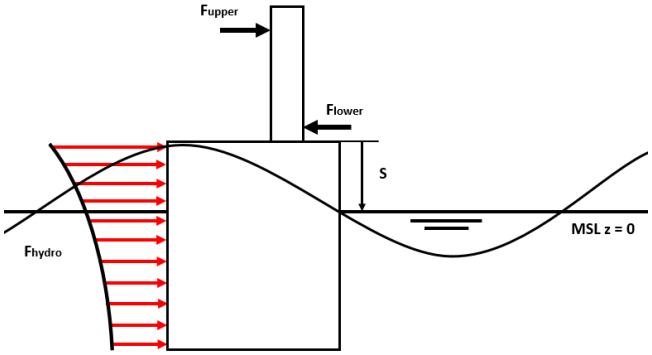

Figure 34: Load case considered for the SP in waves

In Appendix B, the hydrodynamic analysis is worked out in detail. The analysis is performed based on the Morison equation [43] and linear wave theory as proposed in [19]. All other assumptions made for the calculations can be found in this Appendix.

From the analysis results two extreme load cases:

- **Maximum bending moment on the stub:** When the SP is partially submerged the horizontal forces create the maximum bending moment on the stub.
- **Maximum force on the SP:** When the SP is fully submerged, the forces on the SP are maximum.

The reaction forces on the hydraulic grippers are largest during the maximum bending moment load case. The loads and reaction forces on the upper and lower hydraulic ring are displayed in Table 7.

M	25.4	MNm
F	2.33	MN
F_{upper}	6.38	MN
F_{lower}	8.71	MN

Table 7: Maximum bending load case

6.4.1.2 Horizontal loading of the SPIT After the SPs are fully submerged, the SPIT is subjected to the waves. Since the SP is not maximally loaded at this stage, the main members will be sufficiently sized to withstand the direct wave loads. This claim is justified by the results in this paragraph and Appendix F.2. However, the back brace member, strengthening the connection between the pockets of the frame, will be

maximally loaded during horizontal wave impact on the frame. The load case considered here is visualised in Figure 35.

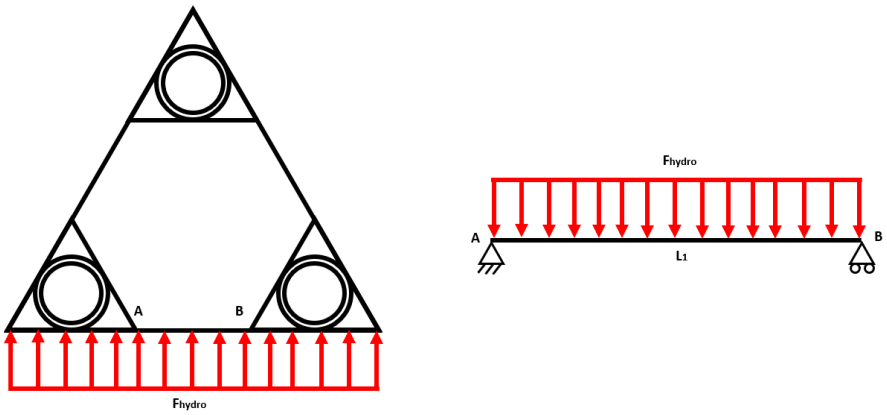

Figure 35: Top view of the SPIT subjected to a horizontal hydrodynamic load. The frame between point A and B is analysed as a hinged beam with a uniform load.

The loads in the back brace are analysed in Appendix C. The analysis is based on the Morison equation and a frame stick model as proposed in [43]. In Figure 36, the cross sectional area of the SPIT frame in the middle of A and B is depicted. The back brace member is indicated by B3 and the main members of the frame are indicated by $B1$ and $B3$. According to the analysis, the beam is subjected to a maximum bending moment of $11.0MN$, resulting in the axial load on the back brace of $3.66MN$. The axial loads in the main members are $1.83MN$. These loads are significantly lower than the axial loads taken from the analysis performed in Appendix F.2. It can be concluded that the main members on the SPIT are sufficiently sized to withstand the direct wave loads. This is because the loads, caused by the SPs, result in the governing load case of the SPIT main members.

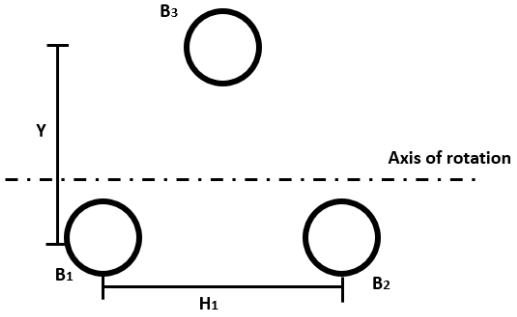

Figure 36: Cross sectional area sketch of the frame between point A and B.

6.4.1.3 Horizontal loads on the SP in the seabed When the SPs are placed on the seabed and during the suction process, the SP can tilt. This tilt will cause a misalignment on the seabed. The function of the hydraulic grippers is to adjust the SP tilt and minimise the misalignment of the SP on the seabed. When the hydraulic grippers make the adjustment on the SP, the soil will resist, resulting in reaction forces of the soil on the SP. To estimate the reaction forces on the SP by the soil the following assumptions are made:

- Due to the controllability of the SP by the hydraulic grippers, the misalignment before the SPs hit the seabed is small and therefore require no further adjustments.
- After a certain penetration length of the SPs, to avoid high reaction forces on the SP and the SPIT, the hydraulic grippers stop adjusting the misalignment of the SPs. The assumed penetration length of the SPs is the self-weight penetration length. This is to adjust the tilt on the SPs induced by the seabed slope and the placement of the SPIT and SPs by the crane. The self-weight penetration is selected based on two factors:
  - The seal around the SPs by the seabed is designed to be sufficient for the pumps to operate after the self-weight penetration.

– The self-weight penetration is the lowest penetration of the SPs in the seabed without the interaction of the crane or the pumps. In this way, the SPIT and SPs can be placed on the seabed. The crane can release the tension in the slings and the tilt adjustment can be made.

When the hydraulic grippers stop adjusting the misalignment of the SPs, the hydraulic grippers will work in a constant tension mode compensating for further tilt of the SP in the seabed. The misalignment of the SP in the seabed after this penetration length is accepted.

The adjustment of the misalignment of the SPs induced by the SPIT and SP placement on a sloped seabed is depicted in Figure 37. The pumps are used to compensate for the height difference, and because the SPs are connected to each other by the SPIT, the tilt of the SP is also adjusted.

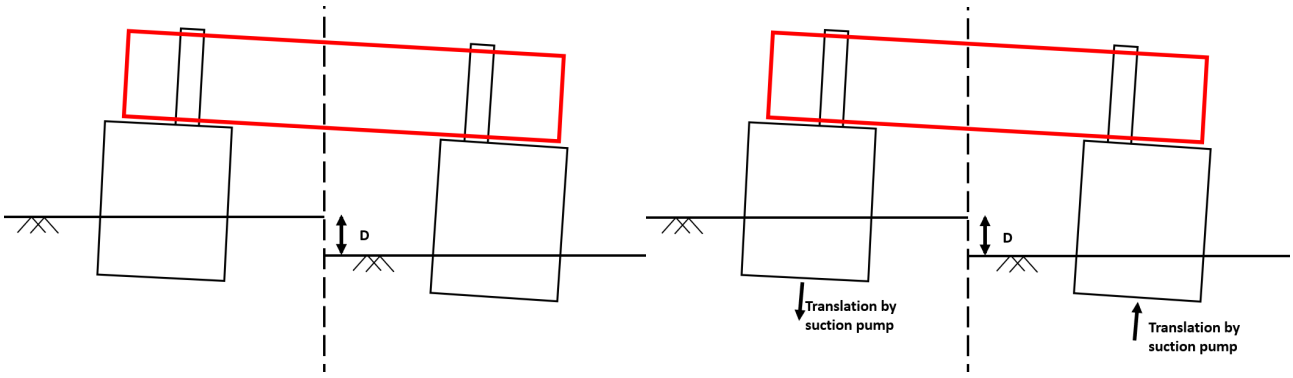

(a) Possible rotation of the SPIT during self-weight penetration. **(b)** Rotation adjustments created by suction pumps.

Figure 37

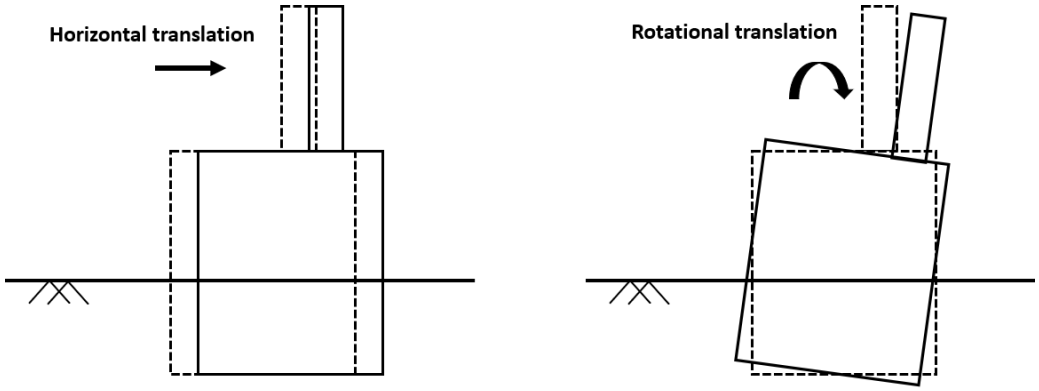

Figure 38: Two reaction types considered for the misalignment adjustments of the SP in the seabed.

During the adjustment operation, the soil around the SP is displaced. The reaction force of the soil on the SP is transferred to the SPIT through the SP stub. The maximum reaction forces of the soil on the SP depends on the soil failure strength. Two reaction types are considered for the misalignment adjustments of the SP in the seabed: horizontal translation and rotational translation. Both types are depicted in Figure 38. The maximum reaction forces are analysed for different soils in Appendix D. In Table 8, the maximum bending moment for each soil type, resulting from the analysis, is displayed .

	Uniform clay	NC clay	Sand
Rotational translation	1.80MNm	0.6MNm	0.41MNm
Horizontal translation	24.5MNm	21.1MNm	74.5MNm

Table 8: Maximum bending moment on the SP stub for each soil type.

From the data in Table 8 can be concluded that the maximum bending loads on the stub will occur for horizontal translation of the SPs. The bending moments resulting from the uniform clay and NC clay are lower than the bending moment induced by the horizontal hydrodynamic loads from section 6.4.1.1. Therefore, these loads will not be governing in the design of the SPIT frame. However, the maximum bending moment in sand is approximately three times larger than the bending moment induced by the horizontal hydrodynamic loads. This will result in governing loads in the design of the SPIT frame.

However, for the design of the SPIT in this thesis, the loads from the bending moments in sand will not be used to size the members of the SPIT frame because of the following considerations:

- If the maximum bending moments in sand are considered for the design loads on the SPIT, the loads on the SPIT will be approximately three times larger than if the governing load case is the hydrodynamic loading of the SPs and the SPIT. The hydrodynamic loads will be unavoidable during the installation sequence. However, the horizontal reaction forces of the soil on the SPs can be reduced during the installation sequence by considering the following: When the SPs require an installation in sandy soils, the induced tilt of the SPs and SPIT on the seabed and the initial penetration length will be reduced. The initial penetration length is reduced by initiating the pumps before the self-weight penetration is reached. The crane lowering speed is also reduced in order for the SP, that first make contact with the seabed, to have sufficient time to penetrate the seabed. This results in the reduced tilt of the SPs and SPIT on the seabed. The pumps do require enough seal to perform the adjustments and the crane lowering speed is impacted by the motion of the crane tip, this limits the minimum lowering speed.
- The estimated reaction forces of the soil on the SPs result from soil failure. However, for small adjustments, the soil will deform elastically. Elastic deformation create lower reaction forces on the SP in comparison with the considered soil failure. Until when elastic deformation occurs and what the reaction forces are, depends on the stiffness of the soil and requires research that is outside the scope of this thesis.

From the simplified models, the behaviour of the SPs in the soil is challenging to model. Therefore, with these considerations, the horizontal reaction forces of the soil on the SPIT are assumed not to be governing in the design of the SPIT frame. Future research that can analyse the soil behaviour and loads on the SPs with the SPIT should justify or rectify the assumptions made in this section.

6.4.1.4 Dynamic responses during the lift of the SPIT

During the lifting procedure of the SPIT, the SPIT is excited by external loads. These loads cause the SPIT to oscillate and accelerate. For lifting procedures, a dynamic amplification factor (DAF) is used to amplify the static forces to adjust for the dynamic behaviour of the lifted object. In this section, the vertical & horizontal dynamic responses are analysed.

Vertical response:
The vertical dynamic response of the SPIT can be modeled as a mass damping spring (MDS) system. Figure 39 depicts the model. The MDS system is simplified to one degree of freedom: the heave motion.

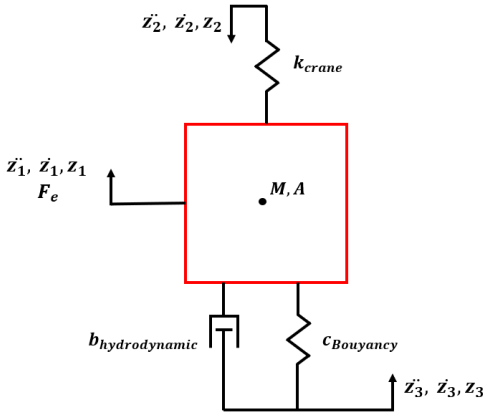

Figure 39: Mass damping spring system of the heave motion of the SPIT

The forces working on the SPIT can be separated into five parts:

- **Lift force:** The SPIT is lifted by a crane. The sling from the SPIT to the crane and the crane itself can be modelled as a spring. In addition, the motion of the crane as the HLV is excited by environmental forces, which should also be taken into account.

The stiffness of the crane spring, k_{crane} is the summation of a spring system containing 5 springs in series:

- Rigging stiffness ($k_{rigging}$)
- Crane wire stiffness (k_{wire})
- Crane boom stiffness (k_{Boom})
- Crane-deck stiffness ($k_{crane-deck}$)
- Vessel rolling stiffness ($k_{rolling}$)

Due to the series of springs, when one of the five springs is significantly lower than the others, this stiffness dominates the spring stiffness k_{crane}. This claim can be derived from the equation for k_{crane}:

$$\frac{1}{k_{crane}} = \frac{1}{k_{rigging}} + \frac{1}{k_{wire}} + \frac{1}{k_{Boom}} + \frac{1}{k_{crane-deck}} + \frac{1}{k_{rolling}} \tag{1}$$

The vessel rolling stiffness has a significantly lower spring stiffness than the rest of the springs in series [39] and therefore k_{crane} can be simplified to $k_{rolling}$. The Orion is equipped with ballasting systems [17] that can change the vessels rolling stiffness. During operations, the ballasting systems can be used to reduce the dynamic response of the SPIT.

- **External forces:** The waves and wind cause external forces on the frame. Both load types have a range of frequencies that will excite the lifted object. Wind has short periods of fluctuations in speed caused by turbulence ranging typically from seconds to 10 minutes [44]. The waves of greatest interest for offshore structures are gravity waves with periods from about $1 - 30s$ [44]. During lift operations, the natural frequency of the lifted object should not overlap with the frequencies of the external forces or damping systems should be introduced to mitigate dangerous dynamic responses of the lifted object. For large flat objects subjected to waves, the slamming force can significantly impact the dynamic response. The top-plates of the SPs should be carefully analysed on the slamming impact of the waves.
- **Hydrodynamic damping force:** This is the energy dissipation caused by the movement between the SPIT and the water. It is common practice to use the water as a damping tool to reduce the dynamic response of the lifted object [39]. This is achieved by partially submerging the lifted object.
- **Buoyancy force:** Hydro-static pressure that forces the SPIT upwards. The buoyancy force can be modelled as a spring. Due to the waves, the water surface is constantly moving. The lowering speed of the crane and the size of the air vents on the SPs should be carefully considered during lift operations of the SPIT. If the air withing the SPs has not sufficient time to escape, an air plug is created. This air plug increases the buoyancy force on the SPIT but also functions as an additional spring to the system. If the buoyancy is increased to a point where the rigging of the SPIT to the crane becomes slack, slack-snap loads can occur, resulting in high loads in the SPIT, rigging and crane [4]. This should be avoided at all times. In Appendix E, an analysis is made to check the lowering speed and air gap size for the SPs used in this thesis. From the results, graphs are made that plot the lowering speed and the minimum air gap of one SP to avoid a floating SP. The plots are shown in Figure 40.

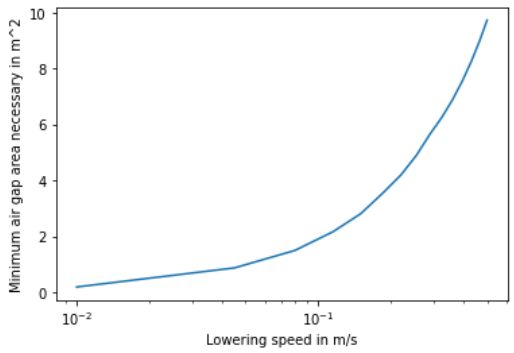

(a) Plot of the minimum air gap area of the SPs to avoid a floating SP

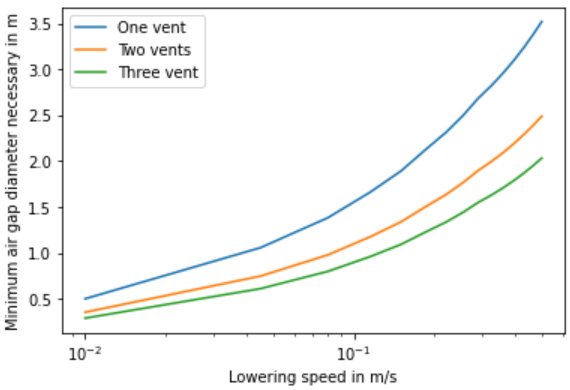

(b) Two rigging configurations for tuggerlines

Figure 40

Sufficient venting can be achieved by one or multiple air gaps. Attention should be given to objects obstructing the vents during operation such as the pump, waves or the SPIT. Additionally, the lowering speed is a combination of the speed of the wire relative to the crane tip and the crane tip relative to the water line. For conditions where the vessel is significantly excited by the waves, the lowering speed of the crane should be adjusted accordingly.

This analysis is performed on a single SP. The additional mass of the SPIT reduces the floating behaviour of the SP. However, according to DNV-RP-N103 [4], 10% of the dry mass of the SPIT and SPs should be the minimum tension on the wire to avoid snap-slack loads. As will be explained in section 6.4.5, the contribution of the SPIT is an estimated 16% of the total dry mass. If the SPs air gaps and lowering speed are adjusted according to the plots in graph 40, the minimum tension in the crane wire should be satisfied.

- **Acceleration of mass:** The forces on the SPIT cause the SPIT to accelerate. Due to the interaction with water, additional water mass is accelerated and should be added to the mass of the SPIT. For a non perforated SP the added mass of the water equals [37]:

$$M_{water} = \pi R^2 \rho_{water}(H + \frac{4}{3}) = \pi \cdot 6^2 \cdot 1025(15 + \frac{4}{3} \cdot 6) = 2670mt \tag{2}$$

For perforated SPs, the added mass can slightly be decreased if the area of perforation is 2 to 3% of the total top-plate [37]. The added mass increases the total submerged dynamic weight of the SP almost 10 times. Submerged accelerations of the SPIT with the SPs should carefully be considered during the operation of the SPIT.

During the lift operation of the SPIT, multiple actions such as water ballasting or water damping can be undertaken to reduce the vertical dynamic response of the SPIT. In addition, a heave compensation tool can be considered [5]. This tool can allow for added damping on the system or increase the range of allowable deflection in the rigging in order to decrease the risk of snap loads occurring [4]. The DAF in dry air from DNV-ST-N001 [5] states that, for lift operations with a static hook load between $1000mt$ and $2500mt$, the DAF equals 1.15. What should be noted is that this DAF is limited to adverse weather conditions. According to DNV-ST-N001 [5], the maximum significant wave height, this DAF can be considered for, is $2.5m$. This is below the required significant wave height mentioned in section 6.1. The DAF for a subsea lift requires detailed analysis that is outside the scope of this thesis. This analysis should consider the slamming loads on the SP top-plate, the air plug created inside the SP, and the added mass of the SP [4] [5]. For a simple one degree of freedom system, the maximum DAF considered is 2.0 [12] [14] and will be used in further calculations in this thesis. For more complex systems, the DAF may be higher [12] [14], but is not probable for the single lift operation of the SPIT [2].

Horizontal response:
The horizontal dynamic response of the SPIT during the lift operation is of greatest importance when the SPIT is lifted and overboarded from deck. Uncontrolled horizontal excursions of the SPIT endanger the crew on board and damage other assets of the vessel or the SPIT itself. Tuggerlines are used to reduce the horizontal response by controlling the tension on the tuggerlines. The tuggerlines pull the SPIT towards its connection point in order to maintain tension during the lift. As mentioned previously, when the SPIT is partially submerged, the water acts as a damping system reducing the horizontal response as long as the wave frequency does not coincide with the natural frequency of the horizontal response of the SPIT.

The horizontal response of the SPIT during lift is simplified with a pendulum system. Depending on the rigging of the tuggerlines the horizontal response natural frequency can be estimated. Figure 41a shows a schematic representation of the pendulum system and Figure 41b for two rigging configurations. In the left configuration, the tuggerlines are directly connected to the SPIT. In the right configuration, the tuggerlines are connected to the lifting bridle.

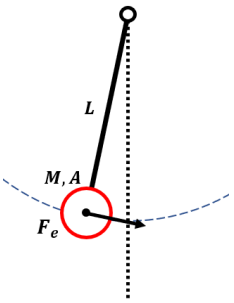

(a) Pendulum system

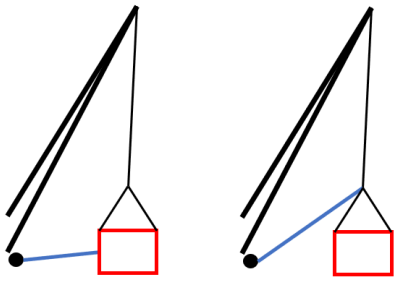

(b) Two rigging configurations for tuggerlines

Figure 41

The natural period of a pendulum system can be calculated with the following equation:

$$T_n = 2\pi\sqrt{\frac{L}{g}} \tag{3}$$

The natural period is dependant on the length of the pendulum and the gravitational constant. In the pendulum system introduced above the length L equals the distance between the bridle and the centre of mass of the SPIT. The left rigging configuration constrains the SPIT such that the pendulum length equals zero. The right configuration only constrains the bridle such that the distance between the bridle and the centre of mass of the SPIT creates a pendulum system. The maximum distance between the bridle and the SPIT is equivalent to the maximum bridle height and is approximately $80m$. The minimum distance of the bridle and the SPIT is equivalent to $25m$ since the sling angle from the SPIT to the bridle should be greater than 45° [5] [26]. The results of the natural period of the pendulum are plotted in Figure 42.

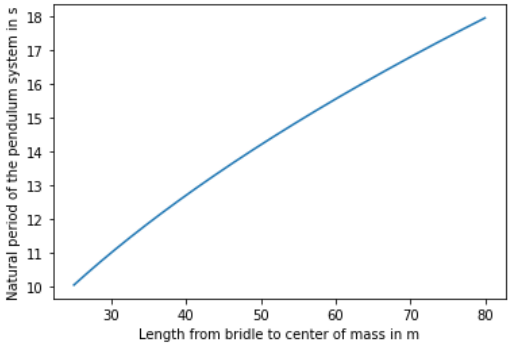

Figure 42: Plot of the natural period of a pendulum system

The range of natural frequencies of the pendulum system, that is caused by this rigging configuration, overlaps with the wave and wind periods offshore [44]. To avoid resonance, the tuggerlines should be directly connected to the SPIT as indicated in the left configuration. Attention should be given to the point of attachment to the SPIT. Additional loads will be introduced to the frame of the SPIT if the configuration is changed.

An additional factor for the rigging should be taken into consideration. The force the tuggerlines exert on the SPIT, are directly compensated by the tip of the crane. This force reduces the crane lift capacity. Attention must be given to correctly adjust the crane curve for the use of tuggerlines during the lift operation.

6.4.1.5 Member checks of the SPIT frame The estimation in paragraph 6.4.1.3 states that the largest loads on the SPIT frame occur during the lift operation of the SPIT and SPs. Therefore, the SPIT frame members are sized according to the following load cases:

- The SPIT is suspended in the air, the vertical dynamic response of the SPs and the SPIT and the horizontal hydrodynamic loads on the SPs result in the loads on the frame.
- The SPIT is submerged and the vertical dynamic response results in the loads on the frame.

- The SPIT frame is subjected to horizontal hydrodynamic loads. The members that are sized for this load case have already been explained in section 6.4.1.2.

To check all unique members of the SPIT frame, the symmetry of the frame is used to simplify the analysis. The member check analysis is based on hinged frame models proposed in [43]. Only three parts of the frame require analysis to find the loads in each unique member. The three parts of the frame are shown in Figure 43 and are explained below:

- **Outside frame (red):** The members on the outer side of the triangular frame are analysed. The frame is analysed for the loads occurring on the SPIT suspended in air or submerged in the water by the crane.
- **Connecting frame (green):** The back brace member is analysed. The horizontal hydrodynamic loading on the frame determines what load to expect in the back brace.
- **Inside frame (blue):** The inside braces of the frame are analysed. The hydrodynamic loads of the SPs will create shear in the upper and lower level of the SPIT that are partially compensated by the inside braces of the frame.

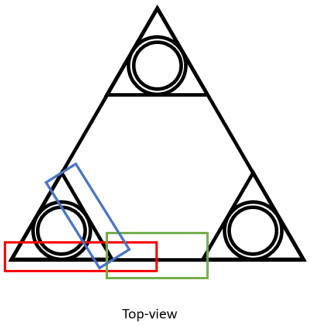

Figure 43: The analysed parts of the truss frame. Red: outside frame. Green: connecting frame. Blue: inside frame.

Each member of the SPIT frame is correctly sized to satisfy two checks:

- Stress check of members
- Buckling check of members

In Appendix F, the stress and buckling checks are performed and the members of the frame are correctly sized to satisfy the strength design requirement. The results are shown in Table 9. The numbering of each member is shown in Figure 44. Each color indicates the load case the member was sized according to. The following colors indicate:

- Red: The SPIT is suspended in air and hydrodynamic loads on the SPs are transferred through the SP stub to the SPIT. This case considered symmetric loading of the SPs
- Purple: The SPIT is suspended in air and hydrodynamic loads on the SPs are transferred through the SP stub to the SPIT. This case considered identical loading of the SPs
- Green: Loads on the inside frame created by the hydrodynamic loads on the SPs.
- Yellow: The SPIT is suspended in the water and a DAF is considered to calculate the static loads in the frame.
- Blue: The SPIT is subjected to hydrodynamic loads.

Other braces of the frame are estimated in size from the considered unique members in the frame. The loads on these braces are estimated not to be critical for the structural strength of the frame. The size is only used to estimate the weight of the frame in section 6.4.5. These braces are labeled in Appendix J to indicate what unique member is used to estimate the size.

	$F_{max}[MN]$	$F_{min}[MN]$	$B_{check}[-]$	$S_{check}[-]$	$L[m]$	$D[mm]$	$T[mm]$	$M[kg]$
1	1.37	-1.37	0.60	0.67	4.64	193	9.7	214
2	8.94	-0.75	0.20	0.67	6.75	494	24.7	2030
3	2.41	-2.41	0.57	0.67	8.19	339	9.7	664
4	4.16	-9.08	0.09	0.67	6.75	498	24.9	2062
5	0.00	0.00	0.00	0.00	4.64	193	9.7	214
6	8.33	-1.36	0.21	0.67	6.75	477	23.8	1892
7	2.41	-2.41	0.57	0.67	8.19	339	9.7	664
8	4.16	-9.08	0.09	0.67	6.75	498	24.9	2062
9	2.24	-2.24	0.37	0.67	4.64	247	12.4	350
10	7.92	-1.77	0.39	0.67	9.00	465	23.2	2398
11	1.90	-1.90	0.65	0.67	6.46	255	10.2	413
12	1.90	-1.90	0.65	0.67	6.46	255	10.2	413
13	4.57	-8.67	0.05	0.67	4.50	486	24.3	1313
14	0.00	-0.00	0.05	0.67	4.50	486	24.3	1313
15	0.00	-7.66	0.00	0.67	4.64	647	16.2	1196
16	3.13	-3.13	0.51	0.67	6.46	292	14.6	680
17	3.13	-3.13	0.51	0.67	6.46	292	14.6	680
18	3.66	-3.66	0.48	0.67	6.75	316	15.8	831

Table 9: Final dimensions for each member with the corresponding buckling & stress check.

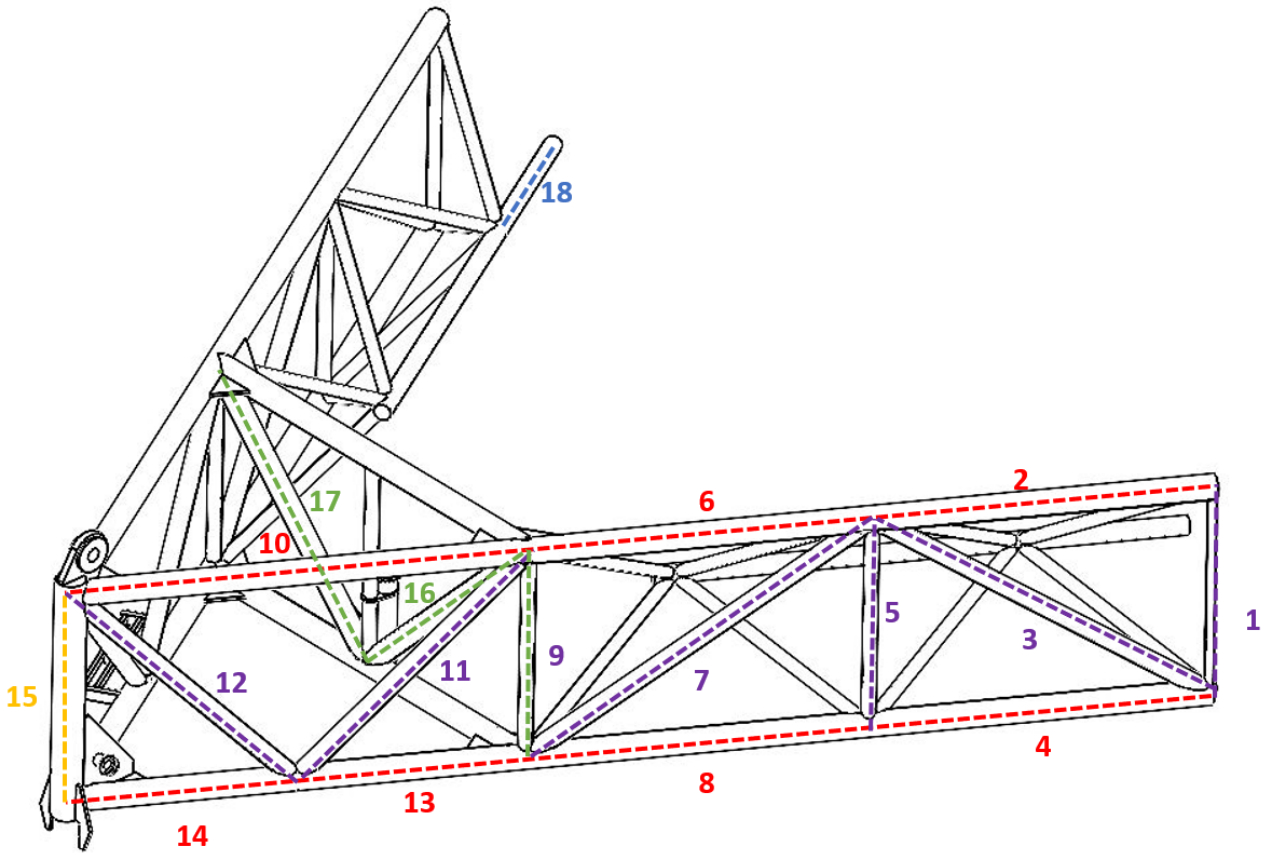

Figure 44: Frame numbering for each unique member

6.4.2 Padeye strength

The padeye size is of importance for the design of the SPIT to estimate the space required for the pad eye connections at the SPIT. The secondary padeyes on the SPs do not impact the design of the SPIT and are therefore not in this analysis.

The padeye check is analysed according to DNV-ST-N001 [5]. The strength of the padeye is checked on three aspects:

- Bearing pressure of the pin against the pin hole of the padeye
- Tear out of the sides of the padeye
- Cheek plate welds

There are two different padeye designs used for the SPIT design:

- **SPIT-crane connection:** The SPIT is connected to the crane by three padeyes located at the top edges of the SPIT frame. In Figure 30, a zoomed in view of on corned shows the location of the padeye. A standard shackle is used to connect the sling to the padeye. The sling is attached to a bridle and the bridle leads up to the crane hook. The shackle pin exerts the forces from the sling to the padeye.

  With the coupling method of the SPIT to the crane, proposed in section 4.1.1, the shackle only has to be removed from the padeye for maintenance during the installation of all the foundations at an OWF. A tight connection between the padeye hole and the pin is preferred as this positively impacts the bearing pressure. For this padeye, minimal side loads can be expected.

- **SP-SPIT connection:** The main padeye on top of the SP is used to connect with the pin-lock mechanism on the lower SPIT corner. Figure 21c in section 5.5 shows the location of the padeye on the stub. Figure 31 shows where the pin-lock mechanism is located. All the vertical forces during the lift sequence of the SP is transferred from the pin of the lock mechanism to the frame of the SPIT.

  The padeye is connected to the SPIT on deck and disconnected after a minimal penetration depth of the SP in the seabed. A loose connection between the padeye hole and the pin is required as slight misalignment can occur of the padeye and the locking mechanism during the installation procedure. For this padeye, minimal side loads can be expected as the constraints on the SP stub should compensate for the side loads.

In Appendix G, the padeyes are correctly dimensioned to satisfy the padeye checks. Tables 10a and 10b show the design load and final dimensions of each padeye. With these results can be estimated how much space is required on the SPIT around the padeyes. Both padeyes should be accessible for the offshore crew to perform maintenance or aid in connecting or disconnecting the padeyes. The accessibility to the padeyes are shown in Figure 30.

F_{sd}	4.99	MN	Maximum design load
D_{pin}	270	mm	Shackle pin diameter
D_H	281	mm	Padeye pin hole
t	300	mm	total thickness of the padeye
R_{pl}	422	mm	Radius of the mainplate
t_{pl}	150	mm	Thickness of the mainplate
R_{ch}	380	mm	Radius of the cheeckplate
t_{ch}	75	mm	Thickness of the cheeckplate

(a) SPIT-crane padeye

F_{sd}	2.26	MN	Maximum design load
D_{pin}	220	mm	Pin diameter
D_H	259	mm	Padeye pin hole diameter
t	188	mm	total thickness of the padeye
R_{pl}	336	mm	Radius of the mainplate
t_{pl}	80	mm	Thickness of the mainplate
R_{ch}	290	mm	Radius of the cheeckplate
t_{ch}	54	mm	Thickness of the cheeckplate

(b) SP-SPIT padeye

Table 10

6.4.3 Capacity of hydraulic cylinders

To perform certain actions done by the SPIT, hydraulic cylinders are used. For the design of these actions, three different hydraulic cylinder types are considered:

- **Lock mechanism:** The hydraulic cylinder in this mechanism pushes or pulls a pin through the padeye on the SP. The lock should always be able to be unlocked. The hydraulic cylinder should therefore exert sufficient force to the pin to overcome the frictional forces on the pin during operations. From the following equation, the friction force on the pin is estimated.

$$F_{friction} = F_{SP} \cdot \mu_{steel} \cdot = 3.34MN \cdot 0.15 = 0.75MN \tag{4}$$

F_{SP} is the normal force on the pin cause by the weight of the SP. The maximum static weight of the SP is $340mt$. This translates to a normal force of $3.34MN$. μ_{steel} is the steel-steel static friction coefficient. For a lubricated steel-steel contact the coefficient equals 0.15 [29]. A safety factor SF of 1.5 is considered. The resulting friction force $F_{friction}$ equals $0.50MN$. The required capacity of the hydraulic cylinder therefore becomes $51mt$. The required stroke of the cylinder is estimated for two times the thickness of the padeye. From Table 10b the thickness equals $190mm$. The required stroke therefore equals $380mm$.

- **Hydraulic ring:** The three cylinders in the ring constrain the SP stub at the upper and lower part by pushing the rods against the stub. The design load for the cylinders is the maximum force exerted from the SP stub to the ring. From section 6.4.1.1 follow that for the upper ring the load equals $8.71MN$ and the lower $6.38MN$. For practical reasons, the upper and lower ring have been made identical. The required capacity of the cylinders equals $888mt$. The stroke of the cylinders should be larger than the maximum tolerance margin to be able to release the SP stub for the retrieval of the SPIT on the seabed. From section 5.4 follows that the maximum tolerance margin of the grout connection equals $260mm$.

- **Individual pile lowering:** The hydraulic cylinder jacks up the SPIT against the SP to maintain horizontal. The cylinder design load should be higher than one-third of the weight of the SPIT and possible friction forces from contact with the SP stub and SPIT. From section 6.4.5, one-third of the weight of the SPIT equals $80mt$. The same equation applies for the friction force as equation 4. However, F_{SP} is now equal to the force exerted by the SP stub to the hydraulic gripper. Friction forces for both the upper and lower ring are considered. This results into the following equation for the required force for the cylinder:

$$F_{friction} = (F_{SP_{upper}} + F_{SP_{lower}})\mu_{steel} = (8.71 + 6.38)0.15 = 2.26MN \tag{5}$$

  The required capacity for the cylinder equals $80mt + 230mt = 310mt$. The cylinder requires a stroke of more than $1500mm$ to satisfy the design requirements regarding the maximum individual pile lowering height difference of $1.5m$.

Standard double acting hydraulic cylinders from ENERPAC [11] have been selected for this design based on the stroke and design load of the cylinder. Table 11 shows the specification of the three cylinder types. The 3D model presented in section 6.3 corresponds to the dimensions of the cylinders in Table 11.

	Capacity	Stroke	Height cylinder	Width cylinder	Weight	Description
Lock mechanism	60mt	380mm	670mm	180mm	41kg	RARH6010 extended
Hydraulic ring	1000mt	300mm	692mm	570mm	1236kg	HCR100012
Jack up	400mt	1500mm	2006mm	358mm	1225kg	RR40048 extended

Table 11: Hydraulic cylinder specifications

6.4.4 Installation tolerance of the SPs with the SPIT

In this section, the installation tolerance of the SPIT is analysed. The analysis checks the tolerances of each DOF of the SP and relates this to the installation tolerance of the SP stub.

In the first phase of the suction process, the SPs are constrained by the SPIT in all six DOF. Figure 24 shows the DOFs for the SP. These constraints have tolerance margins that result in the installation tolerance of the SPs. The yaw DOF does not contribute to the installation tolerance as the axis of rotation of the SP is considered to overlap with the centre axis of the stub. The other five DOF can be sorted in three groups that impact the installation tolerance of the SP:

- **Height of the SP (Heave):** After the installation of the SPs, the absolute height difference between the lowest and highest stub induces the tilt of the jacket structure. The jacket pin inside the SP stub tilts accordingly. This is rectified or amplified during the curement of the grout connection, by the use of pile stoppers. The installation tolerance of the pile stoppers results in a rotational misalignment and must be taken into consideration for the installation of the jacket. Figure 45 depicts how the tilt (α) of the jacket is induced by the height difference (δ) of the stubs and pile stoppers. The length between the stubs (L) will determine the magnitude of the tilt that is induced by the height difference of the stubs.

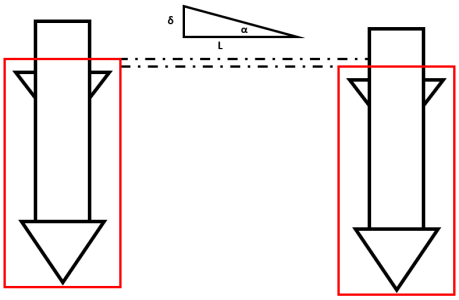

Figure 45: Tilt induced by height difference of the SP stubs

- **Horizontal misalignment of the SP (Surge and sway):** The hydraulic gripper mechanism allows for horizontal translation adjustments. The accuracy of the adjustments depends on the controllability of the hydraulic cylinders and the measuring tools used to measure the horizontal position of the SP. The resulting tolerance δ is depicted in Figure 46.

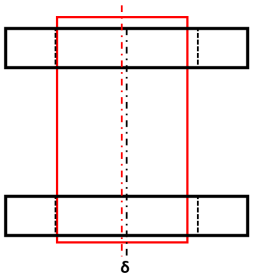

Figure 46: Horizontal misalignment of the SP stub in the SPIT

- **Rotational misalignment of the SP (Pitch and roll):** The hydraulic gripper mechanism also allows for rotational translation adjustments. Figure 47a shows how rotational misalignment of the SP stub is caused by the grippers. The accuracy of the adjustments depends on the controllability of the hydraulic cylinders and the measuring tools used to measure the horizontal position of the SP. After a certain penetration of the SPs, the loads from the soil will become too large to compensate with the hydraulic grippers. When this penetration level is reached cannot be determined by the results from section D. A conservative estimate is taken that directly after contact on the seabed by the SPs, the hydraulic grippers will not be able to adjust the tilt of the SPs. The resulting misalignment is displayed in Figure 47b.

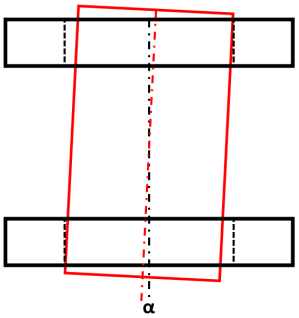

(a) Rotational misalignment of the SP stub in the SPIT

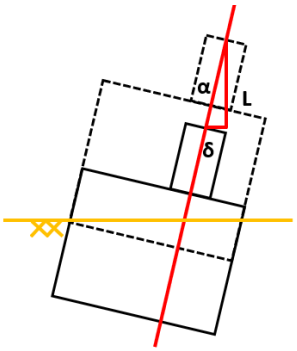

(b) Resulting installation tolerance caused by the misalignment of the SP stub in the SPIT. The black dotted line highlights the initial position of the SP in the seabed. The solid black line highlights the position after PTG is reached.

Figure 47: Rotational misalignment of the SP stub in the seabed

The fabrication tolerances of the SPIT do not have to be considered since the hydraulic grippers can adjust

for this. In Appendix H, the installation tolerances are analysed in detail. Table 12 shows the results of the installation tolerances and the final remaining gap between the JP and the SP stub. From the data can be concluded that the installation tolerance of the SPIT is sufficient.

	Installation tolerance	Total tolerance	Tolerance margin
Upper clash	55mm	147mm	242mm
Lower clash 1	78mm	170mm	232mm
Lower clash 2	51mm	164mm	250mm

Table 12

6.4.5 Weight of the SPIT

The required lift capacity of the installation vessel is dependent on the weight of the SPIT. In this section, the weight of the SPIT is estimated. The members of the SPIT frame make up the largest part of the weight of the SPIT. Since the members are hollow, three different weight cases are looked at:

- **Dry weight:** The weight of the SPIT out of the water. This is calculated according to the following equation:

$$M_{dry} = \sum_{n=1}^{18} \frac{D_n^2 - (D_n - 2T_n)^2}{4} L_n \pi \rho_{steel} N_n \tag{6}$$

  The diameter D_n, thickness T_n, length L_n and number of members in the frame N_n are displayed in Table 13. The used density steel ρ_{steel} equals $7850 m^3/kg$ [29].

- **Submerged weight with flooded members:** The weight of the SPIT when fully submerged in the water. The hollow cylinders are flooded with water. The buoyancy force on the SPIT reduces the weight of the SPIT. However, added mass caused by the enclosed water should be taken into account for dynamic calculations or when the SPIT is retrieved. The submerged flooded weight and the added mass are calculated according to the following equations:

$$M_{subF} = \sum_{n=1}^{18} \frac{D_n^2 - (D_n - 2T_n)^2}{4} L_n \pi (\rho_{steel} - \rho_{water}) N_n \tag{7}$$

  and

$$A_{water} = \sum_{n=1}^{18} \frac{(D_n - 2T_n)^2}{4} L_n \pi \rho_{water} N_n \tag{8}$$

- **Submerged weight with non flooded members:** The weight of the SPIT when fully submerged in the water. The hollow cylinders are sealed, creating large pockets of air. This results in a high buoyancy forces on the SPIT, reducing the weight of the SPIT. The buoyancy forces can cause the SPIT to float in the water, creating slack in the crane wire. This is not preferred for a lift operation [5]. The submerged mass of the SPIT is calculated according to the following equation:

$$M_{subNF} = \sum_{n=1}^{18} \left(\frac{D_n^2 - (D_n - 2T_n)^2}{4} L_n \pi \rho_{steel} - \frac{D_n^2}{4} L_n \pi \rho_{water} \right) N_n \tag{9}$$

For each member, the dimensions and the corresponding weights are shown in Table 13.

The total weight of the SPIT is the summation of all parts of the SPIT. In Table 14, all the parts adding to the weight of the SPIT frame are displayed. For the submerged weight estimations it is assumed that, beside the frame of the SPIT, each part is solid. The convergence rate (CR) for dry weight to submerged weight is:

$$CR = \frac{\rho_m - \rho_{water}}{\rho_m} \tag{10}$$

Where ρ_m is the density of material considered for each part and ρ_{water} the density of the water. The final results are also shown in Table 14. The data of the submerged weight of the SPIT with no flooded members indicate a negative submerged mass. This indicates that the SPIT will float on the water. This should be

	L[m]	D[mm]	T[mm]	M_{dry}[kg]	M_{subF}[kg]	A_{water}[kg]	M_{subNF}[kg]	N
1	4.64	193	9.7	214	186	113	-508	18
2	6.75	494	24.7	2030	1765	1074	-654	6
3	8.19	339	9.7	664	577	674	-1573	6
4	6.75	498	24.9	2062	1793	1090	-643	6
5	4.64	193	9.7	214	186	113	-508	18
6	6.75	477	23.8	1892	1645	1000	-699	6
7	8.19	339	9.7	664	577	674	-1573	6
8	6.75	498	24.9	2062	1793	1090	-643	6
9	4.64	247	12.4	350	304	185	-574	6
10	9.00	465	23.2	2398	2085	1268	-970	9
11	6.46	255	10.2	413	359	285	-911	6
12	6.46	255	10.2	413	359	285	-911	6
13	4.50	486	24.3	1313	1141	694	-449	9
14	4.50	486	24.3	1313	1141	694	-449	9
15	4.64	647	16.2	1196	1040	1409	-1219	3
16	6.46	292	14.6	680	591	360	-839	3
17	6.46	292	14.6	680	591	360	-839	3
18	6.75	316	15.8	831	723	440	-886	18
Weight frame:				138840	120705	80428	-108821	

Table 13: Results from the weight calculations for each member

avoided during lift procedures. The members in the frame should therefore be partially or fully flooded in order to avoid slack in the sling.

Description	Mass in mt	Based on
Total weight of all members of the frame	140	Section 6.4.5
Added steel to improve structural strength of frame	35	25%M_{dry} [39]
Total weight of all cylinders and corresponding equipment	20	Section 6.4.3
Total weight of all pumps and corresponding equipment	10	SPT-offshore [39]
Total weight of all walkways and ladders on the SPIT	35	25%M_{dry} [39]

Dry weight of the SPIT	240
Submerged weight of the SPIT with flooded members	230
Submerged weight of the SPIT with no flooded members	-20

Table 14

6.4.6 Crane curve Orion

The crane curve of the Orion shows the plots of the vertical lift capacity and lifting height over the lifting radius of the crane. This plot is used to indicate if the crane has the required lift height and capacity for the installation operations of the SPs with the SPIT. In Figure 48, the crane curve of the Orion is displayed. This curve corresponds to offshore conditions where maximum crane capacity can be used and is taken from the ScotWind design report [10].

The crane capacity is checked for the use of the main hoist of the Orion. For the considered case study, the estimated weight of SP is $340mt$ and the estimated weight of the SPIT is $240mt$. The corresponding estimated submerged weight of the SP equals $296mt$ and the estimated maximum submerged weight of the SPIT is $230mt$. The dry weight of the SPIT and SPs equals $240 + 3 \cdot 340 = 1260mt$. The submerged weight of the SPIT and SPs equals $1118mt$. The dynamic responses during the lift operation should be considered. For the lift operation in air the DAF equals 1.15 [5]. For subsea lifts, the DAF requires analysis that is outside the scope of research for this thesis. A conservative DAF of 2.0 is considered [12] [14]. The required lift capacity (C_{req}) is calculated with the following equation:

$$C_{req} = SHL \cdot DAF \tag{11}$$

Where SHL is the static hook load. The SHL is different for lift operations in air compared to completely submerged. The SHL for lift operations in air equals the dry weight. The SHL for lift operations for submerged

conditions equals the submerged weight. The maximum required lift capacity results from the submerged conditions and equals $1118 \cdot 2.0 = 2234mt$. The added weight of the rigging is considered 4% [27] of the weight of the SPIT and SPs and equals $50mt$. The necessary lifting radius is estimated to be below $50m$. From the crane curve in Figure 48 can be concluded that the capacity of the Orion is sufficient.

It should be noted that the capacity of the crane decreases by the following two factors:

- When Tuggerlines are used the vertical lift capacity of the crane decreases. The horizontal forces that the tuggerlines exert on the SPIT will be transferred to the crane, increasing the loads on the crane. The vertical lift capacity is reduced to not exceed the maximum loads on the crane. The magnitude of the forces exerted by the tuggerlines depend on the required damping. For calm weather conditions, the tuggerlines exert minimal forces on the SPIT.
- Environmental conditions might change the dynamic behaviour of the Orion and the SPIT. In order to ensure the stability of the vessel the maximum lift capacity is reduced accordingly.

These factors should be taken into account when analysing the workability. This analysis is outside the scope of this thesis. However, for the installation of multiple foundations, a limited workability will have a significant impact on the cost of the installations. The SPIT is designed for multiple foundation installation purposes and therefore, the workability is of concern. From the crane capacity in Figure 48 can be concluded that there is room for a decrease in vertical capacity of the crane. Therefore, in less optimal weather conditions the installation sequence can still proceed. The exact weather conditions that provide the limitations of the installation of the SPIT and SPs requires future research.

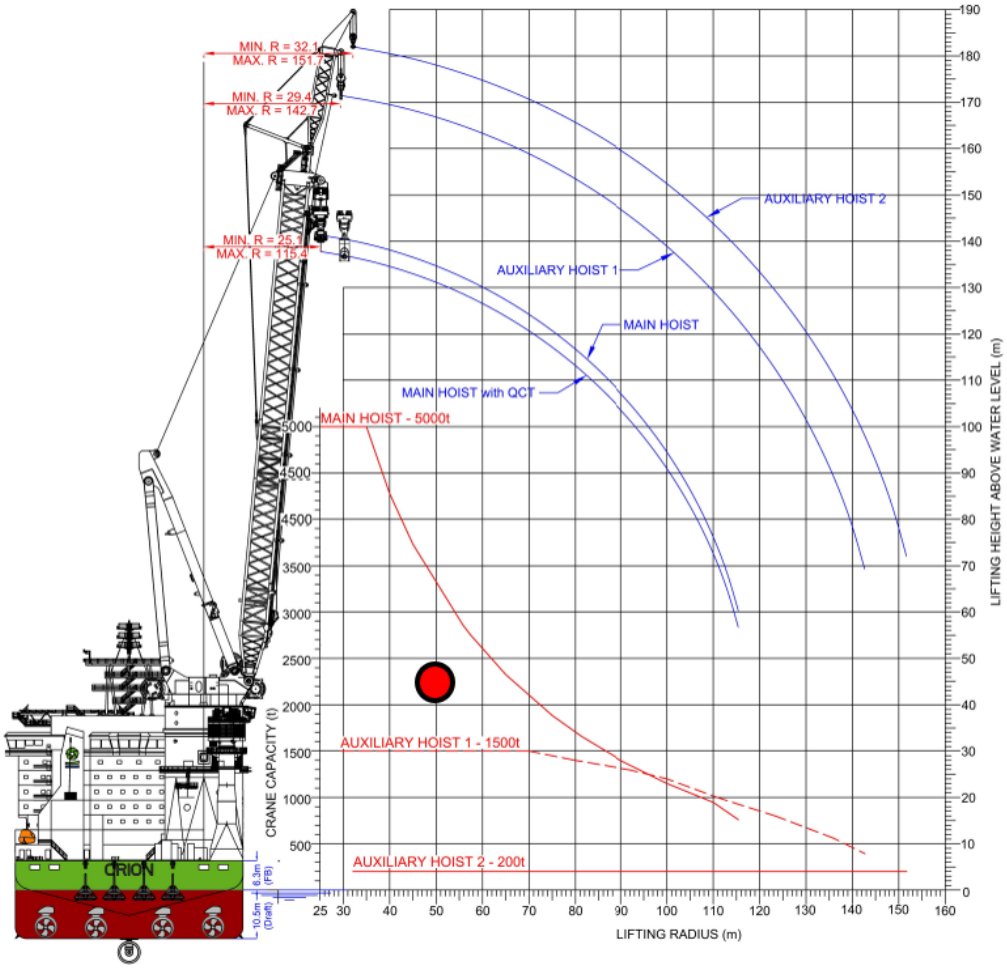

Figure 48: The crane curve of the Orion for standard lifts in optimal weather conditions. The dot indicates the required crane capacity for the SPIT and SPs.

6.5 Answer to the research questions

This section gives an overview of the conclusions following the results of Chapter 6. This is done by answering the third sub research question. The main research question is also answered based on the conclusion of the sub research questions from Chapters 4 and 5.

6.5.1 Sub-research question 3

In this Chapter, the design of the SPIT is visualised. All proposed design requirements in section 6.1 have been included in the design of the SPIT. The answer to the third sub-research question results from the findings.

> **3: How will the design of an installation template for pre-installation of the suction pile foundation for jackets satisfy the design requirements to perform safe offshore operations at a representative OWF?**

Answer: The design choices proposed in section 6.2 provide the SPIT with the necessary features to satisfy for the stated design requirements in section 6.1. The checks performed in section 6.4 justify the design requirements considering the:

- Strength of the frame and important features on the SPIT
- Installation precision of the SPs with the SPIT
- Required crane capacity for the installation sequence

The SPIT design loads that are used for the checks consider the following load cases:

- Horizontal loading of the SPs through the splash zone
- Horizontal loading of the SPIT through the splash zone
- Vertical loading of the crane when the SPIT is submerged
- Horizontal loading of the SPs in the seabed

These load cases are predicted to result in the leading load cases of the design of the SPIT. However, this should be justified by more extensive load analyses in future research of the SPIT. In addition, the claim that the features of the SPIT will perform as intended, requires justification from future research as well.

6.5.2 Main research question

With the help of the three sub-research questions, the answer to the main research question can be answered in more detail. The answer to the main research question is based on the findings in Chapters 4. 5 and 6.

> **What are key design challenges of a suction pile installation template that is used as an installation tool for suction pile jackets for a representative OWF?**

Answer: The main key design challenge of the SPIT is to install the SPs within the required tolerance margins. This design challenge can be separated into three parts. Each part uncovered other key design challenges:

- **SP installation method:** A key design challenge is to figure out how the SPs are connected to the SPIT and the SPIT to the crane. The method of connecting the SPs to the SPIT during the installation sequence determines the layout of the SPIT and how the loads are transferred from the SPs to the SPIT and the crane.

  The proposed installation method is explained in detail in section 6.2 based on the installation sequence in 4.1.2.2. The limitations of this method are based on:

  - The capacity of the installation vessel: The required deck-space and lift capacity of the installation vessel might exceed the capacity of the installation vessel.
  - The practical effectiveness of the proposed method: The measures to constrain the SPs and adjust the SP tilt might, in practice, result in unfavourable consequences. For example, high jamming forces occurring when objects clash during the installation sequence or lower installation precision of the SPIT.

- **Installation tolerance:** A key design challenge is to identify the required installation precision of the SPs with the SPIT. The connection method of the jacket frame and SPs relate to the required installation precision necessary for the SPs by the SPIT.

  The proposed method is explained in detail in section 5. The limitations of this method is based on the practical dimensions of the grouted connection. Therefore, the required installation precision of the SPIT cannot be increased to infinity. The grouted connection demands a certain precision that should be analysed as the installation precision of the SPs is used as an important input for the design requirements of the SPIT.

- **Design loads:** A key design challenge is to identify the SPIT design loads. The magnitude of the loads determines the required size for the SPIT and equipment. This is to ensure the safety throughout the installation sequence and also a precise installation of the SPs.

  The limitations of the performed analyses to estimate the SPIT design loads in section 6.4 are based on the scope of the analyses. The considered load cases in this Chapter only analyse a limited part of the installation sequence. The considered load cases are expected to be the governing load cases, however, this should be justified by future research. It could be that a governing load case has been overlooked.

7 Discussion

Results of the SPIT design requirements check can be questioned on its validity. This can be caused by wrong assumptions or inaccurate models. This Chapter reflects on the most critical results gathered throughout this thesis.

7.1 Hydrodynamic loads on SP

For the hydrodynamic load calculations on the SP, three assumptions are made:

- **Wave load conditions on the SP can be simplified by taking a single wave:** The design requirement of the SPIT states that the SPIT is operable in waves with a $3m$ significant wave height. Therefore, the analysis is performed for waves with a wave height of $3m$ and a design envelope of the wave period from $5 - 20s$. This is based on the metocean data in Appendix I. Since the SP is dominated by hydrodynamic inertia forces, only the acceleration of the wave kinematics is of importance. The smallest wave periods produce the highest accelerations and therefore $T = 5s$ results in the leading load case. This impacts the following two assumptions.
- **The Morison equation can be used for the load estimation:** This assumption is true for two requirements:
  - The analysed member is slender compared to the wave length. For a cylindrical member this would result in a ratio of $D/\lambda \leq 0.2$.
  - The analysed cylindrical member is sufficiently long that the tip effects are negligible.

  For the calculated load case in section 6.4.1.1 ($H_s = 3m$ and $T_s = 5s$), both requirements are not satisfied. However, the research does indicate that if these requirements are not satisfied, the estimated loads are conservative.
- **The SPIT is considered as a fixed structure:** Tuggerlines are used to restrict horizontal motions and rotate the lifted object during crane operations. However, in order to avoid large line tensions in the tuggerlines, the object is not rigidly fixed in place. Therefore, small horizontal motions of the lifted structure are possible. The absolute acceleration between the waves and the structures will be lower as the structure is allowed to move with the wave, reducing also the hydrodynamic load on the SPs. The assumption that the SPIT and SPs are fixed, results in a conservative load estimation.

These assumptions lead to results that will differ from the actual loads on the SP and SPIT. From reasoning of the used assumptions can be concluded that the performed analysis results in conservative estimates. More detailed hydrodynamic load calculations should indicate lower loads on the SP and SPIT.

7.2 Geotechnical analysis

For the SPIT design load estimation, the calculated load cases on the SP during the suction process are not considered governing for the SPIT design. The stated reasons in section D explain the arguments on why it is not considered in this thesis. If future research would indicate that this load case should not be ignored, the members of the frame would require approximately three times more steel to satisfy the structural design requirements. This would result in an estimated increased weight of the SPIT from $240mt$ to $720mt$. The crane curve of the Orion in section 6.4.6 suggest that the required capacity would not exceed the crane capacity of the Orion. The increased weight of the SPIT does not require a change in the installation strategy of the SPIT method.

During the installation of the SPs in the seabed, the soil around the SPs is deformed. When the SPIT is retrieved, the absence of the loads on the SPs by the SPIT allows the elastic deformation of the soil to push the SPs back. Depending on the magnitude of deformation and elastic behaviour of the soil, this movement of the SPs can result in a significant impact on the installation tolerance of the SPs. However, this requires research outside of the scope of this thesis. Future research should analyse the magnitude of the movement of the SP caused by the elastic properties of the soil.

7.3 Weight and structural strength of the SPIT

For the sizing of the members in the SPIT frame, only a single WSD safety factor is considered. This will result in different loads not adjusted according to their load type. The estimated size of the members in the frame should be considered with care to its limitations. According to the crane curve in section 6.4.6, the weight of the SPIT can significantly be increased without exceeding the crane capacity of the Orion. This will reduce the workability of the SPIT. The loads on the members of the SPIT can increase by correctly adding and adjusting the following aspects to the considered loads, analysed in this thesis:

- Fatiguing of the members and joints
- Shear on the members
- Hydrostatic pressure on the members
- Bending on the members

7.4 Jamming forces on the SPIT-SP connection

The design of the SPIT-SP connection is designed to constrain the SP during the installation of the SPs in the seabed. When the SPIT should be retrieved from the seabed, the constraints are lifted. However, if the misalignment of the SPs in the seabed cause the SP to clash with the SPIT, friction between the SP and the SPIT will cause jamming forces. These jamming forces can result in damaging the SPs and the SPIT or the SPIT might not be able to be retrieved from the seabed. Therefore, the hydraulic grippers are selected for the design of the SPIT.

The hydraulic grippers have added to the complexity of the design of the SPIT. A less complex solution is to constrain the SP stubs without the hydraulic cylinders. The hydraulic gripper is changed to a static steel ring. The gap between the SP stub and the ring is reduced. The induced tilt of the SP by the gap should be accepted for the installation tolerance. If the jamming forces on the SP stub and the rings in the SPIT are below the required force for the SPIT to be retrieved from the SP stub, this solution has potential. However, the lack of understanding of how the SP will behave in the soil with the SPIT, prevents the integration of this solution. Future research that provides a better understanding of the SPs in the soil with the SPIT will help to determine this design choice.

7.5 Top-plate grouting

The individual lowering of the SPs into the seabed is assumed to make the top-plate grouting procedure obsolete. This is assumed because the SPs should now be able to lower the SP to the seabed until the inside of the top-plate is in contact with the seabed. In practice, this can be hindered by:

- **Uneven seabed inside the SP:** If the seabed inside the SP is unevenly leveled, the pump inlet can be blocked by the seabed while most area of the top-plate is not yet in contact with the seabed. Insufficient bearing capacity of the SP on the soil can result from this.
- **Insufficient pump capacity:** If the pump capacity is insufficient to lower the SP to the PTG, the top-plate of the SP does not make contact with the seabed. Insufficient pump capacity is caused by unexpected high soil resistance on the SP. This can be caused by wrongly interpreted data from geo-surveys or an oversized design of the SP.

If the SP top-plate is unable to make sufficient contact with the seabed, top-plate grouting should still be considered.

Current research on the necessity of top plate grouting performed by SPT-offshore [39] indicates that for undrained soil types, top-plate grouting can be neglected. If this research can be translated to full-scale practice, the feature of individually lowering SPs by the SPIT can be removed from the design. This results in a reduced weight and cost of the SPIT.

7.6 Orion as installation vessel

The total estimated dry weight of the SPIT ($240mt$) and the three SPs ($3x340mt$) is $1260mt$, resulting from section 6.4. Multiple installation vessels of the DEME fleet are checked in their capacity for the SP installation with the SPIT. Two aspects should be taken into consideration for the required capacity of the installation vessel:

- **Offshore workability:** The difference between the maximum lift capacity and the required lift capacity for the SPIT indicates the offshore environmental condition window. A larger offshore condition window results in an improved workability for the installation vessel. The maximum significant wave height, the SPIT is designed for, is based on the maximum significant wave height design requirement for most pre-piling templates [8]. From the design check, the crane curve of the Orion is sufficient for the design conditions. The maximum wave height condition can be lowered if smaller installation vessels are preferred over the Orion.
- **deck-space:** The required deck-space on the installation vessel for the SPIT is equivalent to the footprint of the SPJ. Extra SPs can be stored on deck to perform multiple installation sequences offshore. Jack-up vessels have a typical lower available deck-area compared to floating installation vessels because of the jack-up legs. From this case study, the footprint of the SPJ approximates $50x45m$, resulting in an estimated required deck-space of $1300m^2$. The minimum width of the SPJ footprint might already exceed the width of the deck of the installation vessel. If required, the deck of the installation vessel can be extended to fit the required footprint of the SPIT. The estimated deck-space required for the SP, considered in this case study, is $220m^2$.

In the current DEME fleet, seven installation vessels are available [15]. In Table 15, the installation vessels are shown with the maximum crane capacity and deck area.

Name:	Type:	Crane capacity [mt]:	Deck area [m^2]
Apollo	Jack-up	800	2000
Innovation	Jack-up	1500	3400
Neptune	Jack-up	600	2000
Orion	Floating DP3	5000	8000
Sea challenger	Jack-up	1600	3350
Sea installer	Jack-up	1600	3350
Green Jade	Floating DP3	4000	8000

Table 15: DEME installation vessels

From the crane capacity of the installation vessels in Table 15 can be concluded that the Apollo and Neptune have insufficient crane capacity. The Innovation, Sea challenger and Sea installer have the lift capacity to lift the SPIT with the SPs. The deck area of the three vessels has the potential to transport SPs for three installations. Jack-up vessels require more time to position the vessel on-site with respect to floating installation vessels. The increased preparation time of jack-up vessels is disadvantageous for the cost of the installation procedure. From this can be concluded that the jack-up installation vessels in the DEME fleet are not preferred for the installation of SPs with the SPIT.

The Orion and Green Jade are similar in dimension. The lift capacity of the Green Jade is lower, but should still be able to perform the lift operations. Since both vessels operate in different locations in the world, the SP dimensions can vary greatly. The hard soils, generally found at the North Sea seabed, translates to SP ratios of $L/D \approx 1$, whereas the seabed in Asia is generally softer, resulting in SP ratios of $L/D > 1$. The SPs in soft soils require more steel than hard soils. More lift capacity is required to lift the SPs and SPIT. On the other hand, the SPs in soft soils have a smaller footprint than SPs in hard soils. The number of installation sequences in one trip can be increased.

8 Conclusion

The results from this thesis indicate that the proposed design of the SPIT provides a solution to extent the installation of SPJ for OWT. The research identifies four key design challenges. The main design challenge is to install the SPs with the SPIT within the required tolerance margins. This challenge uncovered three additional key design challenges:

- Figure out how the SPs are connected to the SPIT and the SPIT to the crane.
- Identify the required installation precision of the SPs with the SPIT.
- Identify the SPIT design loads.

In this thesis, the provided tools to complete each challenge has its limitations and should be considered for a future SPIT design. However, each challenge indicates solvable obstacles to the design of the SPIT. This is because the required crane capacity for the SPIT and installation tolerance of the SPs with the SPIT have a significant margin for error.

The design of the SPIT is visualised and can be seen in section 6.3. The SPIT is designed as a lifting tool for three SPs and has integrated features to support the installation of the SPs on the seabed. Integrated pump systems in the SPIT reduce the required lift operations to attach and remove the pumps from the SPs. The SPIT is designed to allow for individual pile lowering to make top-plate grouting redundant. The installation precision of the SPs with the SPIT is ensured by the hydraulic grippers on the SPIT. These grippers constrain the stub and adjust the misalignment of the SPs before and after contact with the seabed.

From the considered load cases can be concluded that the governing load cases of the SPIT occur when the SPIT is suspended in the air or in the water by the crane. The maximum reaction forces from the soil on the SPs during installation indicate that it can become a governing load case. However, it is estimated that these maximum reaction forces can be avoided. The design of the SPIT can benefit from a more detailed understanding of the interaction of the SPs and the SPIT on the seabed to justify or rectify this claim.

The dry weight of the SPIT is estimated at 240mt. The total dry weight of the SPIT and SPs is estimated to be $1260mt$. The required crane capacity for the SPIT and SPs does not exceed the crane capacity according to the crane curve of the Orion. The maximum deck-space area of the Orion is sufficient for the SPIT and 39 SPs. This translates to 13 foundations that can be installed on a single trip by the Orion.

9 Recommendations

The research described in the master thesis has taken the first step into detailing the SPIT method. Further research is necessary to develop the installation method and justify the claims in this thesis. The following recommendations are made for further research on the SPIT installation method.

9.1 SPIT functions

The functions of the SPIT result in the proposed installation sequence of the SPs with the SPIT. The functions of the hydraulic grippers are key to the success of the SPIT design. The design of the integrated pumps and individual pile lowering are also important functions that have impact on the design of the SPIT. Further research should provide evidence that the proposed functions, in practice, will perform according to the claims made in this thesis. Model testing can help justify the performance of the functions of the SPIT.

9.2 Detailed load analyses

The structural design of the SPIT, in this thesis, is based on limited models and assumptions. Further research is required to justify or rectify the proposed design. Future research in the following topics will improve the understanding of the SPIT design loads:

- Dynamic responses of the SPIT and the SPs during the lift operation
- Geotechnical analysis of misalignment adjustment of SPs in the seabed
- Load distribution through the members and features of the SPIT

More detailed load analyses can be provided by research based on software programs. OrcaFlex can be used to simulate the dynamic responses of the SPIT and SPs. Plaxis can be used for the geotechnical analysis of the SPs. Various FEM programs can be used to identify the load distribution through the SPIT.

9.3 Commercial feasibility

The use and estimated dimensions for the SPIT has indicated the potential of the SPIT installation method. It remains to be seen whether this method will be implemented on large scale. This will depend on the commercial feasibility of the installation method. To estimate the commercial feasibility, further research on the following topics can be considered:

- Workability of the SPIT: Weather conditions for the installation sequence determine if the installation can proceed. In what weather conditions the installation can proceed determines the workability of the SPIT. This is an important factor to consider for the installation time of the foundations.
- SPIT-SPLIT cost comparison: The closest competitor of the SPIT installation method is the split jacket. A cost comparison will indicate which method of installation and when each installation method is more commercially beneficial.
- Reusability of the SPIT: During the lifetime of the SPIT, the frame requires maintenance. The added cost of maintenance and downtime impacts the commercial success of the SPIT. To increase the use of the SPIT, the SPIT or parts of the SPIT, might be reused for other projects. For the recycled parts, structural fatigue will play a more dominant role in the design of the SPIT.

References

[1] Natalia Aleksandrova. Scour protection using artificial vegetation, 2017.

[2] DNV AS. Dnv-rp-h103 modelling and analysis of marine operations, 2011.

[3] DNV AS. Dnvgl-rp-0419 analysis of grouted connections using the finite element method, 2016.

[4] DNV AS. Dnv-rp-n103 modelling and analysis of marine operations, 2017.

[5] DNV AS. Dnv-st-n001 marine operations and marine warranty, 2018.

[6] DNV AS. Dnvgl-st-0126 support structures for wind turbines, 2018.

[7] DOT BV. Slip joint offshore research, 2016.

[8] CATAPULT. *Guide to an offshore wind farm.* The Crown Estate and Offshore Renewable Energy Catapult, Swindon, 1st edition, 2019.

[9] CDWE and COWI. Hai long owf wtg jacket feed design report, 14mw. Technical Report A134331, COWI A/S, Kongens Lyngby, 2020.

[10] DEME Concessions Wind. Jacket benchmark design for site e3, w1 and n1. Technical Report 2020.00632, DEME Offshore, Zwijndrecht, 2020.

[11] ENERPAC. Hydraulic cylinders and jacks https://www.enerpac.com/en-gb/products/gbcylindersandjacks.

[12] Ocean Marine Engineering. Calculation of hydrodynamic effects on structures during lifting through the splash zone http://oceanmarinengineering.blogspot.com/2014/12/calculation-of-hydrodynamic-effects-on.html, 2014.

[13] International Organization for Standardization. Iso 19902 petroleum and natural gas industries — fixed steel offshore structures, 2020.

[14] Victor Giurgiutiu. *Vibration of solids and structures.* Academic press, 2008.

[15] DEME Group. Deme technology https://www.deme-group.com/technology, 2023.

[16] DEME Group. Green jade announcement https://www.deme-group.com/news/revolutionary-offshore-installation-vessel-green-jade-joins-fleet-landmark-moment-taiwans, 2023.

[17] DEME Group. Orion technology specifications https://www.deme-group.com/technologies/orion, 2023.

[18] GWEC. Gwec home webpage, https://gwec.net/.

[19] Leo H. Holthuijsen. *Waves in oceanic and coastal waters.* Camebridge university press, 2009.

[20] Mark Hutchinson and Feng Zhao. Global wind report 2023. Technical Report 1, Global Wind Energy Council, Brussels, Belgium, 2023.

[21] IADC. Subsea rock installation, 2019.

[22] Buhr Ingo. De102012021001a1 verfahren und vorrictung zum herstellen einer gründung für offshore-windenergieanlagen, 2013.

[23] IRENA. Irena home webpage, https://www.irena.org/.

[24] Zhiyu Jiang. Installation of offshore wind turbines: A technical review, 4 2021.

[25] J M J Journée and W W Massie. *Offshore hydromechanics Second Edition.* 2008.

[26] Hermann Kaps and Julia Petzold. *Heavy knowledge.* SAL engineering, 2021.

[27] Li Liang. Heavy lift installation study of offshore structures, 2004.

[28] Alan John MacLeay, Trevor Hodgson, and SNC Lavalin Atkins. Beatrice offshore wind project, wind turbine generator foundation design, 2019.

[29] Mikrocentrum. *Formuleboekje*. werktuigbouw.nl, 8e editie.

[30] Walter Musial et al. Offshore wind market report: 2021 edition. Technical Report 1, National Renewable Energy Laboratory, Denver, USA, 2021.

[31] Charles W. Nelson. Us2018/0195250a1 modular offshore wind turbine foundation and modular substructure with suction caissons, 2018.

[32] Standard Norge. Norsok m101 structural steel fabrication, 2017.

[33] Jorss Blunck Ordemann. Monopile foundations with flanged connections, 2023.

[34] Ramboll. Moray offshore wind east limited grouted connection tolerances. Technical Report 5413-RAM-DS-RPT-14008, Ramboll, Copenhagen, 2018.

[35] Safelifting. Gn h14 wide body shackle 1000 ton https://safelifting.eu/heavy-lifting-equipment/lifting-equipment/shackles/gn-h14-wide-body-shackles-shackles/gn-h14-wide-body-shackle-1000-ton/.

[36] Safelifting. Gp p-6036 heavy duty shackle 800 ton https://safelifting.eu/heavy-lifting-equipment/lifting-equipment/shackles/gp-p6036-heavy-duty-shackles-shackles/gp-p-6036-heavy-duty-shackle-800-ton/.

[37] Frøydis Solaas and Peter Christian Sandvik. Hydrodynamic coefficients for suction anchors during installation operations. 2017.

[38] Ka Young Song, Young Suk You, and Min Young Sun. Ultimate load transfer characteristics of a typical grouted connection used in the monopile foundations of offshore wind turbines. *Ocean Engineering*, 260, 9 2022.

[39] SPT-Offshore. Equipment introduction content, 2022.

[40] Oil States. Hydra-lok ™ connections, 2022.

[41] Rene Thijssen, Robert Jan van Zijl, and Wout Luites. 2021888 suction bucket template, 2020.

[42] Carbon Trust. Offshore wind accelerator suction installed caisson foundations for offshore wind: Design guidelines, 2019.

[43] Jan Vugts. *Handbook of Bottom Founded Offshore Structures*. 2. Eburon Academic Publishers, 2016.

[44] Jan Vugts. *Handbook of Bottom Founded Offshore Structures*. 1. Eburon Academic Publishers, 2016.

[45] Wang Xuefei, Xiangwu Zeng, Jiale Li, Xu Yang, and Haijun Wang. A review on recent advancements of substructures for offshore wind turbines. *Energy conversion and Management*, 158(7):103–119, 2018.

[46] Puyang Zhang, Hongyan Ding, and Conghuan Le. Model tests on tilt adjustment techniques for a mooring dolphin platform with three suction caisson foundations in clay. *Ocean Engineering*, 73:96–105, 2013.

A Suction pile stub analysis

DNVGL-ST-0126 [6] provides a standard code for the design of grout connections. With the help of these standards the stub of the SP can be sized. Figure 49 shows the schematic of a pre-piled jacket-pile connection. This connection type can be used for the jacket-SP connection as well.

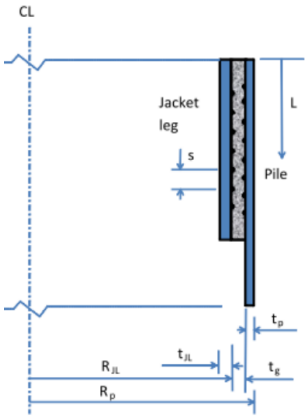

Figure 49: Schematic of the grout connection of a pre-installed pile with a jacket leg

A.1 Design maximum loads

The design loads are based on a grouted connection of the Hai long internal design report [9]. The offshore foundations are designed for $14MW$ ($222m$ rotor diameter) turbines with a hub height of $145mLAT$ and a water depth of $56mLAT$ for offshore conditions in the Formosa Strait west of the coast of Taiwan. For the SPIT calculations, a $18MW$ ($260m$ rotor diameter)turbine with a hub height of $145mLAT$ and a water depth of $70mLAT$ located in the North-Sea east of Scotland is required. The loads are estimated by a linear interpolation scale factor of the turbine diameter with the following equation:

$$\alpha = \frac{D_{18MW}}{D_{14MW}} \approx 1.2 \tag{12}$$

The maximum loads for the grout connection for the SPIT result in the following:

Design loads:	**Axial** P_{ad}	**Bending** M_d	**Shear** Q_d
Hai Long	46.4MN	60.0MNm	8.3MN
ScotWind	55.8MN	72.0MNm	10.0MN

A.2 Design capacity

If the grout capacity is sufficient for the design loads, two different checks should be done regarding:

- Axial capacity
- Nominal radial contact pressure

Due to the heavy fatigue conditions of the grout connection, a 20% reserve is taken into account for the design capacity of the grouted connection. This results in a utilization factor of the design loads that should be 0.8 or lower. The utilization factor for the axial pressure can be calculated with the following equation:

$$UC_{ax} = \frac{F_{design}}{F_{max}} < 0.80 \tag{13}$$

Where F_{design} is the design load per unit length along the circumference of one shear key and F_{max} the characteristic capacity per unit length of one shear key. The utilization factor for the axial pressure can be calculated with the following equation:

$$UC_{pressure} = \frac{\rho_{nom}}{1.5MPa} < 0.80 \tag{14}$$

Where ρ_{nom} is the design nominal radial contact pressure and the $1.5MPa$ is a fixed number as the maximum contact pressure capacity. The equations from DNVGL-ST-0126 [6] results in a conservative estimate of the necessary dimensions of the grout connection. FE analyses according to DNVGL-RP-0419 [3] can be performed to result in less conservative estimates, however, for this analysis, the standard validity checks will be used.

A.3 Grout thickness relation

The SP stub is optimised for the tolerance margin. The tolerance is directly linked to the grout thickness. With the validity check limits provided by DNVGL-ST-0126 [6], the maximum grout thickness can be related to the stub outer diameter.

The grout thickness T_g is the space between the stub and the jacket leg and can be calculated with the following equation:

$$Tg = \frac{D_p - 2T_p - D_j}{2} \tag{15}$$

To maximise the grout thickness T_g, the stub outer diameter D_p, should be maximised, while the stub thickness T_p and the jacket leg outer diameter D_j are minimised.

For the stub radius-thickness ratio the upper limit equals:

$$limit => R_p/T_p = 70 \tag{16}$$

Rewritten to relate the stub thickness by the stub outer diameter gives:

$$T_p = \frac{D_p}{70 \cdot 2} \tag{17}$$

For the grout diameter-thickness ratio the upper limit equals:

$$limit => \frac{D_g}{T_g} = 10 \tag{18}$$

Where D_g equals:

$$D_g = D_p - 2T_p \tag{19}$$

With this upper limit, the jacket leg outer diameter can be rewritten:

$$\frac{D_p - 2T_p}{\frac{D_p - 2T_p - D_j}{2}} = 10 \tag{20}$$

$$5 = \frac{D_p - \frac{D_p}{70}}{D_p - \frac{D_p}{70} - D_j} \tag{21}$$

$$Dj = \frac{135}{175} D_p \approx 0.79 D_p \tag{22}$$

Rewriting equation 15 results in:

$$T_g = \frac{D_p - \frac{D_p}{70} - 0.79 D_p}{2} \approx 0.1 D_p \tag{23}$$

From this result, it can be concluded that the maximum grout limit is approximately 10% of the pile diameter D_p.

A.4 Results

To visualise the effect of the sizing of the stub diameter and the stub length a plot is made. Since only the axial capacity is dependent on the length of the stub, only the axial capacity is plotted in the Figures.

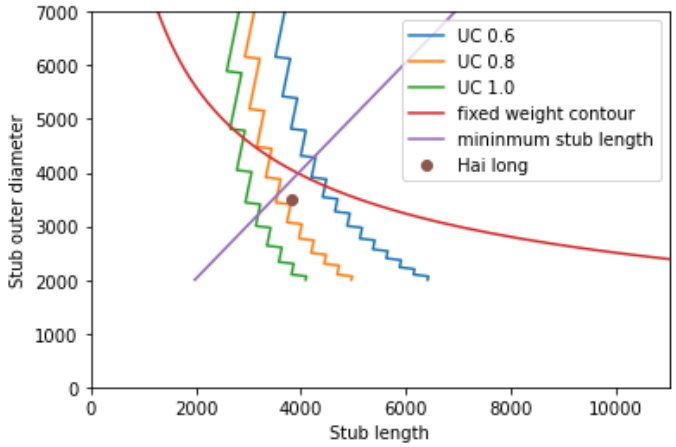

Figure 50: Stub outer diameter over stub length calculations with UC contour lines under axial loading

The red line indicates a fixed weight contour. On this line the weight is kept constant while varying the stub length. From this line can be concluded that increasing the length of the grout connection, while the UC factor is kept constant, increases the weight efficiency.

The purple line indicates the practical upper boundary for the minimum stub length. Dimensions above this line are not feasible.

In the plot, the dot indicates the design location from the Hai Long project. The dot is close to the minimum stub length line, indicating that the design was partially optimized to minimize the stub length.

In Figure 51, the maximum design loads for the SPIT are implemented into the calculations. The UC contour lines are slightly shifted to the upper right corner. To maximise on the grout thickness, the stub diameter is maximised for the necessary UC. In the Figure, the dimensions for the stub are indicated by the dot. In Table 16, the stub diameter and grout length of the Hai long project and the SP are displayed. The calculated dimension for the SP stub and the jacket pin are shown in Table 17. These dimensions also satisfy for the nominal radial contact pressure criterion explained in section A.2.

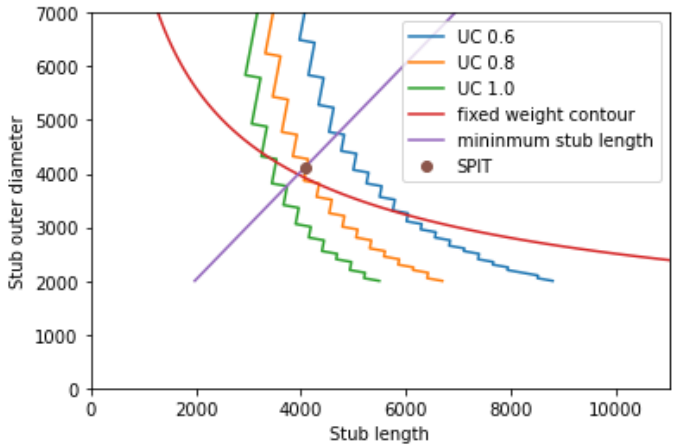

Figure 51: Stub outer diameter over stub length calculations with UC counter lines under axial loading

	Grout length stub	Stub outer diameter
Hai long	3810mm	3500mm
SPIT	4100mm	4100mm

Table 16: Grout length stub and stub diameter

D_p	4100	mm	Stub outer diameter
T_p	30	mm	Stub thickness
D_j	3240	mm	Jacket leg outer diameter
T_j	80	mm	Jacket leg thickness
D_g	4040	mm	Grout annulus diameter
T_g	400	mm	Grout thickness
S	300	mm	Shear key spacing
W	17	mm	Width of weld bead
H	11	mm	Height of weld bead
n	11	-	Number of shear keys
$fcck$	80	MPa	Grout strength (C80)
E_s	210	GPa	Elastic modulus
υ	0.3	-	Poisson ration steel
L_{geff}	3300	mm	Effective grout length
L_g	4100	mm	Grout length
UC_{ax}	0.75	-	Utilization factor axial capacity
$UC_{pressure}$	0.78	-	Utilization factor contact pressure

Table 17: Parameters used for the grout calculations

A.5 Total stub length

The total length of the stub depends on the stab in length of the jacket pin. The jacket pin length consist of several parts which are indicated in Figure 52.

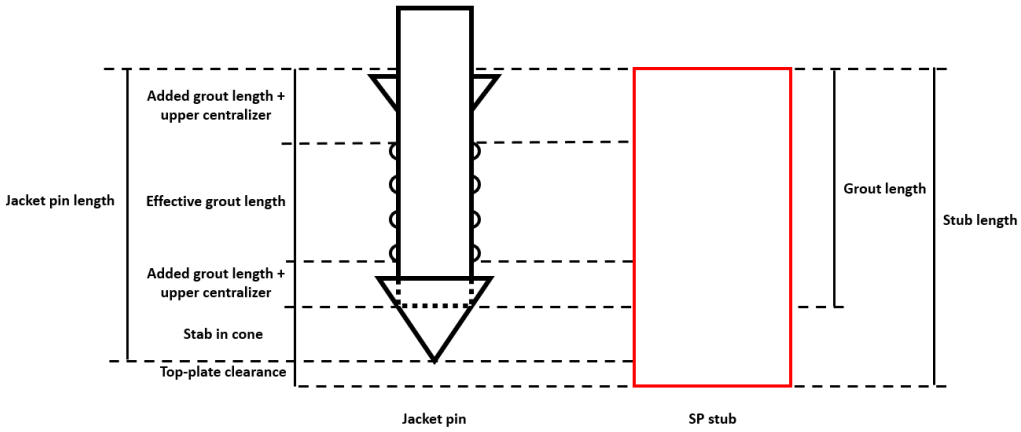

Figure 52: Schematic sketch of the jacket pin and SP stub length

The effective grout length is the length between the highest and lowest welded bead. An additional length for the grout is required above the highest weld bead and below the lowest weld bead. The upper and lower centralizers are integrated into this additional length. The stab in cone located at the bottom of the jacket leg is added to the jacket pin to make the insertion of the jacket pin into the stub easier. The grout length, consisting of the effective grout length plus the added length with the centralizers, is displayed in Table 17 and equals $4100mm$. The stab in cone requires an estimated additional $2000mm$. The total stab in length of the jacket leg is therefore $6100mm$. An additional clearance gap between the tip of the pin and the SP top-plate of $200mm$ is considered. The total minimum stub length therefore equals $6300mm$.

Individual lowering of the SPs should also be considered for the total length of the stub. Individual pile lowering will be performed if the SPs are installed on a sloped seabed. The tip of the stub for each SP should be located at the same height, otherwise when the jacket frame is placed on top of the SPs, the jacket will tilt. The assumed maximum height difference that can occur at the considered OWF between the SPs is 1.5. The maximum stub length equals $6400mm + 1500mm = 7900mm$.

B Horizontal hydrodynamic load analysis on the SP

The horizontal motions during lift operations offshore are limited by tuggerlines. The tuggerlines act as an active damping system for the pendulum motions occurring due to the wave interaction on the ship and the lifted object. Also, the tuggerlines are used to steer the object when necessary.

For the horizontal hydrodynamic load calculations, the interaction of the object with the tuggerlines is not analysed. For the preliminary conservative calculations, it is assumed that the tuggerlines have sufficient capacity to compensate the motion of the lifted object, resulting in a fixed object relating the current and the waves. To quantify the loads on the SPIT during the lift through the waterline, the maximum loads on a single SP are analysed. Fluid-structure interaction loads can be estimated with the Morison equation. The Morison equation gives the force over a structure per meter length. The general Morison equation is as follows:

$$F_n(t) = -\rho C_a A\ddot{r} + \rho C_m A\dot{v} + \frac{1}{2}\rho C_D D(v - \dot{r})|v - \dot{r}| \tag{24}$$

C_a, C_m and C_D are the added mass, mass and drag coefficients respectively.ρ is the density of the medium, A is the area normal to the flow, $\ddot{r}$ and $\dot{r}$ are the acceleration and speed of the object parallel to the flow. $\dot{v}$ and v are the acceleration and speed of the medium normal to the member.

The general Morison equation can be simplified for fixed slender cylinder members. The cylinder is assumed slender when $\frac{D}{\lambda} < 0.2$. Where D is the diameter of the cylinder and λ the wave length of the incoming wave. With this simplified equation the horizontal hydrodynamic loads on a single SP is calculated:

$$F(t) = \frac{\pi}{4}\rho C_M D^2 \dot{u}(t) + \frac{1}{2}\rho C_D D u(t)|u(t)| \tag{25}$$

C_M is the added coefficients of the mass of the structure and the added mass of the cylinder. C_D is the drag coefficient of the cylinder. D is the outer diameter of the cylinder and ρ the water density. u and $\dot{u}$ are the velocity and acceleration of the water particle perpendicular to the cylinder. In this analyses the assumption is made that the SP is in the vertical axial direction and the analysed water motions are horizontal.

The Morison equation can be separated into two terms:

- Inertia term: Corresponds to the first part of the equation.
- Drag term: Corresponds to the second part of the equation.

In specific design regions, one term can become dominant in which the other term can be neglected. The Morison equation in this way can be even further simplified. The specific design regions are determined based on the Keulegan-Carpenter (KC) number. The three design regions are:

- KC < 3: The inertia term is dominant and the drag term can be neglected.
- $3 <$ KC < 45: Both terms need to be considered for the Morison equations.
- KC > 45: The drag term is dominant and the inertia term can be neglected.

In the next section the KC number will be determined.

B.1 Morison coefficients

The coefficients are estimated by the experimental data gathered in [25]. The estimations are based on 3 factors:

- Keulegan-Carpenter number
- Reynolds number
- Surface roughness cylinder

The dimensionless KC number can be calculated with the following equation:

$$KC = \frac{u_a T}{D} \tag{26}$$

Where u_a is the speed amplitude of a linear wave, T the oscillating period of that wave and D the diameter of the cylinder. For deep water conditions, the KC number can be simplified to the following equation:

$$KC = 2\pi \frac{\zeta_a}{D} \tag{27}$$

Where ζ_a is the wave amplitude and D the diameter of the cylinder. Since both of these values are know due to the design requirements stated in section 6, the KC number results in:

$$KC = 2\pi \frac{1.5m}{12m} = 0.79 \tag{28}$$

The dimensionless Reynolds number can be calculated with the following equation:

$$Rn = \frac{u_a D}{\upsilon} = \frac{2\pi\zeta_a D}{T\upsilon} \tag{29}$$

Where ζ_a is the wave amplitude, D the diameter of the cylinder, T the oscillating period of the wave and υ the kinematic viscosity of sea water. Filling in the numbers for the maximum values result in a Reynolds number of:

$$Rn = \frac{2\pi \cdot 1.5m \cdot 12m}{4s \cdot 1.19 \cdot 10^{-6} m^2 s} = 2.4 \cdot 10^7 \tag{30}$$

Due to the large diameter of the cylinder and the low surface roughness of steel, the cylinder can assumed to be smooth. Added surface roughness by marine growth is non existent for the SP during the installation of the SP.

In [25], 5 different standard approaches are mentioned for the determination of the coefficients. The results are shown in Table 18.

	C_M	C_D
Sarpkaya	2.0	0.9
Clauss	2.0	0.6
DNV	2.0	0.6-1.0
API	1.6	0.65
SNAME	2.0	0.65

Table 18: Drag and inertia coefficients according to 5 different approaches.

From the different approaches can be concluded that $C_M = 2.0$ is a good estimate. C_D shows significant variance in the results. However, due to the small KC number (<3), the Morison equation is dominated by the inertia forces. The drag term can be neglected.

B.2 Water particle motions

The particle acceleration and speed of waves can be linearised by the dispersion relation. Since the drag term can be neglected, the water particle speed of the wave and current can be ignored. The water particle acceleration can be described with the following equation:

$$\dot{u}(t) = -\zeta_a \omega^2 \frac{cosh(k(h+z))}{sinh(kh)} sin(\omega t) \tag{31}$$

Where ζ_a is the wave amplitude, ω the wave frequency and k the wave number. h is the water depth of the mean sea level and z the vertical coordinate ranging from 0 to -h at the sea bed.

The longer the wave is with respect to the water depth, the more the particles interact with the seabed. The water particle trajectories therefore change depending on the wave and water depth. Figure 53 shows the water trajectories from a linearised long or shallow water wave. The horizontal motion is largest at the wave crest but slowly decreases towards the seabed.

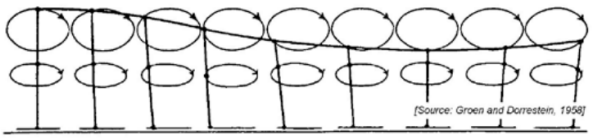

Figure 53: Water particle trajectory from a linearised long or shallow wave

Figure 54 shows the water trajectories from a linearised short or deep water wave. The horizontal motion is largest at the wave crest and quickly decreases towards the seabed. This trajectory creates localised water particle motions near the surface of the water. The effect of the hydrodynamic loads with the different motion trajectories on the SP will be explained in detail in the next section.

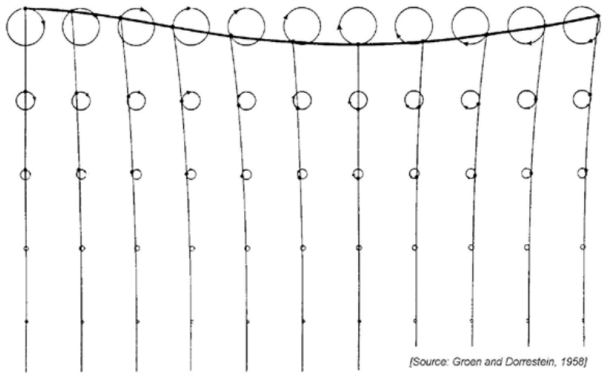

Figure 54: Water particle trajectory from a linearised short or deep water wave

The water particle acceleration expressed in equation 31 is only valid in the range of $0 \geq z \geq -h$. Where $z = 0$ is the mean sea level. In order to incorporate the added height due to the wave amplitude, wave profiles can be extended. In this analysis the wheeler profile stretching method is used. Equation 31 requires the substitution for z to z'. z' is calculated with the following equation:

$$z' = qz + h(q-1) \text{ where } q = \frac{h}{h + \zeta_a} \tag{32}$$

Now z' has a computational vertical coordinate range of $-h \geq z' \geq 0$ and z has the actual vertical coordinate range of $-h \geq z \geq \zeta_a$. Figure 55 shows the comparison of the wheeler stretching method horizontal water particle velocities with the extrapolated stretching method. The wheeler stretching method estimates more accurate loads compared to the extrapolated linear theory.

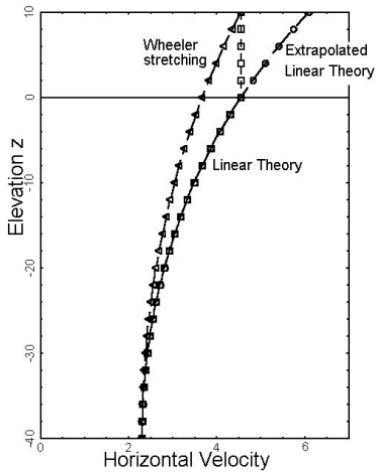

Figure 55: The wheeler stretching method compared to the extrapolated linear theory

The design envelope of the waves that can be expected are based on the metocean data set provided by DEME. In Appendix I, the rate of occurrence for different T_s and H_s values are given. The maximum H_s for safe operations is set at 3m. The design envelope of different T_s range from 5s to 15s.

B.3 Load case

When the shell of the SP is lifted through the water plane, the loads transferred to the SPIT will be largest. The horizontal force loaded onto the shell due to the inertia forces, need to be compensated by the stub. The

stub is constrained by the hydraulic mechanism, explained in section 6, by clamping the lower and upper part of the stub, representing F_{upper} and F_{lower} in Figure 56. S indicates the submerged length of the SP as the vertical distance from the top-plate to the mean sea level (MSL), in the analysis done this dimension is varied to check when maximum bending moments occur at specific submerged lengths.

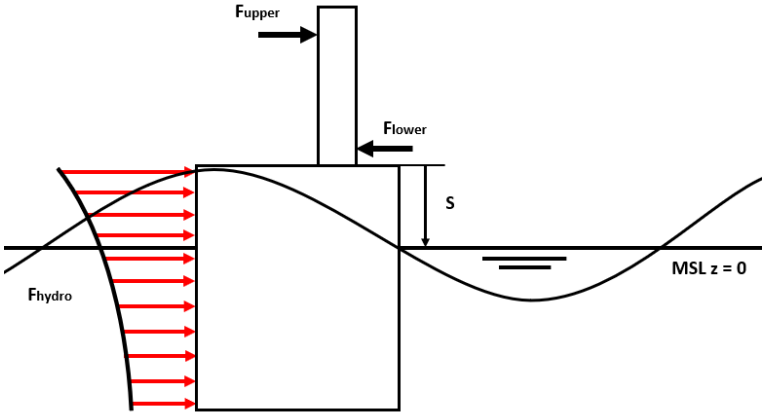

Figure 56: Schematic Figure of the load case considered for the horizontal hydrodynamic loads

For static equilibrium two equations need to be satisfied:

$$\sum F = 0 \text{ and } \sum M = 0 \tag{33}$$

For this load case only the horizontal 2D forces need to be taken into account for the two equilibrium equations. The equations can be filled in resulting in:

$$\sum F = F_{hydro} + F_{upper} - F_{lower} = 0 \tag{34}$$

$$\sum M_{topplate} = F_{upper} \cdot r_{upper} - F_{lower} \cdot r_{lower} - F_{hydro} \cdot r_{hydro} = 0 \tag{35}$$

Where r_{hydro} is the distance from the centre of forces from the hydrodynamic loads to the top-plate. r_{upper} is the distance from F_{upper} to the top-plate and r_{lower} is the distance from F_{lower} to the top-plate.

B.4 Results

Figure 57a and 57b show the maximum wave impact loads on the SP when the SP is fully submerged. From the data can be concluded that higher frequency waves, result in more horizontal load. However, the bending moment observes an optimum around $T_s = 6s$.

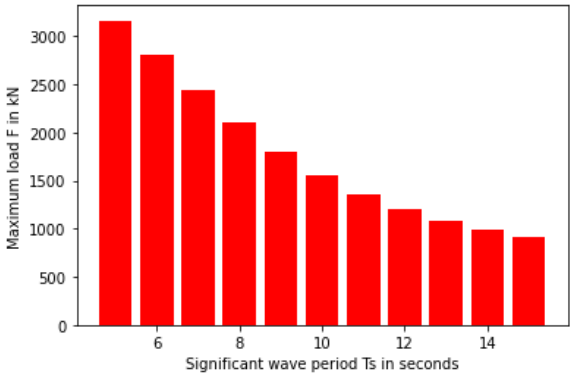

(a) Horizontal load on the skirt of the SP

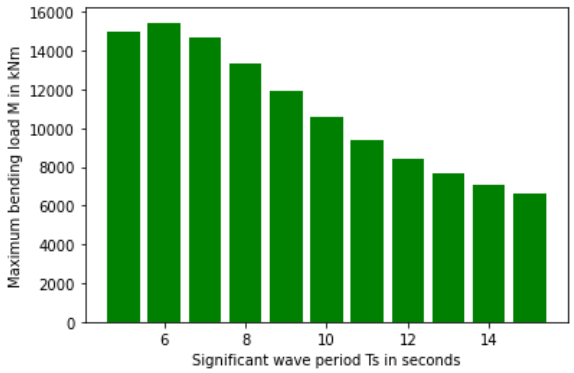

(b) Bending moment on the top-plate

Figure 57: Loads on the SP during a wave impact with $H_s = 3.0m$ when the SP is fully submerged

For high frequency waves, or short waves, the water particle trajectory is localised at the top of the surface. The centre of forces by the hydrodynamic loads is therefore closer to the top-plate in comparison to longer waves. The load distribution for different periods is plotted in Figure 58.

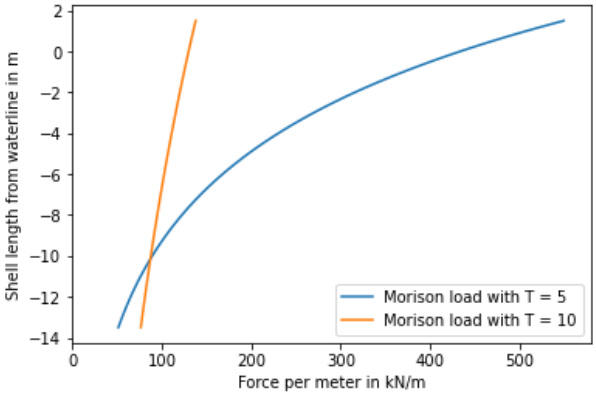

Figure 58: Morison load distribution over the shell wall of the SP for different wave periods

If the SP would be loaded when not fully submerged, the total horizontal load would decrease, but at a specific submerged length the bending moment would be maximised. Figure 59 shows the plot of the bending moment versus the length S of the SP for different wave periods. For short waves, the bending moment can be significantly increased when the optimal submerged length is reached. For long waves the bending moment will only decrease.

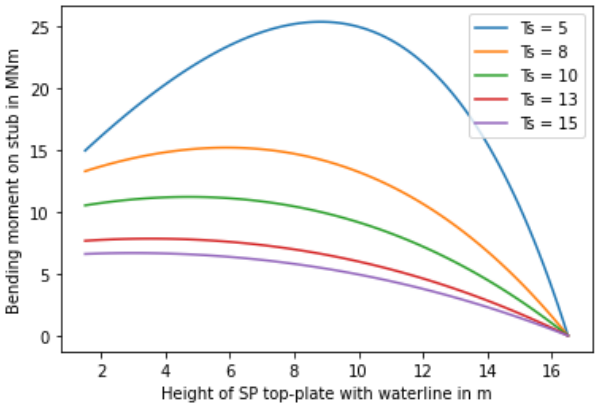

Figure 59: Bending moment versus the distance from top-plate to the MSL S

From Figures 57a and 59 can be read that the maximum horizontal load equals $3160kN$ and the bending moment equals $25.4MNm$. The maximum loads occur at a wave height of $3.0m$ and wave period of $5s$. What has to be noted however is that the applied Morison equation is only suitable for slender cylinders where $\frac{D}{\lambda} < 0.2$. For wave periods smaller than $6.1s$, this limit is exceeded. The loads calculated by the Morison equation for wave periods smaller than $6.1s$ will result in conservative estimates. For the high level design of the SPIT, these load estimations will suffice.

B.5 Stub loads

The reaction forces on the stub of the SP due to the hydrodynamic loading on the SP can now be calculated. Figure 60 shows the sketch of the stub on the top-plate.

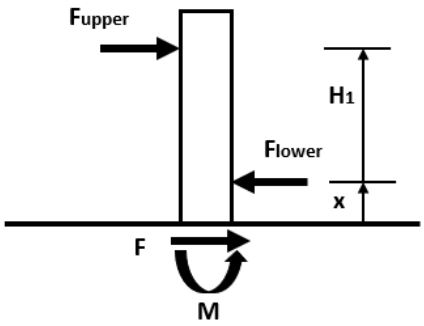

Figure 60

The lower hydraulic gripper has an offset $x = 1.8m$ with respect to the top-plate. F_{upper} and F_{lower} are spaced with length $H_1 = 4.64m$. Loads F and M are calculated in the previous subsection. The reaction forces F_{upper} and F_{lower} can be calculated by the equilibrium equations $\sum M_{top-plate}$ and $\sum F_x$:

$$\sum M_{top-plate} = F_{upper}(H_1 + x) - F_{lower}x - M = 0 \tag{36}$$

$$\sum F = F_{upper} + F - F_{lower} = 0 \tag{37}$$

These equations can be rewritten to find the reaction forces:

$$F_{lower} = \frac{M + F(H_1 + x)}{H_1} \tag{38}$$

$$F_{upper} = F_{lower} - F \tag{39}$$

The reaction forces are calculated for two cases:

- Maximum bending at the top-plate
- Maximum force on the SP

The results with the corresponding M and F are shown in Tables 19a and 19b. These results only show for a positive direction load, but both positive and negative should be considered. The maximum bending load case results in the largest reaction forces. The maximum force load case will be neglected for further calculations.

M	25.4	MNm
F	2.33	MN
F_{upper}	6.38	MN
F_{lower}	8.71	MN

(a) Maximum bending load case

M	15.0	MNm
F	3.16	MN
F_{upper}	4.46	MN
F_{lower}	7.62	MN

(b) Maximum force load case

Table 19

To check if the stub will not yield due to the reaction forces, the maximum stress in the stub should be below the yield stress of the material. The equation is as follows:

$$\sigma_{max} = \frac{M_{max} y_{max}}{I_{stub}} < \sigma_y \tag{40}$$

For a one clamped-end and one free-end beam, the maximum bending force M_{max} can be calculated with the following equation:

$$M_{max} = F_{upper} H_1 \tag{41}$$

Where y_{max} is the radius and I_{max} the area moment of inertia of the stub. The results are displayed in Table 20. For a medium grade steel, the yield strength is 350MPa. The current maximum stress caused by the reaction forces is less than the yield strength. It can be concluded that the stub has sufficient strength to withstand these

loads. Attention should be given to possible local failures in the stub if the load distribution is too centralised. FEM analysis in a later design stage should indicate if local failure can occur and if strengthening of the stub is required.

y_{max}	2.05	m
H_1	4.64	m
I	0.79	m^4
M_{max}	29.6	MNm
σ_{max}	76.8	MPa
σ_y	350	MPa

Table 20

C Horizontal hydrodynamic load analysis on the SPIT frame

When the SPIT is lowered through the splash zone, the impact of the waves on the frame is largest in the connecting frame, connecting the frame pockets. This is because large bending moments act on this part of the frame during wave loading. In Figure 61, the part of the frame is indicated between A and B. The horizontal hydrodynamic load causes a distributed force over the frame. This analysis checks if the members are properly sized to withstand the horizontal loading. A hinged beam model is taken to simplify the frame between A and B as indicated in Figure 61.

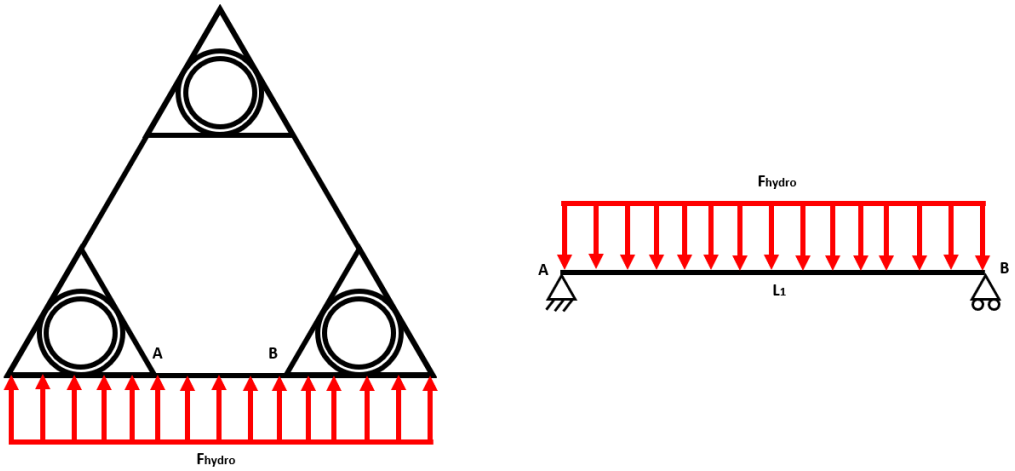

Figure 61: Top view of the SPIT subjected to a horizontal hydrodynamic load. The frame between point A and B is analysed as a hinged beam with a uniform load.

The distributed load over the beam can be calculated with the morison equation introduced in section B. In this morison equation the stick-model 21c is adopted to simplify the frame as a single tubular.

$$F(t) = \frac{\pi}{4}\rho C_M D_{ie}^2 \dot{u}(t) + \frac{1}{2}\rho C_D D_{de} u(t)|u(t)| \tag{42}$$

Diameters D_{ie} and D_{de} are the summed diameter of the members for the inertia and drag term:
For horizontal braces the corrected diameters are:

$$D_{ie} = \sqrt{LD} \text{ and } D_{de} = L \tag{43}$$

For vertical braces the corrected diameters are:

$$D_{ie} = D \text{ and } D_{de} = D \tag{44}$$

For diagonal braces perpendicular to the incoming wave, the corrected diameters are:

$$D_{ie} = \frac{D}{\sqrt{sin(\theta)}} \text{ and } D_{de} = \frac{D}{sin(\theta)} \tag{45}$$

For diagonal braces parallel to the incoming wave, the corrected diameters are:

$$D_{ie} = D\sqrt{cos(\beta)} \text{ and } D_{de} = Dcos^2(\beta) \tag{46}$$

The simplified beam exists of 5 different types of members. These types are shown in Figure 62. The stick-model can now be made. Since the type 4 braces are spaced in all three dimensions, the braces are simplified to a diagonal brace perpendicular to the wave direction (same as the type 2 members).

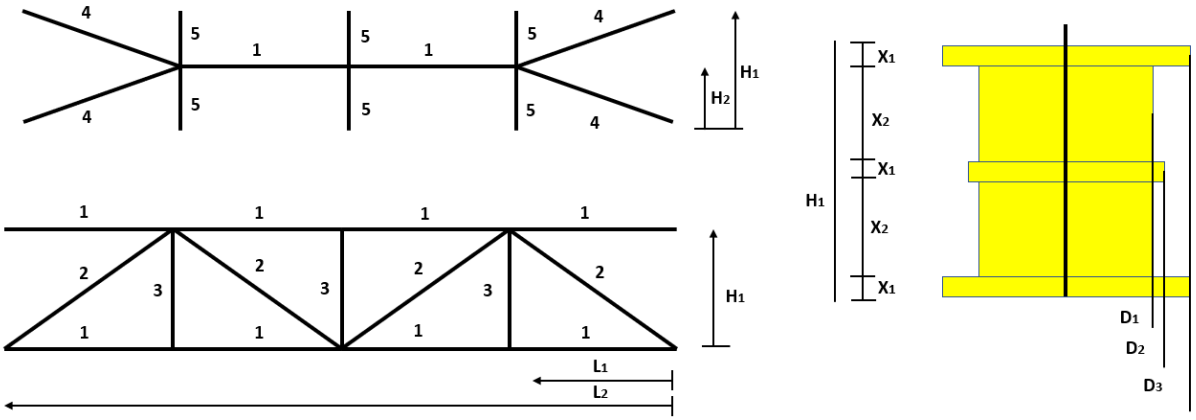

Figure 62: The member numbering of the brace between point A and B. The simplified stick-model is displayed on the right.

D	350	mm
H_1	4.64	m
H_2	2.32	m
L_1	27.00	m
L_2	6.75	m
θ	34.5	deg
β	37.7	deg
X_1	350	mm
X_2	1.80	m
Y	3.00	m

(a) Parameters used for the dimensions of the frame.

	D_{ie} [m]	D_{de} [m]
1	1.54	6.75
2	0.45	0.59
3	0.35	0.35
4	0.45	0.59
5	0.21	0.27
D_1	10.72	32.18
D_2	4.57	5.18
D_3	7.64	18.68

(b) Corresponding D_{ie} and D_{de} for each member type and the summation used for the stick-model.

$u_{current}$	2	m/s [m]
H_{wave}	3	m
T	5	s
ζ_a	1.5	m
ω	1.26	rad/s
k	0.16	rad/m
h	70	m
z	0	m

(c) Parameters used for calculating the maximum wave kinematic that can occur during lift operation.

Table 21

For the wave kinematics the following equations are used to acquire the speed and acceleration of the incoming wave:

$$u(t) = \zeta_a \omega \frac{cosh(k(h+z))}{sinh(kh)} cos(\omega t) + u_{current} \tag{47}$$

$$\dot{u}(t) = -\zeta_a \omega^2 \frac{cosh(k(h+z))}{sinh(kh)} sin(\omega t) \tag{48}$$

For this analysis, the constant kinematics wave profile will be used to simplify the calculations for the Morison equation. This results in a uniform speed and acceleration over the complete frame taken from $z = 0$. The total force on the frame between point A and B is calculated with the following calculation from the stick-model:

$$F_{total} = 2F(D_1, t)X_1 + F(D_2, t)X_2 + 2F(D_3, t)X_3 \tag{49}$$

From this equation results a maximum total force on the frame of $1.59MN$. Now the maximum bending in the frame is calculated with the following equation:

$$M_{max} = \frac{F_{total} L}{4} = 11.0MNm \tag{50}$$

The maximum bending occurs in the middle of the beam. The cross section area sketch of the middle of the beam is shown in Figure 63. The maximum axial force occurs in the member B3. The axial force in this member is calculated with the following equation:

$$F_{axial} = \frac{M_{max}}{Y} = 3.66MN \tag{51}$$

To satisfy static equilibrium, the loads in the main members B1 and B2 equal $3.66/2 = 1.83MN$. The members B_1 and B_2 in Figure 63 correspond with members 2 & 4 from the analysis in section F.2. The member corresponding to B_3 will be labeled as member 18 in Table 39a in section F.5, where the overview of all the beams is displayed.

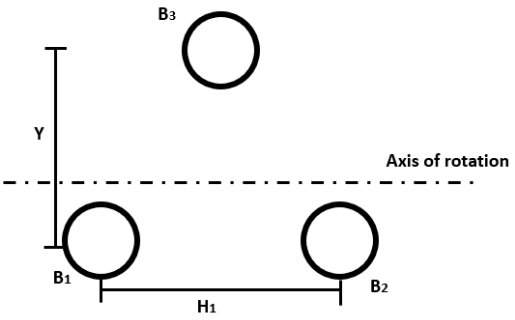

Figure 63: Cross sectional area sketch of the frame between point A and B.

D Soil pile interaction

The considered load case for the geotechnical analysis is depicted in Figure 64a. The loads are calculated based on the geotechnical models proposed in [4], [42] and [43].

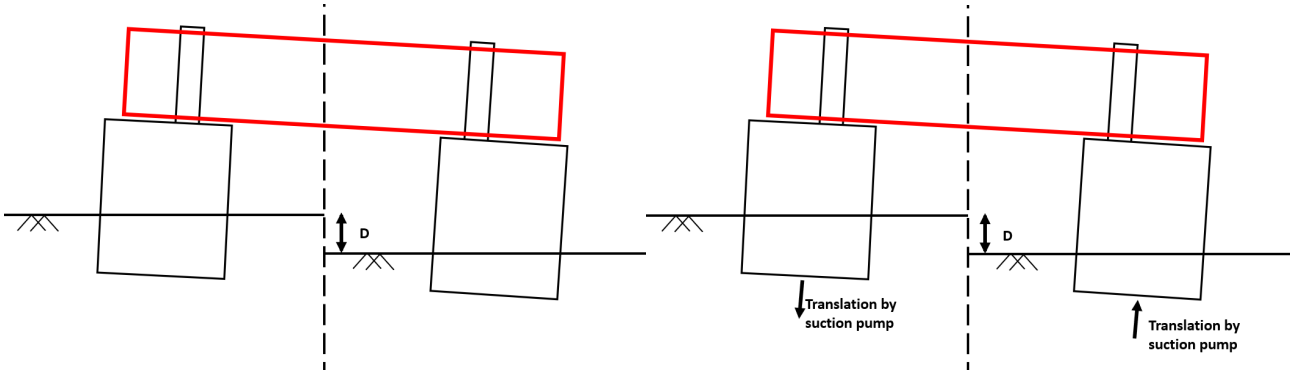

(a) Possible rotation of the SPIT during self-weight penetration. **(b)** Rotation adjustments created by suction pumps.

Figure 64: Geo-technical load case considered for SPIT design

Depending on the centre of rotation of the SPs and SPIT, the horizontal forces and bending moment will be created by a combination of horizontal and rotational translations displayed in Figure 65. Both reaction types are based on the lateral soil pressure. The horizontal and rotational translations can take place when the maximum lateral soil pressure is exceeded and the soil fails. Pure horizontal translations cause for the largest soil-pile interaction loads. To reduce the loads transferred to the pile and the SPIT, a pure rotational translation is preferred.

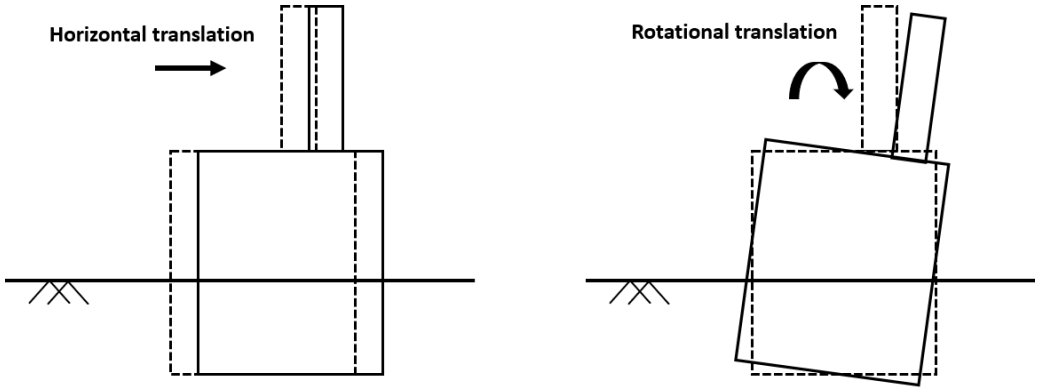

Figure 65: Two reaction types on a SP during horizontal and bending loads on the stub.

In Figure 66, a linear and uniform soil profile is sketched. Pure uniform or linear soil profiles will not be encountered in practice but for the high level design of the SPIT, these profiles are sufficient. L is the embedded length of the pile in the soil, S_{lin} and S_{uni} is the distance from the seabed to the centre of rotation. This distance is dependent on the loads transferred from the SPIT through the stub through the SP.

Both soil profiles satisfy two equilibrium equations:

$$\sum F = 0 \text{ and } \sum M = 0 \tag{52}$$

If the stub is purely loaded with a bending moment ($F_{stub} = 0$), the maximum bending moment can be related to the maximum lateral soil pressure. M_{stub} corresponding to the linear soil profile becomes:

$$M_{stub} = P_{max} L^2 (\frac{1}{3} - \frac{2}{3} x^3) = 0.01 L^2 P_{max} \tag{53}$$

Where $x = \frac{S_{lin}}{L} = \frac{\sqrt{2}}{2}$. M_{stub} for the uniform soil profile becomes:

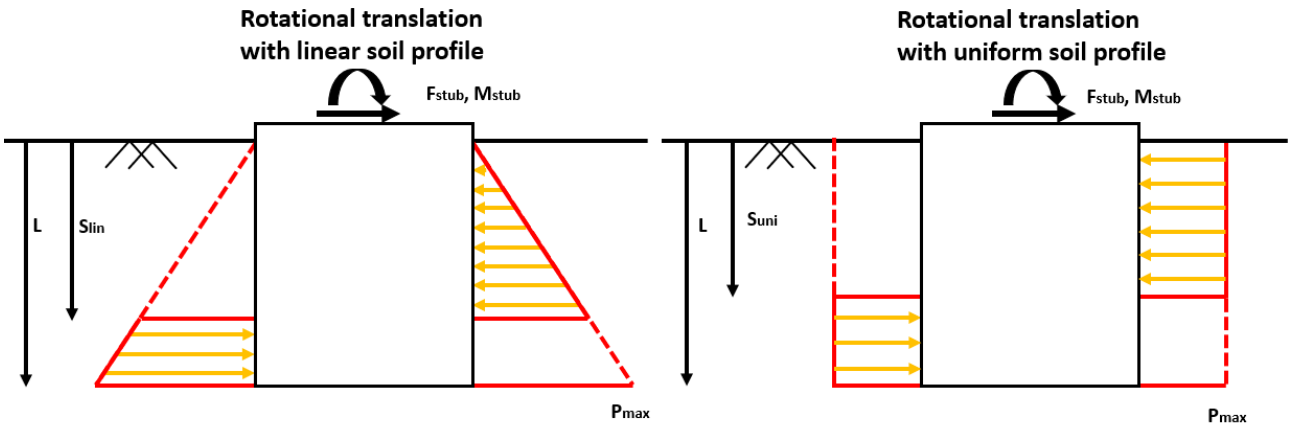

Figure 66: Lateral maximum soil pressure profiles on a shallow foundation pile.

$$M_{stub} = P_{max}L^2(\frac{1}{2} - x + x^2) = \frac{1}{4}L^2P_{max} \tag{54}$$

Where $x = \dfrac{S_{uni}}{L} = \dfrac{1}{2}$. P_{max} for both soil profiles depend on the type of soil.
If the pile approaches a horizontal translation where $S \approx L$, F_{stub} & M_{stub} are maximum. For the linear soil profile both equations become:

$$F_{lin} = \frac{1}{2}P_{max}L \text{ and } M_{stub} = F_{lin}(H - \frac{1}{3}L) \tag{55}$$

Where H is the total length of the SP. For the uniform soil profile both equations become:

$$F_{uni} = P_{max}L \text{ and } M_{stub} = F_{uni}(H - \frac{1}{2}L) \tag{56}$$

In the next subsections the soil-pile interaction for clay and sand will be analysed.

D.1 Clay

For the calculations of the soil-pile interactions the self-weight penetration should be calculated first. The self-weight penetration equilibrium equation for clay soils is:

$$V' = L\alpha s_{u1}(\pi D_o) + L\alpha s_{u1}(\pi D_i) + (\gamma' L N_q + s_{u2}N_c)(\pi D t) \tag{57}$$

Where $D_o, D_i \& D$ is the outer, inner and mean diameter of the SP respectively. L is the self-weight penetration of the SP in the soil. t is the SP thickness. α is the adhesion factor. N_c and N_q are the undrained cohesion and overburden capacity factors respectively. s_{u1} is the mean undrained shear strength along the embedded wall and s_{u2} the undrained shear strength at the tip of the SP.

The maximum lateral soil pressure for clays against shallow foundations (z < 3D) can be written as:

$$P_{max} = 2Ds_u \tag{58}$$

The P_{max} value is dependent on the clay type and the soil profile. In the following subsections the bending moments on the stub will be calculated.

D.1.1 Uniform clay

At the ScotWind project location, soft clay soils can be encountered. The expected design envelope for the undrained shear strength and soil unit weight is shown in Table 22.

Uniform soft clay	Lower bound	Upper bound
Unit weight γ	$13kN/m^3$	$16kN/m^3$
Undrained shear strength s_u	$20kPa$	$40kPa$

Table 22: Uniform clay design envelope

Equation 57 can be rewritten to find the self-weight length L:

$$L = \frac{V' - s_u N_c \pi D t}{\alpha s_u \pi (D_o + D_i) + \gamma' D t \pi N_q} \tag{59}$$

D_o	12000	mm
D_i	11900	mm
D	11950	mm
t	50	mm
V'	450	mt
H	15	m
α	0.6	-
N_c	9	-
N_q	1	-

Table 23: parameters used for clay

Figure 67 shows the maximum bending moment over the undrained shear strength of the uniform clay. The difference in soil density does not influence the bending load significantly. The softer the soil, the more the pile penetrates the soil, resulting in a larger bending moment. The estimated bending moment for uniform soft clays is $1.8MNm$.

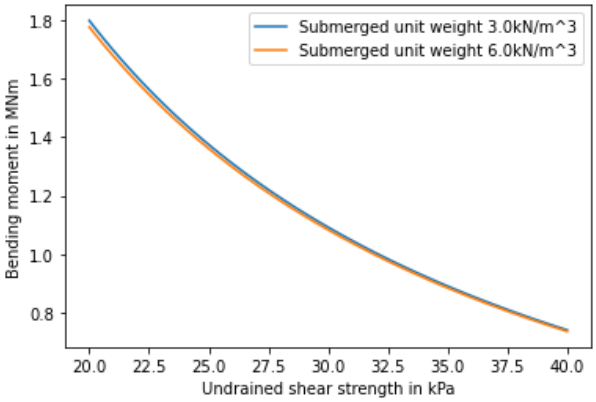

Figure 67: Bending moment on the SP versus the undrained shear strength

figures 68a and 68b show the maximum loads that can occur during horizontal translation. The maximum force is calculated for $s_u = 20kPa$ and equals $1.86MN$. The maximum bending moment shows an optimum for $s_u = 25kPa$ and equals $24.5MNm$.

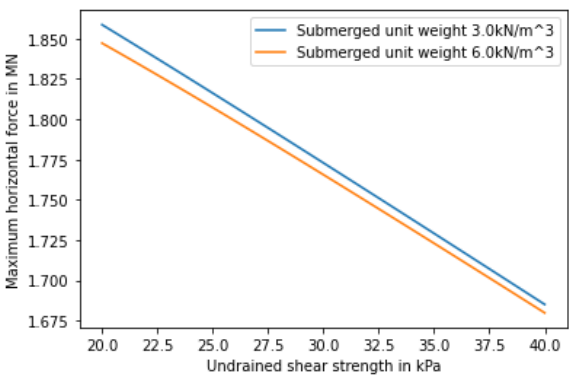

(a) Maximum horizontal force at the stub

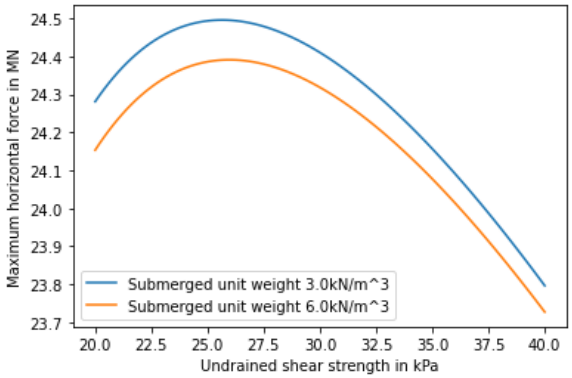

(b) Maximum bending moment at the stub

Figure 68: Maximum loads at the stub of the SP for uniform clay

D.1.2 Normally consolidated clay

The undrained shear strength for NC (normally consolidated) clays can be expressed with the following linear equation:

$$s_u = 0.22\gamma' z \tag{60}$$

Where z is the vertical coordinate where the undrained shear strength acts on the pile. NC clays have a linear soil profile as the equation shows. The design envelope of the unit weight of clay is the same for the uniform clay profile and can be seen in Table 22. The self-weight penetration of the NC clay can be rewritten from equation 57 to the following equation:

$$L = -\frac{b}{2a} + \sqrt{(\frac{b}{2a})^2 - \frac{c}{a}} \tag{61}$$

Where:

$$a = \alpha\pi\frac{0.22}{2}\gamma'(D_o + D_i) \tag{62}$$

$$b = (\gamma' N_q + 0.22\gamma' N_c)(\pi D t) \tag{63}$$

$$c = -V' \tag{64}$$

Table 23 also shows the parameters used for these equations. Figure 69 shows the bending moment over the submerged unit weight of clay. The softer the soil, the more the pile penetrates the soil, resulting in a larger bending moment. The estimated bending moment for uniform soft clays is $0.6MNm$. The embedded length however exceeds the total length of the SP. The current SP is therefore not properly dimensioned for NC soft clays.

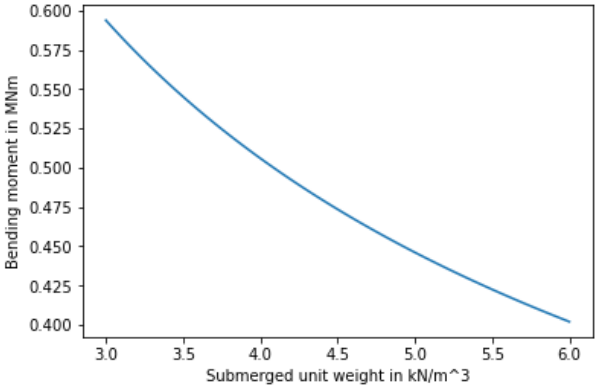

Figure 69: Bending moment on the SP versus the saturated unit weight of clay.

Figures 70a and 70b show the maximum loads that can occur during horizontal translation. The maximum force is calculated for $\gamma' = 3.0kN/m^3$ and equals $1.92MN$. The maximum bending moment is calculated for $\gamma' = 6.0kN/m^3$ and equals $21.1MNm$.

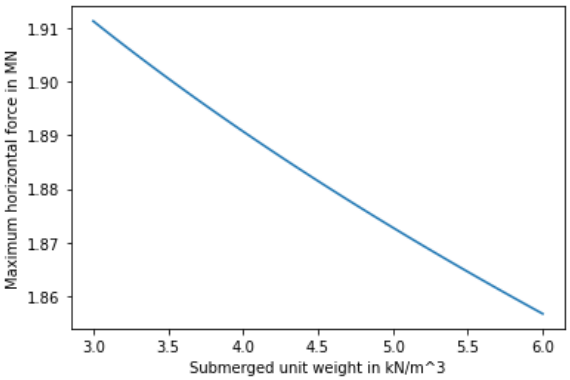

(a) Maximum horizontal force at the stub

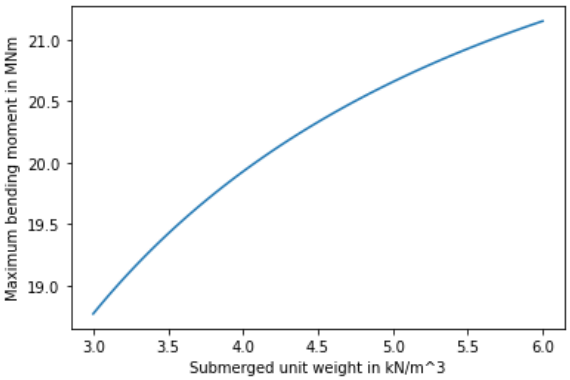

(b) Maximum bending moment at the stub

Figure 70: Maximum loads at the stub of the SP for NC clay

D.2 Sand

For the calculations of the soil-pile interactions, the self-weight penetration should be calculated first. The self-weight penetration equilibrium equation for sand soils is:

$$V' = \frac{\gamma' L^2}{2}(Ktan\delta)_o(\pi D_o) + \frac{\gamma' L^2}{2}(Ktan\delta)_i(\pi D_i) + (\gamma' L N_q + \gamma' \frac{t}{2} N_\gamma)(\pi D t) \tag{65}$$

Where $D_o, D_i \& D$ is the outer, inner and mean diameter of the SP respectively. L is the self-weight penetration of the SP in the soil. t is the SP thickness. δ is the soil/wall friction angle K the earth pressure coefficient. N_γ and N_q are the drained soil-weight and overburden capacity factor respectively.

The maximum lateral soil pressure equation for sand indicates that the soil profile is linear and can be written as:

$$P_{max} = DK_p^2 \gamma' z \tag{66}$$

Where K_p is the passive earth pressure coefficient and can be calculated with the following equation:

$$K_p = \frac{1 + sin\phi}{1 - sin\phi} \tag{67}$$

Where ϕ is the internal friction angle of the sand.

At the ScotWind project location, a sand top-layer can be encountered. However the sand specifications are not yet known. The design envelope will therefore be:

Sand design envelope	Lower limit	Upper limit
Internal friction angle ϕ	30°	40°
unit weight γ	$13kN/m^3$	$18kN/m^3$

Table 24: Design envelope of sand

For the self-weight penetration length, equation 65 can be rewritten as:

$$L = -\frac{b}{2a} + \sqrt{(\frac{b}{2a})^2 - \frac{c}{a}} \tag{68}$$

Where:

$$a = \frac{\gamma'}{2} K_p tan(\delta)\pi(D_o + D_i) \tag{69}$$

$$b = \gamma' N_q \pi D t \tag{70}$$

$$c = -V' + \gamma' \frac{t}{2} N_\gamma \pi D t \tag{71}$$

The parameters used for these equations are shown in Table 25.

D_o	12000	mm
D_i	11900	mm
D	11950	mm
t	50	mm
V'	450	mt
H	15	m
α	0.6	-
N_q	20	-
N_γ	0	-

Table 25: parameters used for sand

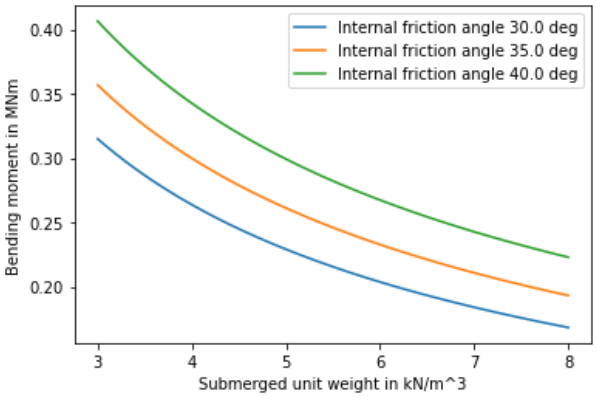

Figure 71: Bending moment on the SP versus the saturated unit weight of sand. Different internal friction angles of sand are shown in the plot.

Figures 72a and 72b show the maximum loads that can occur during horizontal translation. The maximum force is calculated for $\gamma' = 3.0 kN/m^3$ and equals $5.4 MN$. The maximum bending moment is calculated for $\gamma' = 3.0 kN/m^3$ and equals $74.5 MNm$. Both loads are maximum for the sand corresponding with the 40° internal friction angle.

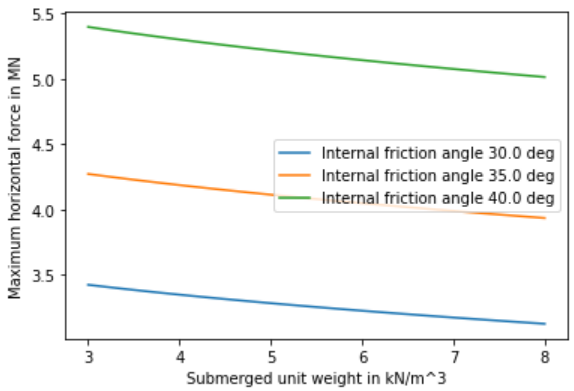

(a) Maximum horizontal force at the stub

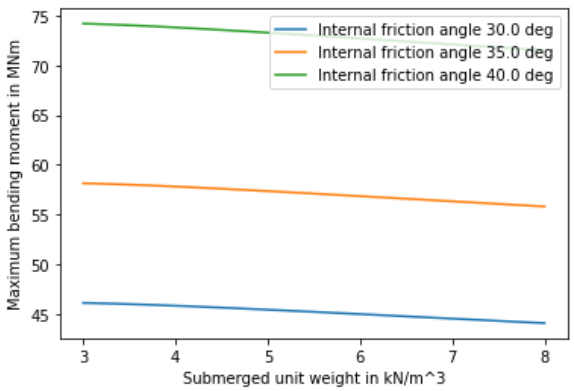

(b) Maximum bending moment at the stub

Figure 72: Maximum loads at the stub of the SP for sand

In Table 26, the maximum bending moment for each soil type is displayed.

	Uniform clay	NC clay	Sand
Rotational translation	1.80MNm	0.6MNm	0.41MNm
Horizontal translation	24.5MNm	21.1MNm	74.5MNm

Table 26: Maximum bending moment on the SP stub for each soil type

E Venting of a SP

In this analysis a single SP is lowered through the water surface from a fixed crane tip. Water is simulated as a non-viscous flow, resulting in no damping or friction between the water and pile. Because of the hollow inside of the SP, air pressure inside the pile rises during lowering. Depending on the venting and lowering speed of the SP, the air escapes at a certain velocity. The air pressure lifts the SP, reducing the lift load. The aim of these calculations is simulating the buoyant behaviour of a vented SP and the effect it has on the lift load. In these calculations the effect of the lowering speed and perforation rate(vent size) is analysed.

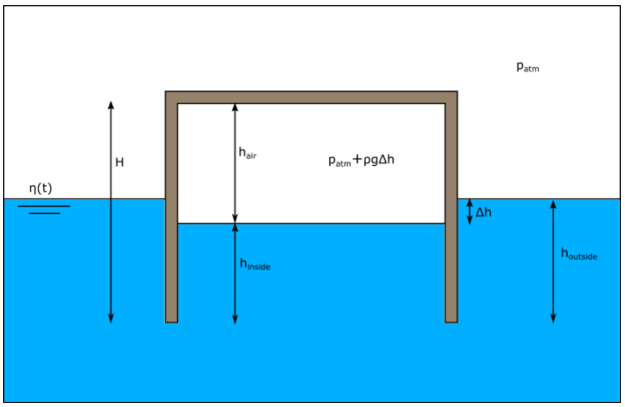

Figure 73: Schematic picture of lowering process

In Figure 73, the overview of the problem is depicted with the correct parameters. The lift load is calculated with the following equation:

$$F_{line} = F_{gravity} - F_{buoyancy} - F_{aircushion} = mg - \nabla\rho_{water} - \rho_w g\Delta h A_{in} \tag{72}$$

With m the mass of the pile, calculated with the following equation:

$$m = (A_s H + A_{out} h_{topplate})\rho_{steel} \tag{73}$$

Where A_s is the cross sectional area of the cylinder. A_{out} is the area of the top of the pile. $h_{topplate}$ is the thickness of the top plate of the pile.

∇ is the wetted volume of the pile and is calculated with the following equations:

$$\nabla = A_s h_{submerged} \quad for \quad h_{submerged} \leq H - h_{topplate} \tag{74}$$

$$\nabla = A_s h_{submerged} + A_{out}(h_{submerged} - (H - h_{topplate})) \quad for \quad h_{submerged} > H - h_{topplate} \tag{75}$$

Where $h_{submerged} = h_{outside}$, if the parameter is smaller than the height of the pile. Otherwise the structure is fully submerged and therefore ∇ is constant where $h_{submerged} = H$.

The Δh is solved by the subtraction:

$$\Delta h = h_{outside} - h_{inside} = h_{outside} - (H - h_{air}) \tag{76}$$

Where $h_{outside}$ depends on the lowering speed of the crane and the wave height and is calculated as follows;

$$h_{outside} = v_{lowering} t \tag{77}$$

The height of the air pocket is calculated by using the ideal gas law for isothermal processes:

$$p_1 V_1 = p_2 V_2 => (p_{air} h_{air})_{i+1} = (p_{air} h_{air})_i \tag{78}$$

Solving this system results in the following equation for h_{air}:

$$h_{air}(i+1) = -0.5(\frac{p_{atm}}{\rho_w g} + h_{submerged} - H) + \sqrt{0.25(\frac{p_{atm}}{\rho_w g} + h_{submerged} - H)^2 + \frac{h_{air}(i) p_{air}(i)}{\rho_w g}} \tag{79}$$

The height of the air plug can now be solved by time iterations. The new air pressure is calculated by:

$$p_{air}(i+1) = p_{air}(i)(\frac{h_{air}(i)}{h_{air}(i+1)}) \tag{80}$$

During lowering of the SP, the vents of the SP allow the air to escape. The equation for the speed of air escaping the SP is:

$$v_{air} = \sqrt{\frac{2\Delta p}{k_{flow}\rho_{air}}} \tag{81}$$

Where Δp is the pressure difference between the inside and outside of the SP, k_{flow} the blocking factor of air through a circular hole and ρ_{air} the air density. The discharge of air leaving the SP can be calculated by multiplying the speed of air times the vent area. The perforation parameter indicates the percentage of the top-plate that is used for venting.

E.1 Buoyancy development over time

The results of the calculations are shown below. The standard calculation has been done with the following parameters:

Parameter	Value	Unit
D	12	m
H	15	m
Mm	340	mt
P	2.0	%
k_{flow}	1.75	-
$v_{lowering}$	0.1	m/s

Table 27

The results of the buoyancy developing over time is graphed in the plots in Figures 74a and 74b.

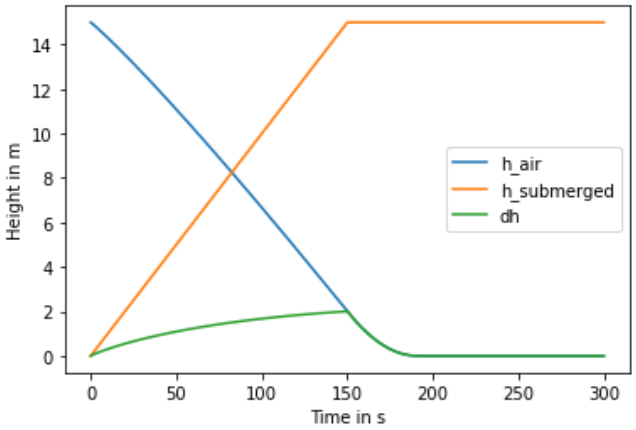

(a) Height parameters varying over time

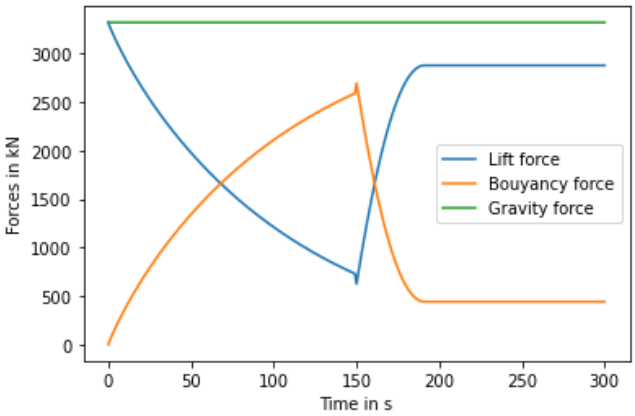

(b) Forces on the SP varying over time

Figure 74

In Figure 74a, the plot shows the moment when the SP is submerged at $h_{submerged} = 15m$. All air has escaped the SP when $h_{air} = 0m$. In Figure 74b, the plot shows the lift force reducing until the SP is fully submerged. The plot in Figure 74b indicates that the buoyancy force does not exceed the gravity force. The SP will not float during the lifting procedure and the lift wire is constantly kept in tension. The next section will indicate the minimum perforation of the SP before the buoyancy force exceeds the gravity force for different lowering speeds.

E.2 Minimum perforation

The minimum perforation of the SP depends on the lowering speed during the submergence of the SP. Figures 75a and 76 show the results of the venting necessary to remain tension in the crane wire. The calculations are performed based on a constant lowering speed during operations. However, the motion of the vessel and waves will create varying lowering speeds. If large vessels motions or swell waves are expected during the lift operation, the operation might be temporarily stopped in order to create extra time to let the air escape from the inside of the SP.

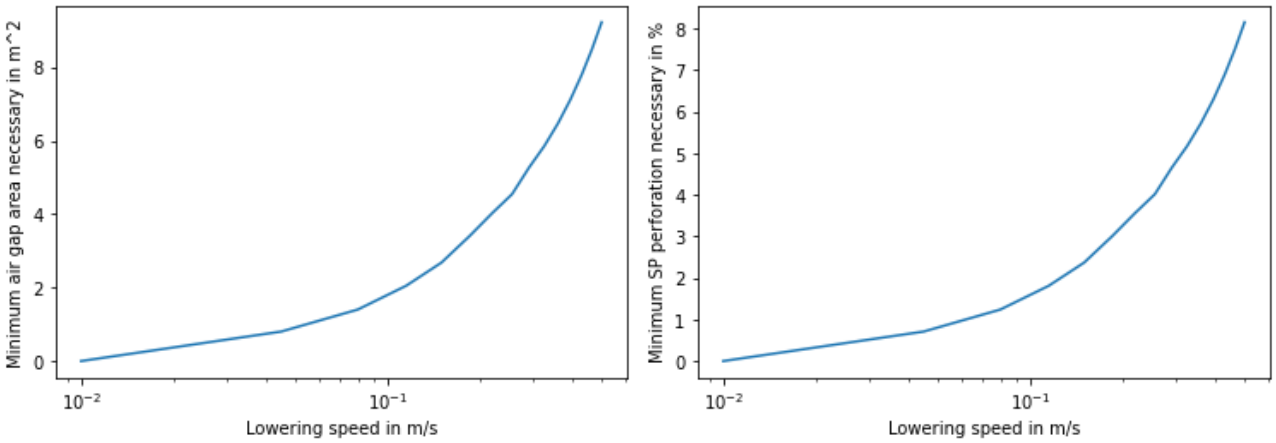

(a) Air gap area plotted over the lowering speed

(b) SP perforation plotted over the lowering speed

Figure 75

The air gap area and perforation rate can be translated to the air gap diameter. Multiple vents can be made on the SP to reduce the size of on air gap.

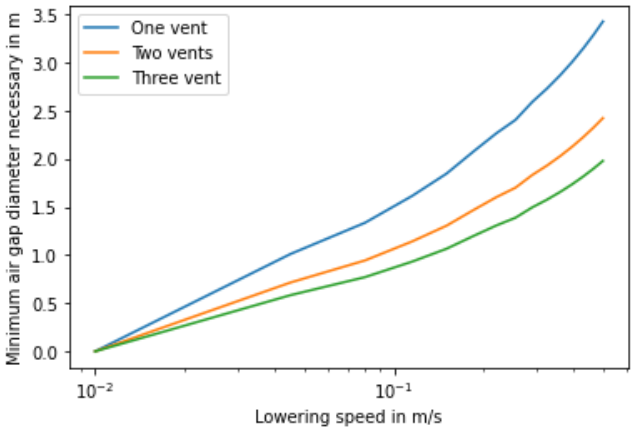

Figure 76: Air gap diameter plotted over the lowering speed

F Truss frame analysis

A 2D schematic is shown in Figures 77 and 78 of the side-and top-view of the SPIT. In this analysis the frame is simplified to a beam model with only hinged members. Due to the symmetry of the SPIT only specific parts of the frame are analysed.

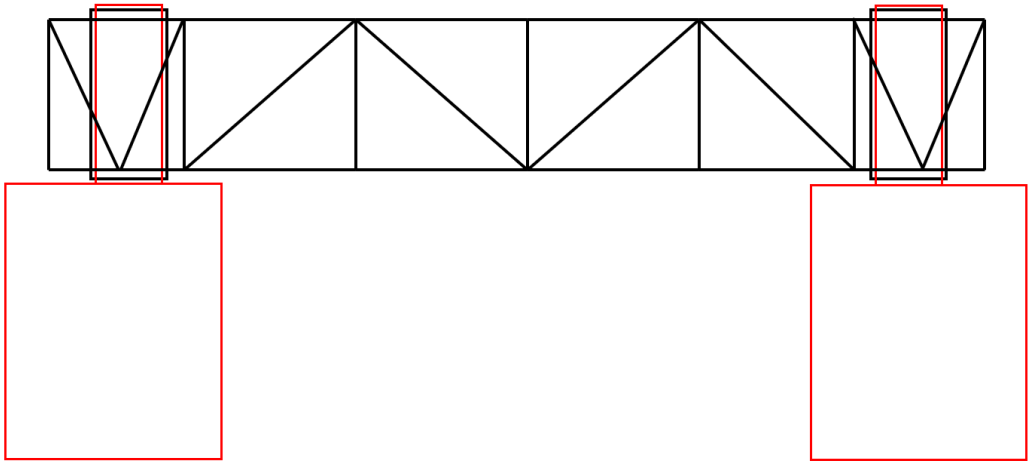

Figure 77: 2D side-view schematic of the SPIT

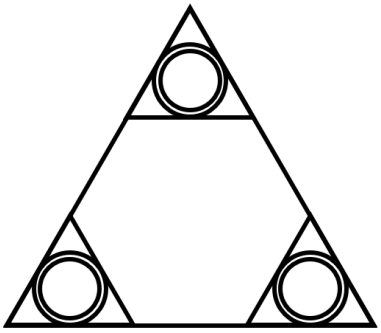

Figure 78: 2D top-view schematic of the SPIT

For the calculations of the frame, the member loads are split into 4 parts:

- Load distribution from the gripper ring to the frame
- Loads on the SPIT main members during operation
- Shear in the frame caused by bending during operation
- Hydrodynamic loads on the members of the frame

The frame is checked on 3 aspects:

- Total stress in each member
- Buckling failure in each member
- Maximum deflection of the frame

The total stress in each member should not exceed the yield strength (σ_y) of that member. The equation should satisfy:

$$\frac{|\sigma_t|}{\sigma_y} = \frac{|F_a|}{Dt\pi\sigma_y} < \frac{1.0}{SF} \tag{82}$$

Where F_a is the axial force in the member. D and t are the diameter and thickness of the member. SF is the global safety factor considered for this analysis.

The maximum deflection of the frame should be within the allowed tolerance margins (δ_{max}) taken from the design requirements in 6. By simplifying the framework into all hinged members, the deflection check can be computed with the help of the virtual work method for truss frames 21c. The equation should satisfy:

$$\delta_f = \sum_{n=1}^{k} \frac{n_i N_i L_i}{A_i E_i} < \frac{\delta_{max}}{SF} \tag{83}$$

Where δ_f is a specific deflection on a point in the frame. k is the number of members making up the frame. n and N is the virtual and actual load on each member. L and E is the length and elastic modulus for each member respectively.

The buckling check is done with the Euler buckling method for a beam with 2 hinged ends. The equation should satisfy:

$$\frac{L^2 F_a}{\pi^2 EI} < \frac{1.0}{SF} \tag{84}$$

Where F_a is the axial force on the member where only compression forces are considered for the buckling check.

F.1 Load distribution from gripper ring to the frame

The distribution of forces in the frame due to the hydrodynamic loads on the SP can be estimated by simplifying the hydraulic ring where the stub of the SP is clamped and the triangular frame holding the ring in place. Figure 79 shows the schematic from the top-view of the triangular frame and the FBD.

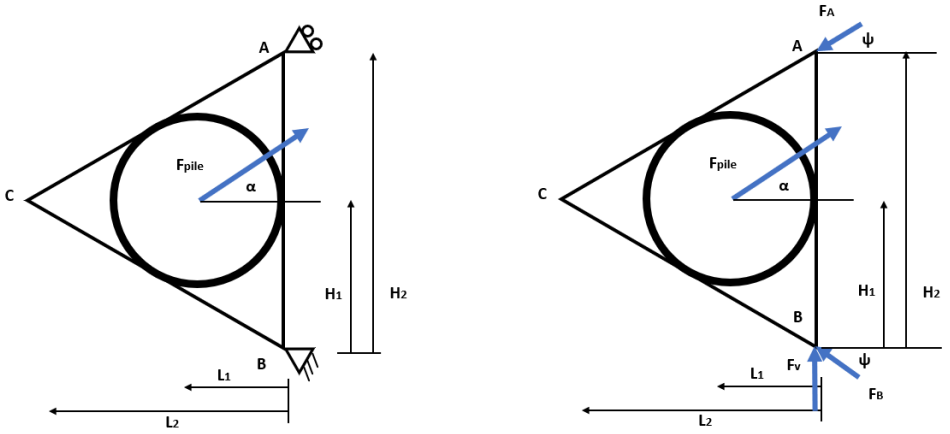

Figure 79: Top-view sketch and FBD of the hydraulic ring inside the triangular frame.

The triangle is supported by the two frames connecting the three pockets to each other. These connections are made in point A and B in the Figure. With the force equilibrium equations, forces F_A, F_B and F_v can be calculated. The equations used are as follows:

$$\sum F_x = 0 \text{ and } \sum F_y \text{ and } \sum M_B = 0 \tag{85}$$

$$\sum F_x = -F_A cos(\psi) - F_B cos(\psi) + F_{pile} cos(\alpha) = 0 \tag{86}$$

$$\sum F_y = -F_A sin(\psi) + F_B sin(\psi) + F_{pile} sin(\alpha) + F_v = 0 \tag{87}$$

$$\sum M_C = L_2 F_v + L_1 F_{pile} sin(\alpha) = 0 \tag{88}$$

In Table 28, the parameters used for the calculations are shown. F_pile is taken as the unit load. The reaction forces F_A, F_B and F_v result in the amplification factor that will be used in the next sections.

L_1	9.00	m
L_2	4.50	m
H_1	9.00	m
H_2	4.5	m
F_{pile}	1	N/N
ψ	30	deg

Table 28: Parameters used for the analysis

Since the SP can be loaded in all directions, angle α is variable. For the analysis of the frame, the maximum forces are of interest. Figure 80 shows the reaction forces plotted over angle α.

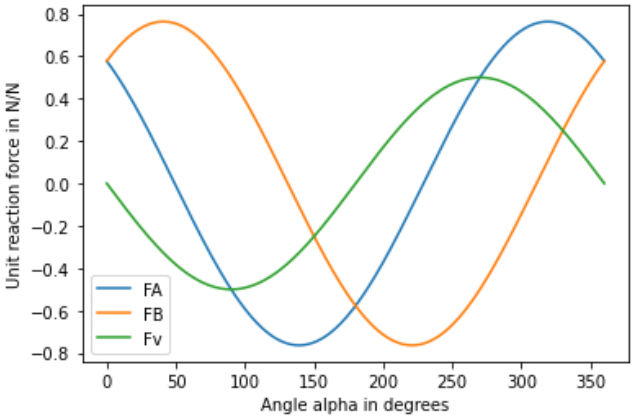

Figure 80: The reaction forces plotted over angle α

The maximum forces for each reaction force is different for a certain angle. The absolute value of the maximum and minimum value for each force is also the same. The results from the plot are shown in Table 29.

F_A	0.76	N/N
α	319	deg
F_B	0.76	N/N
α	41	deg
F_v	0.50	N/N
α	270	deg

Table 29: Result of the maximum reaction forces corresponding to a specific angle α.

F.2 Loads on the main members of the SPIT

The main members of the frame are the members on the outside of the SPIT frame. Because the frame of the SPIT has symmetry, the calculations can be based on one half of the frame on one side of the triangular SPIT frame. This part of the frame is highlighted in Figure 81a. The loading on the main members of the SPIT is analysed for two load cases:

- The SPIT is lifted in the air and the SPs are loaded by the waves
- The SPIT is lifted but fully submerged. The impact of the waves on the SPs is neglected.

Figure 81b shows the FBD for both load cases considered. The external loads indicated in the Figure vary, depending on the load case.

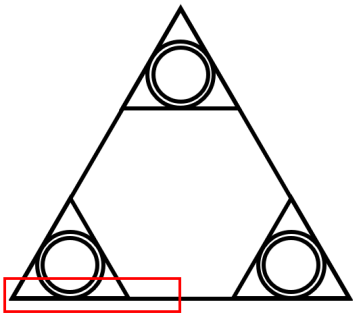

(a) 2D top-view schematic of the SPIT. In red indicated the part of the frame analysed in this subsection.

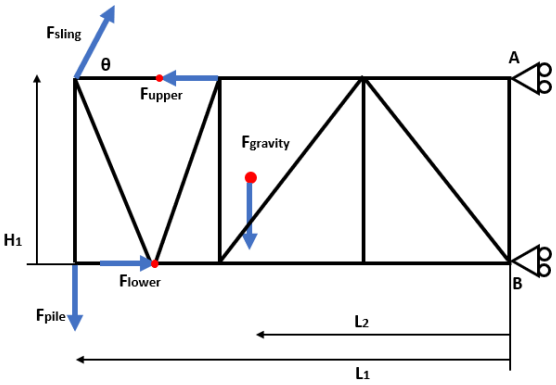

(b) 2D sketch of external loads on the main members of the SPIT during lift operation

Figure 81

The gravity force displayed in Figure 81b represents the gravity force of that particular part of the SPIT. The SPIT is horizontally restrained to represent the other half of the frame.

The corners of the frame are labeled from A to I. The frame consists of 15 members. Figure 82 shows the schematic of the frame with the corresponding labels. The weight of the frame is lumped on each of the top corners (A,C,E,G) and equally distributed over each corner. This is done to satisfy the equilibrium equations for each corner. However, the gravity forces are significantly less than the other induced forces on the frame and therefore no detailed weight distribution analysis on each corner will be performed as the effect will be insignificant.

The sizing of the members will be an iterative process. Table 30 shows the initial dimensions for the members.

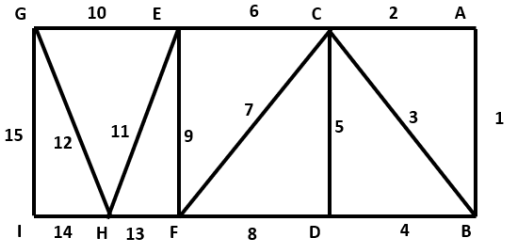

Figure 82: Schematic of the frame

Nr.	Location	Length (m)	Diameter (mm)	Thickness (mm)	Mass (kg)
1	AB	4.64	350	20	786
2	AC	6.75	350	20	1143
3	AD	8.19	350	20	1387
4	BD	6.75	350	20	1143
5	CD	4.64	350	20	786
6	DE	6.75	350	20	1143
7	DF	8.19	350	20	1387
8	CE	6.75	350	20	1143
9	EF	4.64	350	20	786
10	EG	9.00	350	20	1524
11	EH	6.46	350	20	1094
12	GH	6.46	350	20	1094
13	FI	4.50	350	20	762
14	GI	4.50	350	20	762
15	GI	4.64	350	20	786

Table 30: Initial member dimension for the frame

To get the internal forces of each member, the reaction forces in point A & B and the sling load (F_{sling}) need to be calculated. This can be done with the following static equilibrium equations:

$$\sum F_x = 0 \text{ and } \sum F_y \text{ and } \sum M_B = 0 \tag{89}$$

The three unknowns are F_{sling}, F_A and F_B. With the three equilibrium equations the unknowns can be solved. Figure 83 shows the FBD correlating with these equations. The equations can be rewritten as:

$$\sum F_x = F_{sling}cos(\theta) - F_A - F_B - F_{upper} + F_{lower} = 0 \tag{90}$$

$$\sum F_y = F_{sling}sin(\theta) - F_{pile} - F_{gravity} = 0 \tag{91}$$

$$\sum M_B = H_1F_A + L_2F_{gravity} + L_1F_{pile} - H_1F_{sling}cos(\theta) - L_1F_{sling}sin(\theta) + H_1F_{upper} = 0 \tag{92}$$

From section 6.4.1.4, two DAF factors have been selected. The DAF for the first load case where the SPIT is in the air equals 1.15. The gravity forces of the SP and the SPIT should be adjusted according to the following equation:

$$F_{adjusted} = M_{dry} \cdot g \cdot DAF \tag{93}$$

The dry weight of the SP is $340mt$ and the dry weight of the SPIT is estimated to be 300mt. The weight of the analysed SP is one-half of the total SP and the frame is one-sixth of the weight of the SPIT. The DAF for the second load case when the SPIT is fully submerged equals 2.0. The gravity forces of the SP and the SPIT should be adjusted according to the following equation:

$$F_{adjusted} = M_{wet} \cdot g \cdot DAF \tag{94}$$

The wet weight of the SP is $290mt$ and the dry weight of the SPIT is estimated to be $150mt$. The weight of the analysed SP is one-half of the total SP and the frame is one-sixth of the weight of the SPIT. Table 31 shows the parameters used for the equilibrium equations.

θ	60.0	deg
H_1	5.04	m
H_2	2.52	m
L_1	22.50	m
L_2	10.70	m

(a) Parameters used for the equilibrium equations

	Load case 1	Load case 2	
	DAF = 1.15	DAF = 2.0	
F_{pile}	1.92	3.83	MN
$F_{gravity}$	0.56	0.49	MN

(b) SP and SPIT gravity forces adjusted for the DAF

Table 31

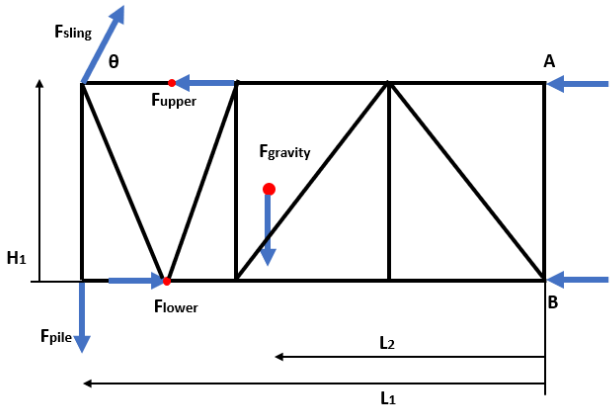

Figure 83: 2D FBD of part of the SPIT during lift operation

The results from the equations are displayed in Tables 32a and 32b. When the SPIT is not subjected to environmental loads, F_{upper} and F_{lower} are loaded due to the COG of the pile not being perfectly aligned with

the padeye location on the SP. The created moment of the SP is countered by the hydraulic rings. F_{upper} and F_{lower} result in the following equation:

$$F_{upper} = -\frac{F_{pile} r}{H_1} \tag{95}$$

Where r is the offset from the COG to the padeye and is estimated to be $3.0m$. The added forces due to the hydrodynamic load on the SP are calculated in Appendix B. For this frame part, the factor of 0.76 is applied according to section F.1. The hydrodynamic loads on the SPs are considered in load case 1. For load case 1, both direction of the hydrodynamic loading is considered.

	Mo+	Mo-	
F_{sling}	2.86	2.86	MN
F_{upper}	3.61	-6.09	MN
F_{lower}	5.38	-7.86	MN
F_A	-0.75	8.94	MN
F_B	3.96	-9.28	MN

(a) Parameters considered for load case 1

F_{sling}	4.99	MN
F_{upper}	-2.48	MN
F_{lower}	-2.48	MN
F_A	6.22	MN
F_B	-3.72	MN

(b) Parameters considered for load case 2

Table 32

Tables 33a and 33b show the results of the axial loading on each member.

	Mo+	Mo-	
F1	0.14	0.14	MN
F2	-0.75	8.94	MN
F3	-0.25	-0.25	MN
F4	4.16	-9.08	MN
F5	0.00	0.00	MN
F6	-1.36	8.33	MN
F7	0.49	0.49	MN
F8	4.16	-9.08	MN
F9	-0.28	-0.28	MN
F10	-1.77	7.92	MN
F11	0.59	0.59	MN
F12	-0.59	-0.59	MN
F13	4.57	-8.67	MN
F14	0.00	0.00	MN
F15	-1.92	-1.92	MN

(a) Axial forces of each member in load case 1. Tension is indicated with a negative sign.

F1	0.12	MN
F2	6.22	MN
F3	-0.22	MN
F4	-3.54	MN
F5	0.00	MN
F6	5.69	MN
F7	0.43	MN
F8	-3.54	MN
F9	-0.24	MN
F10	5.33	MN
F11	0.51	MN
F12	-0.51	MN
F13	-3.19	MN
F14	0.00	MN
F15	-3.83	MN

(b) Axial forces of each member in load case 1. Tension is indicated with a negative sign.

Table 33

The axial forces in members 1 & 14 should be doubled since these members overlap with the other part of the SPIT frame. The method used to calculate the axial forces in members 5 and 14 result in 0MN. However, this does not mean that these members are redundant. Member 5 increases the buckling resistance of the frame and member 14 adds extra stability to the SPIT-SP connection point. For fabrication efficiency, members 4, 8 13 and 14 will have the same size as well as members 2, 6 and 10. The size of member 5 will be the same as member 1.

F.3 Shear in frame due to bending moments

In the previous calculation, the assumption that the loads on one side of the frame is mirrored on the other side is made. However, during operations it can occur that the loads induced in the hydraulic rings create bending moment in identical direction. Figure 84 indicates the identical bending moments in the frame. The bending moment creates shear in the frame and is compensated by the diagonal and vertical members of the frame.

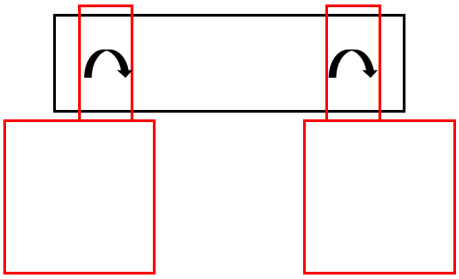

Figure 84: Same direction bending on the SP (indicated in red) creating shear loads in the frame.

In this analysis, only the diagonal and vertical member axial forces are of interest since the horizontal members maximum axial load occurs in the analysis in section F.2. To check the maximum axial forces in the diagonal members, the horizontal constraints of the FBD in the previous section is changed to vertical restraints. Figure 85 shows the new configuration of constraints on the frame.

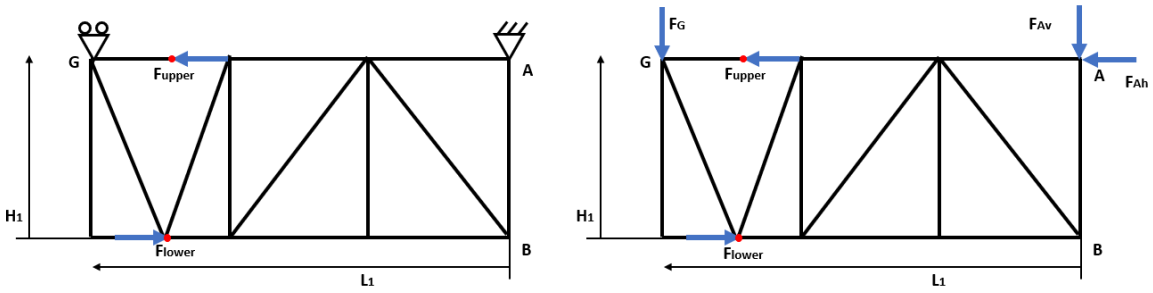

Figure 85: 2D sketch of the FBD considered for the shear analysis of the frame.

The reaction forces in A, F_{Ah} & F_{Av}, and G, F_G, can be calculated with the following equilibrium equations:

$$\sum F_x = F_{lower} - F_{upper} + F_{Ah} = 0 \tag{96}$$

$$\sum F_y = F_G + F_{Av} = 0 \tag{97}$$

$$\sum M_A = H_1 F_{lower} + L_1 F_G = 0 \tag{98}$$

L_1	22.50	m
H_1	4.64	m
F_{upper}	4.85	MN
F_{lower}	6.62	MN
F_{Ah}	-1.77	MN
F_{Av}	-1.37	MN
F_G	1.37	MN

Table 34: Parameters used and the resulting forces from the equilibrium equations

Table 35 shows the results of the axial forces on the vertical and diagonal members.

F1	-1.37	MN
F3	2.41	MN
F5	0.00	MN
F7	-2.41	MN
F9	1.37	MN
F11	-1.90	MN
F12	1.90	MN
F14	0.00	MN
F15	0.00	MN

Table 35: Forces on each member of the frame when lifted with no bending moment in the stub due to hydrodynamic forces. Tension is indicated with a negative sign.

Table 36

F.4 Shear in pocket frame

So far the analysis has covered the maximum forces that are parallel to the frame. If the SP is loaded more perpendicular to the side of the frame. The bracing between these frames, indicated in red in Figure 86, should resist the shear between the upper and lower hydraulic rings. The FBD is sketched in Figure 87.

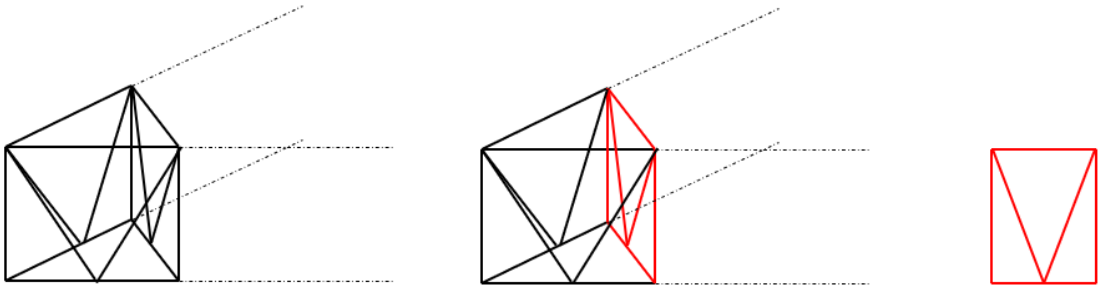

Figure 86: Schematic sketch of the pocket of the SPIT. The dotted lines indicate the bracings to the other pockets. The indicated red bracing is considered for this shear analysis.

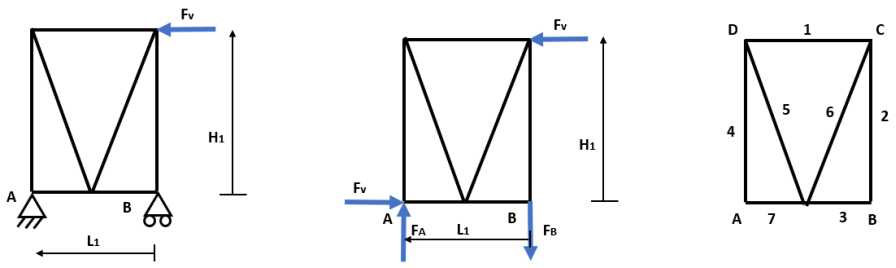

Figure 87: A sketch of the 2D problem with the corresponding numbering of each member.

The horizontal force F_v can be calculated from the maximum force on the hydraulic ring and the amplification factor of F_v calculated in section F.1.

$$F_v = 0.50 F_{lower} = 0.50 \cdot 8.71 = 4.36 MN \tag{99}$$

Table 37, shows the parameters used to calculated the axial forces in each member.

H_1	4.64	m
L_1	9.00	m
F_v	4.36	MN

Table 37: Parameters used for the calculations

The resultant forces F_A and F_B can be calculated to satisfy the static equilibrium:

$$F_A = F_B = F_v \frac{H_1}{L_1} = 2.25MN \tag{100}$$

The results from the calculations with the corresponding minimum and maximum axial force for all members are displayed in Table 38.

	F_{max}	F_{min}
F_1	2.18	-2.18
F_2,F_4	2.24	-2.24
F_3,F_7	4.36	-4.36
F_5,F_6	3.13	-3.13

Table 38: Results from the calculations of the shear load in the triangular frame

Member 2 and 4 corresponds with member 9 from Figure 82. The axial forces in members 2 & 4 are larger for this analysis compared to the analysis in section F.2 and will thus be the governing load case. Members 1,3 & 7 have lower axial forces in this analysis compared to the analysis in section F.2 and will not be the governing load case. Diagonal members 5 & 6 will be labeled as members 16 & 17 respectively in Table 39a in section F.5, where the overview of all the members are displayed.

F.5 Member sizing

The axial loading for each critical member has been calculated. The buckling stress and deflection checks will show if the members are correctly sized. Table 39a shows the maximum and minimum axial force in each member filtered from the results of the analyses performed in this Appendix. The initial diameter and thickness of each member is the same and displayed in Table 39b.

	$F_{max}[MN]$	$F_{min}[MN]$
1	1.37	-1.37
2	8.94	-0.75
3	2.41	-2.41
4	4.16	-9.08
5	0.00	0.00
6	8.33	-1.36
7	2.41	-2.41
8	4.16	-9.08
9	2.24	-2.24
10	7.92	-1.77
11	1.90	-1.90
12	1.90	-1.90
13	4.57	-8.67
14	0.00	0.00
15	0.00	-7.66
16	3.13	-3.13
17	3.13	-3.13
18	3.66	-3.66

(a) The maximum and minimum axial loads in each member with the corresponding buckling and stress check

D	350	mm
t	20	mm
I	$2.83 \cdot 10^{-}4$	m^4
ρ_{steel}	7850	kg/m^3
σ_y	350	MPa
E	210	GPa
SF	1.5	-

(b) Parameters used for the buckling and stress check of the members before the first iteration

Table 39

With the global safety factor (SF) of 1.5, B_{check} andS_{check} should be less than 0.67 for sufficient sizing. For efficient sizing, the necessary area of the member is calculated for the stress check:

$$A_{min} = SF \frac{F_A}{\sigma_y} \tag{101}$$

This also result in the minimum weight of the member. Now, the diameter of the member can be calculated with the following equation:

$$D = \sqrt{(}A_{min}\frac{tr}{\pi}) \tag{102}$$

Where tr is the thickness ratio of the member. The practical lower limit for $tr = D/t = 20$ and the upper limit is $D/t = 60$ [43]. The thickness ratio is optimized for each member. The final results are shown in Table 40.

	$F_{max}[MN]$	$F_{min}[MN]$	$B_{check}[-]$	$S_{check}[-]$	$L[m]$	$D[mm]$	$T[mm]$	$M[kg]$
1	1.37	-1.37	0.60	0.67	4.64	193	9.7	214
2	8.94	-0.75	0.20	0.67	6.75	494	24.7	2030
3	2.41	-2.41	0.57	0.67	8.19	339	9.7	664
4	4.16	-9.08	0.09	0.67	6.75	498	24.9	2062
5	0.00	0.00	0.00	0.00	4.64	193	9.7	214
6	8.33	-1.36	0.21	0.67	6.75	477	23.8	1892
7	2.41	-2.41	0.57	0.67	8.19	339	9.7	664
8	4.16	-9.08	0.09	0.67	6.75	498	24.9	2062
9	2.24	-2.24	0.37	0.67	4.64	247	12.4	350
10	7.92	-1.77	0.39	0.67	9.00	465	23.2	2398
11	1.90	-1.90	0.65	0.67	6.46	255	10.2	413
12	1.90	-1.90	0.65	0.67	6.46	255	10.2	413
13	4.57	-8.67	0.05	0.67	4.50	486	24.3	1313
14	0.00	-0.00	0.05	0.67	4.50	486	24.3	1313
15	0.00	-7.66	0.00	0.67	4.64	647	16.2	1196
16	3.13	-3.13	0.51	0.67	6.46	292	14.6	680
17	3.13	-3.13	0.51	0.67	6.46	292	14.6	680
18	3.66	-3.66	0.48	0.67	6.75	316	15.8	831

Table 40: Final dimensions for each member with the corresponding buckling & stress check.

G Padeye analysis

DNV-ST-N001 [5] provides a standard code for the design of padeye connections. With the help of these standards the sizing of the padeyes are performed. Figure 88 shows the typical padeye layout.

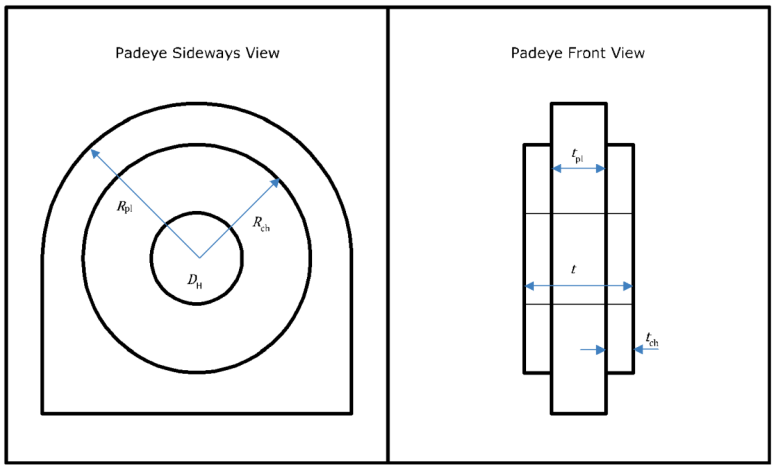

Figure 88: Typical padeye layout from DNV-ST-N001 [5]

Two different padeyes are considered in this analysis:

- SPIT-sling padeye: The padeye at each corner of the frame of the SPIT that is connected to a shackle. This shackle makes the connection with the sling to the crane hook.
- SPIT-SP padeye: The padeye at the top-plate of the SP. A pin lock mechanism on the SPIT creates the connection with the padeye.

The padeyes will be analysed on three checks:

- **Bearing pressure:** Checks if the bearing pressure on the inside of the padeye hole is within design limits. For $\frac{D_{pin}}{D_H} < 0.96$ the following criteria applies:

$$\frac{\sigma_y}{\gamma_m} \geq 0.18\sqrt{\frac{F_d(\frac{1}{D_{pin}} - \frac{1}{D_H})E\beta}{t}} \tag{103}$$

  For $\frac{D_{pin}}{D_H} \geq 0.96$ the following criteria applies:

$$\frac{\sigma_y}{\gamma_m} \geq 0.036\sqrt{\frac{F_d E\beta}{D_H t}} \tag{104}$$

- **Tear out:** Checks if the padeye will not tear out at the sides of the padeye and is within design limits.

$$\frac{\sigma_y}{\gamma_m} \geq \frac{1.7F_d}{(2R_{pad} - D_H)t} \tag{105}$$

- **Cheek plate welds:** Checks if the cheek plates of the padeye are correctly welded to the main plate and is within the design limits.

$$\frac{\sigma_y}{\gamma_m} \geq \frac{F_d t_{ch}}{1.5tD_{ch}a}\delta \tag{106}$$

  where

$$\delta = \frac{4tan(v)h}{t} + 1 \tag{107}$$

All definitions of each parameter can be found in Table 41.

F_{sd}	Design load in sling or pin	MN
γ_c	Consequence factor	-
γ_f	Load factor	-
F_d	padeye design load in line with padeye plate	MN
σ_y	Yield stress of padeye material	MPa
γ_m	Material factor	-
E	elastic modulus	GPa
D_{pin}	Diameter of shackle	m
D_H	Diameter of pinhole	m
β	Adjustment factor - bearing pressure	-
δ	Adjustment factor - lateral load	-
v	Sling out-of-padeye plane angle	deg
a	Thickness of weld throat	m
h	Distance between top of the shackle pin and application of force	m
t	Total thickness of padeye at hole including cheek plates	m
R_{pad}	Radius of padeye	m
R_{pl}	Minimum distance from centre hole to edge of plate	m
R_{ch}	Radius of cheek plates	m
t_{pl}	Thickness of the padeye plate	m
t_{ch}	Thickness of the cheek plate	m

Table 41: Definitions of parameters used for the padeye checks

R_{pad} is taken from the following equation:

$$R_{pad} = (R_{pl}t_{pl} + 2R_{ch}t_{ch})/t \tag{108}$$

All constant used for the padeye calculations are explained in Table 42.

γ_c	1.3	Consequence factor taken for padeye connections
γ_f	2.0	According to the maximum assumed DAF 6.4.1.4
σ_y	350 MPa	Standard yield strength of offshore steel grade
γ_m	1.15	For structural steel
E	210 GPA	Standard elastic modulus for steel
β	0.7	Adjustment factor for padeyes that will be used for multiple lifts without pin rotation.
v	3%	Minimum out of plane angle

Table 42

Additional design requirements for the padeye design are:

- The outside radius of the padeye main plate R_{pl} shall be no less than the diameter of the pin hole D_H
- The padeye thickness t shall not be less than 75% of the inside of the shackle (L_{pin}).
- The cheek plate thickness t_{ch} shall not exceed the main plate thickness t_{pl} and has a symmetric thickness for either cheek plates.
- The minimum gap between the pin D_{pin} and the pin hole D_H is $2mm$ or 3% of the pin diameter up to a maximum of $6mm$.

G.1 SPIT-sling padeye

This padeye connection is made with a shackle attached to the sling leading to the crane hook. The padeyes are used to lift the SPIT with the SPs from deck to the seabed. The design load in sling direction for the padeye (F_{sd}) corresponds with the calculated design load in Appendix F.2 and equals $4.99MN$. However, this has been calculated for a DAF of 2.0 and only one side of the frame. Therefore the static design load equals

$4.99MN$ and a DAF of 2.0 is considered. A standard shackle size with a $1000mt$ capacity has been selected for this connection [35]. The corresponding parameters for the shackle can be seen in Table 43.

Capacity	1000	ton
Width	1091	mm
Length	1490	mm
Mass	2200	kg
D_{pin}	270	mm
L_{inside}	400	mm
h	850	mm

Table 43: Shackle dimensions

In Figure 89, a schematic sketch of the shackle-padeye connection is illustrated. When the sling is out of plane with the padeye, a bending moment is introduced to the padeye. To keep the impact small of this bending moment, the gap between shackle pin and padeye hole should be minimal. For practical limits the gap on each side is $7mm$.

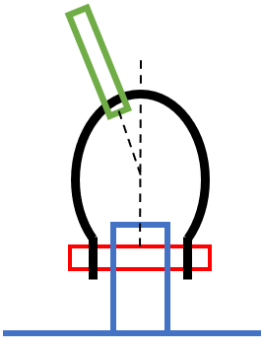

Figure 89: Schematic view of the shackle padeye connection. The shackle is highlighted in black. The padeye is highlighted in blue, The pin is highlighted in red and the sling is highlighted in green.

The final dimensions of the padeye with the corresponding checks can be seen in Table 44.

F_{sd}	4.99	MN
D_H	284	mm
t	300	mm
R_{pl}	422	mm
t_{pl}	150	mm
R_{ch}	380	mm
t_{ch}	75	mm
R_{pad}	400	mm
a	12	mm

(a) Padeye dimensions

σ_y/γ_m	304	MPa
Bearing pressure check	150	MPa
Tear out check	109	MPa
Cheek plate welds check	291	MPa

(b) Design check results for the padeye

Table 44

G.2 SPIT-SP padeye

This padeye connects the SPIT to the SP. On the top-plate of the SP the padeye is located. In the lower corners of the SPIT the pin-locking mechanism is located. The maximum load on the padeye is the weight of the SP. For the design load of the padeye, the submerged weight of the SP and the 2.0 DAF for the submerged lift is taken. This results in the design load of $2.26MN$. The schematic of the locking mechanism can be seen in Figure 90. The dimension of the pin should have enough strength to survive the loads during the closed and open load case. A solid pin with a diameter of $220mm$ satisfies the strength requirements assumed from a shackle pin diameter with a capacity of $800mt$ [36].

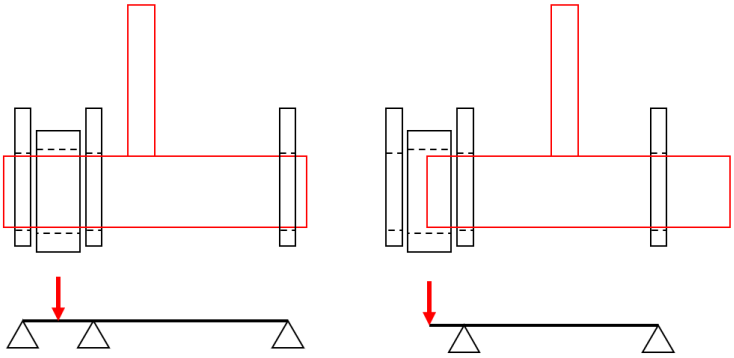

Figure 90: Schematic of the locking mechanism of the pin (red) and the padeye (black).

The gap between the pin and the padeye has been made substantially larger than for typical padeye connections. This is to ensure that slight misalignment of the SPs in the preparation area is acceptable in order to place the SPIT on top of the SPs. This negatively impacts the bearing pressure but, with correct sizing of the padeye, is manageable. The final dimensions of the padeye with the corresponding checks can be seen in Table 45.

F_{sd}	2.26	MN
D_{pin}	220	mm
D_H	259	mm
t	188	mm
R_{pl}	336	mm
t_{pl}	80	mm
R_{ch}	290	mm
t_{ch}	54	mm
R_{pad}	310	mm
a	5	mm

(a) Padeye dimensions

σ_y/γ_m	304	MPa
Bearing pressure check	280	MPa
Tear out check	114	MPa
Cheek plate welds check	298	MPa

(b) Design check results for the padeye

Table 45

H Tolerance analysis for the SP-jacket connection

The accuracy of the placement of the SPs depends on the connection between the jacket pins and the suction pile stub. For the designed grout connection, no steel-steel contact is allowed between the stub and the jacket pin. This tolerance analysis looks into three potential clashes that can occur during the installation of the jacket on the SPs:

- Upper clash: The upper centralizer on the jacket pin collides with the top part of the stub.
- Lower clash 1: The lower centralizer on the jacket pin collides with the lowest shear key on the inside of the stub.
- Lower clash 2: The lower centralizer on the jacket pin collides with the top part of the stub.

Figure 91 indicates the potential clashes.

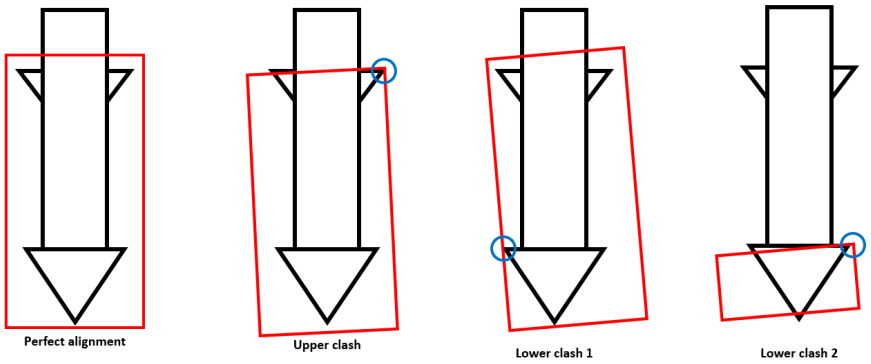

Figure 91: Clash cases considered for the tolerance study of the SP stub and JP.

The upper and lower clash can occur because of tolerances in the fabrication and installation process for both the jacket pin and the SP. The jacket pin and the SP tolerance analysis can be separated into horizontal misalignment and rotational misalignment. Figures 92a and 92b show sketches of the misalignment types. The summation of each tolerance margin caused by the misalignment types corresponding to the correct clash case provides the total tolerance margin necessary for this connection. Each misalignment type can consist of fabrication tolerances and installation tolerances. Table 46, indicates the cause of the misalignment for each type.

	Type	Fabrication tolerance	Installation tolerance
Jacket pin	Horizontal	X	
	Rotational	X	X
SP stub	Horizontal	X	X
	Rotational	X	X

Table 46

The horizontal misalignment of the SP stub or the jacket pin translates directly to the induced tolerance of the connection. The rotational misalignment of the SP stub or the jacket requires the following equation to translate to the induced tolerance of the connection:

$$\delta = sin(\alpha) \cdot L \tag{109}$$

Where δ is the induced tolerance, α the angle of the misalignment and L the length of the point of rotation to the contact area of the clash case. For the rotational misalignment of the jacket pin, the point of rotation can be taken from the joint at the lowest brace. For the rotational misalignment of the SP stub, the point of rotation can be taken from the lower hydraulic ring. Figure 93 displays the used lengths L for the SP stub and the jacket pin to its point of rotation. The maximum stub length results in the largest induced tolerance for rotational misalignment. Therefore the maximum stub length is considered for the tolerance analysis.

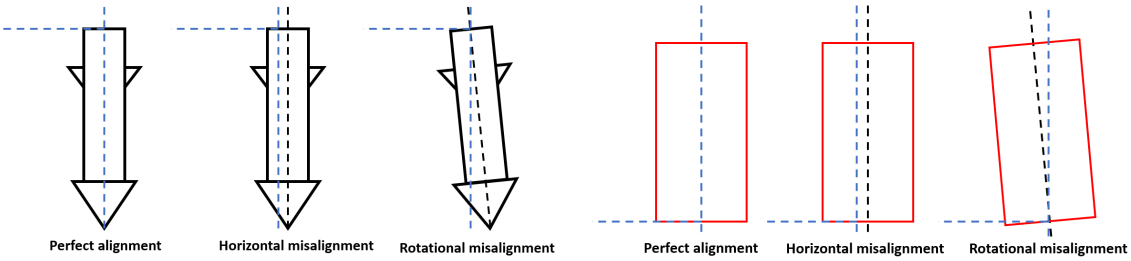

(a) Jacket pin misalignment **(b)** SP stub misalignment

Figure 92

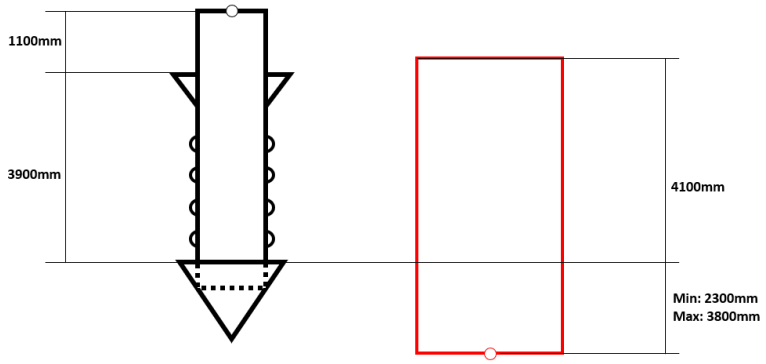

Figure 93: Lengths of the SP stub and jacket pin with respect to their point of rotation

H.1 Fabrication tolerances

The fabrication tolerances of the jacket pin and the SP stub are based on ISO19902 [13] and NORSOK M101 [32]. The total fabrication tolerances are used in Chapter 5.4 to calculate the maximum installation tolerance for the SPIT design requirement.

H.1.1 Jacket pin

The contribution of each fabrication tolerance of the jacket pin (JP) is listed in Table 47.

	Description	Source	upper clash	lower clash 1	lower clash 2
JP diameter	Min. of 1% circumference or 13	ISO19902	4mm	4mm	4mm
JP out-of-roundness	Min. of 1% nominal diameter or 8mm	NORSOK M-101	8mm	8mm	8mm
JP out-of-straightness	1.0mm per meter	NORSOK M-101	1mm	5mm	5mm
JP separation	20mm for offshore structures	ISO19902	20mm	20mm	20mm
JP out-of-verticality	0.25degrees	NORSOK M-101	5mm	22mm	22mm
Total			38mm	59mm	59mm

Table 47: JP fabrication tolerances

H.1.2 SP stub

The contribution of each fabrication tolerance of the SP stub is listed in Table 48.

	Description	Source	upper clash	lower clash 1	lower clash 2
Stub diameter	Min. of 1% circumference or 13	ISO19902	4mm	4mm	4mm
Stub out-of-roundness	Min. of 1% nominal diameter or 8mm	NORSOK M-101	8mm	8mm	8mm
Stub out-of-straightness	1.0mm per meter	NORSOK M-101	8mm	4mm	8mm
Stub out-of-verticality	0.25degrees	NORSOK M-101	34mm	17mm	34mm
Total			54mm	33mm	54mm

Table 48: SP stub fabrication tolerances

H.1.3 Total fabrication tolerances

The total fabrication tolerances are the sum of the SP stub and JP fabrication tolerances. The results are listed in Table 49.

	Fabrication tolerance
Upper clash	92mm
Lower clash 1	92mm
Lower clash 2	113mm

Table 49: Total fabrication tolerances

H.2 installation tolerances

From Chapter 5 results the total allowable tolerance margin of the SP. In the previous section, the fabrication tolerance has been calculated. The remaining tolerance equates to the required installation tolerance of the SPs in the seabed. Because of the function of the hydraulic grippers, the fabrication tolerances of the SPIT can be compensated. The misalignment of the SPs result from the tolerances of the hydraulic gripper and measuring equipment. According to section 6.4.4, the following cases are considered for the installation tolerance of the SPs.

H.2.1 Height of the SP (Heave):

The misalignment from the jacket placement results from the tilt of the jacket. Figure 94 indicates how the tilt is created. From previous project the installation tolerance of a SP is estimated to be $10mm$ SPT [39]. The installation precision of the pile stopper has been estimated at $100mm$ by previous reports from DEME [9] [34]. The minimum absolute distance between two SP stubs equals $\sqrt{36^2 - (36/2)^2} = 31.2m$ from the footprint of the jacket. The tilt of the jacket α results in $0.20°$ and translates directly to the rotational misalignment of the jacket pin. This tolerance will only occur after the jacket has been successfully lifted into the SP stub. Therefore, the clash case of lower clash 2 can be ignored.

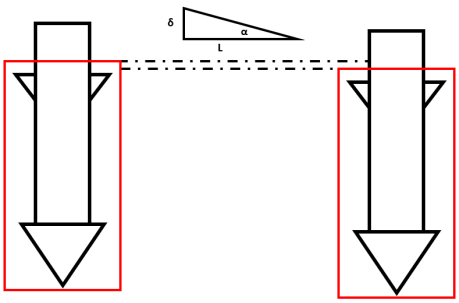

Figure 94: Tilt induced by height difference of the SP stubs

	Description	Source	Upper clash	Lower clash 1	Lower clash 2
Jacket tilt	0.20° installation precision of pile stoppers	SPT & DEME practice [9] [34] [39]	4mm	17mm	0mm

Table 50: Installation tolerance of the JP

H.2.2 Horizontal misalignment of the SP (Surge and sway)

The misalignment resulting from the hydraulic stroke precision and the measuring equipment is depicted in Figure 95. The results are displayed in Table 51.

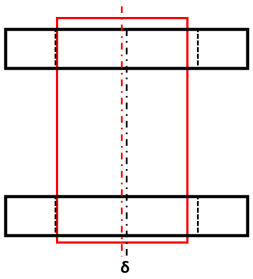

Figure 95: Horizontal misalignment of the SP stub in the SPIT

	Description	Source	Upper clash	Lower clash 1	Lower clash 2
Hydraulics	1% of stroke	Enerpac [11]	3mm	3mm	3mm
Measuring equipment	10mm	DEME practice [9]	10mm	10mm	10mm
Total			13mm	13mm	13mm

Table 51: Installation tolerance resulting from the horizontal misalignment of the SP

H.2.3 Rotational misalignment of the SP (Pitch and roll):

The rotational misalignment resulting from the hydraulic stroke precision and the measuring equipment is depicted in Figure 96a. The conservative estimate is made that after contact on the seabed, the SPs can not be adjusted by the hydraulic grippers. The installation tolerance creating the rotational misalignment is depicted in Figure 96b. The maximum rotational misalignment creating the precision of the hydraulic grippers ($13mm$) and the height between the hydraulic grippers ($4640mm$). The angle α equals $0.16°$. Length L results from the required penetration length necessary to reach PTG. For this case study it equals the SP's height of $15m$. The installation tolerance δ for each clash case is displayed in Table 52.

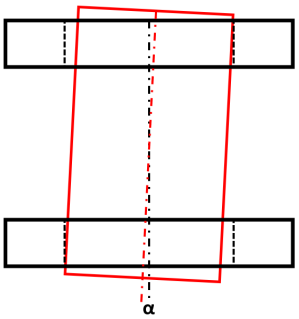

(a) Rotational misalignment of the SP stub in the SPIT

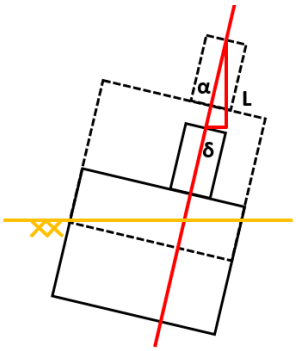

(b) Resulting installation tolerance caused by the misalignment of the SP stub in the SPIT

Figure 96: Rotational misalignment of the SP in the seabed

	Description	Source	Upper clash	Lower clash 1	Lower clash 2
Precision of grippers	0.16° SP stub rotation	table 51	38mm	48mm	38mm

Table 52: Installation tolerance resulting from the rotational misalignment of the SP

H.2.4 Total installation tolerances

The total installation tolerances are the sum of the SP stub and JP installation tolerances. The results are listed in Table 53.

	Installation tolerance
Upper clash	55mm
Lower clash 1	78mm
Lower clash 2	51mm

Table 53: Total installation tolerances

H.3 Total tolerances

The total tolerances is the sum of the fabrication and installation tolerance. In Table 54 can be seen that the calculated total tolerance of each clash case does not exceed the tolerance margin of the grouted connection. The design requirement of the SPIT installation precision is satisfied.

	Total tolerance	Tolerance margin
Upper clash	147mm	242mm
Lower clash 1	170mm	232mm
Lower clash 2	164mm	250mm

Table 54: Total tolerances for the grout connection

I Metocean data

In this Appendix, the metocean data, provided by DEME from ScotWind NE2 OWF site, is displayed. In the sheet below, the probability of occurrence of a specific wave is indicated. On the horizontal axis are the wave periods depicted with increments of 1s. On the vertical axis are the significant wave height depicted corresponding with the wave period with increments of $0.2m$. From this sheet can be concluded that for a significant wave height of $3.0m$, the corresponding wave period ranges from $5 - 16s$ at this location.

	lower	0	1	2	3	4	5	6	7	8	9	10	11
lower	upper	1	2	3	4	5	6	7	8	9	10	11	12
0	0,2				0,1%	0,1%	0,1%	0,1%	0,1%	0,1%	0,0%	0,1%	0,1%
0,2	0,4				0,7%	0,2%	0,4%	0,4%	0,3%	0,2%	0,2%	0,3%	0,2%
0,4	0,6				1,5%	0,5%	0,6%	0,7%	0,6%	0,5%	0,4%	0,4%	0,5%
0,6	0,8				2,6%	0,7%	0,7%	1,2%	1,1%	0,5%	0,4%	0,6%	0,6%
0,8	1				2,2%	2,0%	0,7%	1,5%	1,0%	1,1%	0,8%	0,6%	0,5%
1	1,2				0,5%	3,6%	0,7%	1,1%	1,6%	1,2%	0,6%	0,5%	0,6%
1,2	1,4				0,1%	3,3%	1,2%	0,5%	1,9%	0,8%	0,6%	0,4%	0,4%
1,4	1,6				0,1%	2,2%	1,6%	0,5%	1,5%	0,8%	0,7%	0,4%	0,3%
1,6	1,8				0,0%	1,3%	1,6%	1,0%	0,6%	0,8%	0,7%	0,4%	0,3%
1,8	2					0,6%	1,5%	1,1%	0,5%	0,6%	0,6%	0,4%	0,2%
2	2,2					0,1%	1,1%	1,0%	0,4%	0,6%	0,5%	0,4%	0,2%
2,2	2,4					0,0%	0,8%	0,9%	0,3%	0,5%	0,8%	0,2%	0,0%
2,4	2,6					0,0%	0,4%	0,6%	0,4%	0,3%	0,7%	0,2%	
2,6	2,8						0,3%	0,4%	0,4%	0,5%	0,5%	0,2%	0,1%
2,8	3						0,1%	0,3%	0,3%	0,6%	0,3%	0,1%	0,1%
3	3,2						0,0%	0,2%	0,3%	0,5%	0,3%	0,1%	0,0%
3,2	3,4						0,0%	0,1%	0,1%	0,5%	0,3%	0,1%	0,0%
3,4	3,6						0,0%	0,1%	0,1%	0,4%	0,3%	0,1%	0,0%
3,6	3,8							0,0%	0,1%	0,4%	0,2%	0,1%	0,0%
3,8	4							0,0%	0,0%	0,3%	0,2%	0,1%	0,0%
4	Inf							0,0%	0,0%	0,6%	0,8%	1,1%	0,5%
	total	0,0%	0,0%	0,0%	7,7%	14,7%	11,6%	11,7%	11,5%	12,0%	10,1%	6,8%	4,5%

	lower	12	13	14	15	16	17	18	19	20	
lower	upper	13	14	15	16	17	18	19	20	Inf	total
0	0,2	0,1%	0,0%	0,1%	0,0%	0,0%	0,0%	0,0%		0,0%	0,9%
0,2	0,4	0,3%	0,2%	0,1%	0,0%	0,1%	0,0%	0,0%		0,0%	3,5%
0,4	0,6	0,3%	0,1%	0,1%	0,1%	0,0%	0,0%	0,0%	0,0%	0,0%	6,4%
0,6	0,8	0,5%	0,3%	0,1%	0,1%	0,1%	0,0%	0,0%			9,5%
0,8	1	0,3%	0,5%	0,3%	0,1%	0,0%	0,1%		0,0%		11,8%
1	1,2	0,5%	0,1%	0,4%	0,1%	0,0%	0,1%	0,0%	0,0%	0,0%	11,7%
1,2	1,4	0,4%	0,4%	0,0%	0,2%	0,1%		0,0%		0,0%	10,3%
1,4	1,6	0,3%	0,3%		0,2%	0,0%		0,0%		0,0%	8,8%
1,6	1,8	0,2%	0,2%	0,2%		0,0%	0,0%	0,0%	0,0%		7,3%
1,8	2	0,1%	0,1%	0,1%		0,0%	0,0%		0,0%		6,0%
2	2,2	0,1%	0,1%	0,1%		0,0%	0,0%		0,0%		4,6%
2,2	2,4	0,1%	0,1%	0,1%		0,0%	0,0%				3,8%
2,4	2,6	0,1%	0,1%	0,0%	0,0%	0,0%	0,0%		0,0%		2,8%
2,6	2,8	0,0%	0,0%	0,0%	0,0%		0,0%				2,3%
2,8	3		0,0%	0,0%	0,0%						1,9%
3	3,2		0,0%	0,0%	0,0%						1,5%
3,2	3,4		0,0%	0,0%	0,0%						1,2%
3,4	3,6		0,0%	0,0%	0,0%						1,0%
3,6	3,8	0,0%	0,0%	0,0%	0,0%						0,8%
3,8	4	0,0%		0,0%							0,6%
4	Inf	0,1%		0,0%							3,2%
	total	3,3%	2,6%	1,7%	0,8%	0,5%	0,2%	0,1%	0,0%	0,0%	99,9%

J Frame numbering

In this Appendix the frame numbers are indicated. The calculated unique braces are numbered in Figure 98. The added braces are numbered in Figure 99 according to their estimated size from the unique members. Brace X is only added to create a point of attachment for the hydraulic jack mechanism. The weight of the brace is included in the added steel displayed in Table 14 in section 6.4.5.

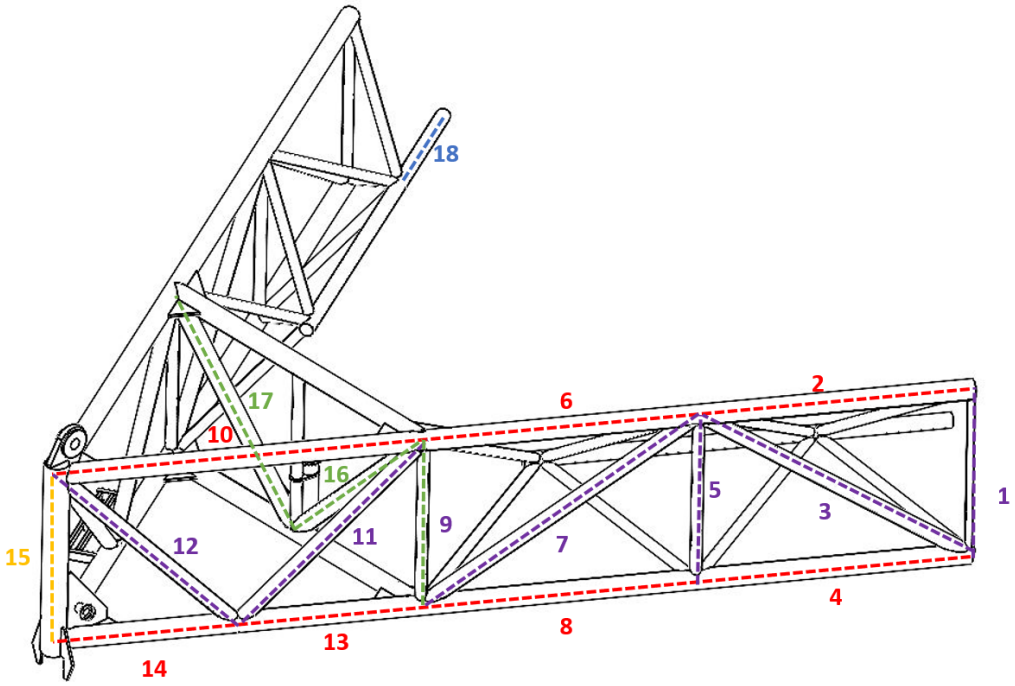

Figure 98: Frame numbering for each unique member

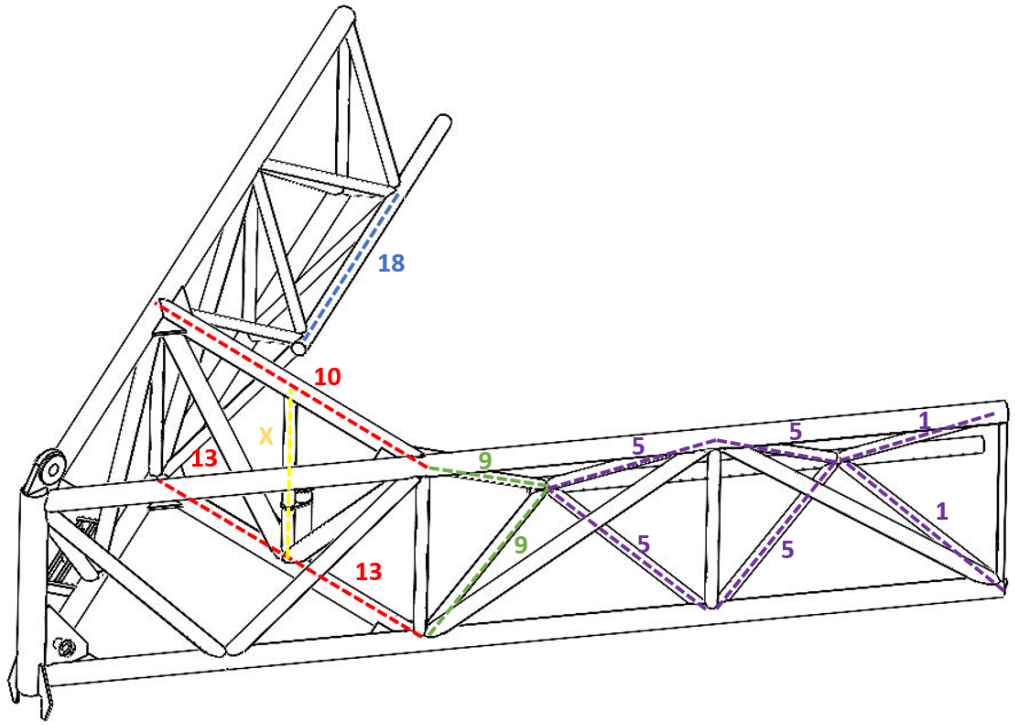

Figure 99: Frame numbering for added braces